UNIVERSITY OF THE
WITWATERSRAND,
JOHANNESBURG

Modelling of the distribution of coal tar product qualities from a tar distillation plant

MSc Research Dissertation

Prepared by

Lehlohonolo Christopher Mokoena

(375984)

Submitted to

A dissertation submitted to the Faculty of Engineering and the Built Environment, University of the Witwatersrand, Johannesburg, in fulfilment of the requirements for the degree of Master of Science in Engineering.

Supervisors: Professor Kevin Brooks and Professor Jean Mulopo

August 2024

Declaration

I. Lehlohonolo Christopher Mokoena, declare that this dissertation is my unaided work. It is being submitted to the Degree of Master of Science in Engineering at the University of the Witwatersrand, Johannesburg. It has not been submitted before for any degree or examination to any other University.

……

(Signature of Candidate) Lehlohonolo Christopher Mokoena

…23rd…day of …August, …2024…in…Vanderbijlpark..

Modelling of the distribution of coal tar product qualities from a tar distillation plant

Abstract

This work presents the simulation modelling and optimisation of a coal tar distillation process to improve the product qualities and increase overall product revenue. The coal tar distillation process consists of three vacuum distillation units and a flash column. The system produces four distillate products: light oil, refined chemical oil (RCO), light creosote, and heavy oil, as well as the residue pitch used as a binder in the manufacturing of electrodes in the aluminium industry.

The simulation model was developed in HYSYS using the actual plant mass balance and operating conditions for the production of a residue pitch product with a softening point of 115 – 118 Metller and associated distillates as reference. A mass balance reconciliation technique using an optimiser in HYSYS was applied to fit the plant quality and distillate rate data through adjustment of the Murphee tray efficiencies for each column. The simulation model was validated by simulating the manufacturing of a softer pitch product of softening point 68 – 73 Ring and ball using conditions specified for this particular product and its related distillate products. Through this process, the base conditions were established for the hard and soft pitch production processes. The resultant pitch yield of softening point 115 – 118 M was 42 %, with the light creosote distillate yield at 27 %, as for the softer pitch, the initial yield was estimated at 65 %, and the light creosote at 9,6 %.

Following the model development and the establishment of base conditions, a sensitivity analysis focusing on product quality distribution was done to develop an operating philosophy of the process followed by an optimisation process carried out using HYSYS original optimiser to maximise the objective function defined as the sum of product revenue sales with constraints placed on product qualities and adjustable parameters selected as column reflux and boil up ratio as well as the top and bottom temperatures. From the optimisation results, the general adjustment on the first two columns was the drop-down of column top and bottom temperatures by increasing the reflux ratio and reducing the boil-up rate. The light oil product quality in the simulation of a 115 – 118 M pitch improved by decreasing the naphthalene content from 48 % to less than 8,0 % as required by standard operation, with the naphthalene recovery in the RCO stream increasing from 44 % to 67 %.

The optimisation process had a large impact on the product yields, where the pitch product 115 – 118 M showed an increase in yield from 42 % to 49 %, which is close to the general yield of 50% mentioned in the literature and normally expected from a coal tar distillation process. and the light creosote distillate product had a positive yield increase of 14 % from the initial value. The overall revenue benefit for the production of a hard pitch improved by an estimated figure of 3,1 % per annum from the initial value (non-optimised condition). In the production of a softer pitch product, the total revenue benefit was 3,2 % higher per annum in comparison to the non-optimised condition.

This research dissertation is dedicated to my mother, Julia Mokoena.

I am grateful and deeply honoured for the boundless love, endless support, and countless sacrifices that you have made for me. You have played a significant role in shaping me into the person I am today. Even during moments of self-doubt, you have consistently believed in me, which I appreciate immensely. I feel incredibly blessed to have you in my life.

Acknowledgements

I would like to express my gratitude and appreciation:

To my supervisors, Professor Kevin Brooks and Professor Jean Mulopo, for their guidance, expertise, and valuable insights, as well as supervision of this research.

To ArcelorMittal for providing financial support and resources that made this research project possible.

To my partner, Ayanda Mahlangu, for your support and encouragement throughout my research journey. I am grateful for your patience, understanding, and emotional support, which helped me stay focused and motivated during these difficult times. I am truly fortunate to have such a supportive partner by my side; thank you for everything you have done.

Contents

List of Figures

List of Tables

Nomenclature

Temperature	$T\ (°C)$
Pressure	$P\ (kPa)$
Liquid fraction	x
Vapour fraction	y
Gibbs free energy	G
Fugacity	f
Gas constant	$R(\frac{8,314J}{mol}.k)$
Equilibrium constant	K

Subscripts

Average	avg
Number of elements	n

Greek

Fugacity coefficient	φ
Density	ρ

Viscosity	μ
Relative volatility	α
Accentric factor	ω

Abbreviations

Minimum	min
Maximum	max
Hard pitch softening point Mettler	$115 - 118\ M$
Soft pitch softening point Ring and Ball	$68 - 73\ RB$

1 Introduction

The drive for cleaner fuels to reduce harmful greenhouse gas emissions has resulted in declining coal consumption in most parts of the world. However, despite the ongoing efforts to reduce coal use worldwide, it is still a valuable resource and is part of the energy mix, mostly in developing countries (Li, Feng-Hua, & Hua-Ling, 2009). One of the major applications of the coal resource is in the carbonisation industry, where bituminous coal is converted into metallurgical coke for use in the blast furnace to produce pig iron. Coke serves three essential functions in the blast furnace, which are to provide mechanical stability (burden) and permeability for molten iron and gases, it also serves as a reductant and an energy source. The carbonisation process of coal is a high-temperature process usually carried out in a slot-type recovery oven at temperatures around 1050 – 1200 °C, thus leading to thermal degradation of coal macromolecules where metallurgical coke, as well as condensable (coal tar and ammonia liquor) and non-condensable (coke oven gas) by-products, are formed and collected by a series of physical and chemical processes (Granda et al, 2014). Coke oven gas is an important source of energy in the steel industry used for battery under-firing. It can also be supplied to various other users for heating purposes, allowing for more efficient energy integration.

The current research is concerned with the condensable by-product recovered from the coking process, namely coal tar, which is a complex mixture of aromatic hydrocarbons, polycyclic hydrocarbons (PAHs), and heterocyclic compounds (Kozlov et al, 2020). It is an important raw material for the carbo-chemical industry, and conversion into saleable products is generally performed by fractional distillation, where products such as light oil, phenols, naphthalene, creosote, and pitch residue are recovered. These aromatic raw chemicals are a major part of the chemical and medical industry, where they are further refined into solvents, dyes, drugs, disinfectants, explosives, fuel oil, and wood preservation, and the pitch residue is used as a binder in the manufacturing of electrodes for the aluminium industry (Kumar Gupta et al, 2021).

Coal tar has a long and successful history as an organic raw material and was the sole source of aromatic chemicals from the second half of the 19th century until the mid-20th century (Diez & Garcia, 2018). After the Second World War, petroleum was produced on a larger scale as it took over the organic chemical market. However, coal tar is still in use as an alternative because of its highly aromatic composition derived from the carbonisation process and constitutes high content of naphthalene and other high molecular weight compounds such as anthracene and pyrene, which can only be found from coal sources (Granda et al, 2014). Coal tar pitch constitutes about 50% yield of the total feed to the distillation plant and has superior binding and impregnating properties when compared to petroleum pitch, thereby justifying its use in the aluminium industry for the manufacturing of electrodes and graphite for electric arc furnaces as well as the continued production of coal tar.

Satisfying the existing and growing market demand for the chemical industry creates a bigger challenge for the engineers and planning teams at the tar distillation plants to produce more product tonnages within specific quality limits and environmental laws. To gain an advantage on production and quality targets in a coal tar distillation process, the crude tar feed quality and the plant operating conditions are parameters of utmost importance and must be managed properly. However, feed tar quality is usually unstable due to inconsistencies in coking

conditions, and this necessitates parameter changes in the distillation process to try and meet the production and quality demands.

The available literature on the coal tar distillation process focuses primarily on optimising the yield and quality improvement of residue pitch products. As aforementioned, pitch residue constitutes half the production in coal tar distillation, and it is in great demand for anode and graphite manufacturing, yielding high revenues; hence, it has been the focus of research. Process parameters that affect pitch quality were investigated in a lab experiment performed by Ajay Kumar *et al. It* was found that the distillation temperature and isothermal holding time have a greater impact on pitch quality, and the heating rate was found to have little effect on the resultant pitch quality (Kumar Gupta et al, 2021). Kozlov *et al.* developed a regression model to predict pitch characteristics based on experimental data (Kozlov et al, 2021), but there is not enough literature published on the performance characteristics and optimisation of a coal tar distillation process. Romanova *et al.* investigated the effect of azeotropes on naphthalene purity in coal tar distillation processing using HYSYS simulation modelling and proposed a three-column system with energy recovery to improve naphthalene purity, recovery and energy optimisation (Romanova et al, 2018).

Modelling of vacuum distillation units has been carried out. However, the focus is mainly on crude oil processing; S X H'ng *et al.* investigated the optimisation of heavy vacuum gas oil by developing a linear regression model to capture the relationship between input and output variables of a vacuum distillation unit (H'ng et al, 2021). Expert systems for crude oil distillation were developed using artificial neural networks for the optimisation of oil production rates within product quality requirements (Liau et al, 2004). Process models work better when coupled with an optimiser where operating conditions, product quality, and production rates are adjusted to maximise plant profits, taking into account environmental emissions and equipment safety.

Several research developments have been carried out using simulators to model the process behaviour with an optimiser applied to search for the best operating conditions and improvement to valuable product yields. Lopez used metamodels to develop a crude oil distillation process model using data from a simulator (López et al, 2013). A non-linear programming model was then applied to maximise profits by optimising crude oil blending and operating conditions. In the current study, a process optimisation model for a coal tar distillation plant is developed to investigate the optimum operating conditions for improved yields and product quality distribution using a specific crude tar feedstock. This work will broaden the existing engineering knowledge base on vacuum distillation and provide insight into the optimisation of coal tar distillation plants, as well as in training inexperienced engineers and operators to make better decisions.

1.1 **Problem Statement**

The increased demand for coal tar distillation products and challenges in the stability of feedstock quality from the coke oven batteries in the industry have motivated engineers to search for ways to adjust the coal tar distillation operating strategy to improve yields and consistently produce good quality products. Hence, the current study investigated the optimum operating conditions and product quality distribution of a specific coal tar distillation process by developing a simulation model that will describe the behaviour of the process and thus predict the quality output based on specified input variables, with an optimiser applied to the

simulation model to increase overall product revenues by increasing the yield of valuable products within specified quality limits.

This research addressed the following questions:

- What is the base product yield with the current crude tar feedstock qualities and operational conditions?
- Which operational parameter changes should be made to achieve maximum product revenue?
- Is the naphthalene oil composition produced from the different pitch grades the same?
- Can the model developed be used in practical plant operation?

1.2 **Aim and Objectives**

The project aims were to evaluate the distribution of coal tar product qualities from a tar distillation plant by developing a steady-state distillation process simulation model and optimising the plant performance through product revenue maximisation.

The objectives of this research were:

- To develop a steady-state model that best describes the coal tar distillation process.
- To identify the process conditions that influence product yields and qualities.
- To investigate the optimum operational parameters.
- To evaluate product quality distribution at different pitch grades.

1.3 **Overview of the Dissertation**

This dissertation describes the methodology taken to develop a coal tar distillation model which is applied to investigate the effects of process conditions on product qualities of the different distillates produced. The optimisation process is also described to develop an operating strategy that maximises product revenue and improves product quality.

The research dissertation begins with the literature review section in Chapter 2, which provides an overview of coal tar, its chemical composition, and its physical properties. This section goes on to explain the fundamentals of distillation, including the theories behind simulation models. Finally, optimisation methods in process engineering and those applicable to distillation processes are discussed in detail to conclude the literature review section.

The methodology followed in the development of a coal tar distillation process is described in Chapter 3; this includes feed characterisation, model development, thermodynamic model and simulation model selection, as well as the optimisation method applicable.

Chapter 4 presents the simulation results for changes in operational parameters and their impact on product quality. It also presents a case for optimising operations for two pitch products.

Chapter 5 summarises the results and discusses their implications for coal tar distillation processes.

In Chapter 6, recommendations are made regarding future studies and how the coal tar distillation modelling can be improved to provide accurate results.

2 Literature Review

2.1 **Coal**

Coal played a very important role in the Industrial Revolution and the advancement of modern civilisation. It has been the most reliant and abundant energy source since its discovery in the Middle Ages and has given birth to many industries that shaped the world into what it is today. Countries that discovered their coal reserves much earlier have now transformed into developed countries (Li et al, 2009).

In its physical state, coal is an organic sedimentary rock with colour ranging from brown to black, easily fractured, and has formed over millions of years through the partial decomposition of vegetable material in freshwater swamps (Viswanathan, 2017). Due to the biological and geological actions during the coalification process, original plant matter progressively changes to a fibrous brown deposit known as peat. With continual changes in temperature and pressure over millions of years, peat evolves into brown coal (lignite). The organic material progresses from lignite to semi-bituminous, bituminous, semi-anthracite and anthracite (Sundholm et al, 1999) .

The coal characteristics depend on the type of vegetation, deposition, and environmental conditions during the coalification process. Most European coals are of higher rank when compared to those found in the southern hemisphere (Brazil, Africa, and Australia), and this is attributed to the climate and type of vegetation found in respective geological areas (Franck & Stadelhofer, 1988). The emergence of coal petrographic studies, which examine the visible structure of coal, has led to an improved way of classifying the different types of coals by quantifying the different maceral groups (vitrinite, clarain, durain, and inertinite) present in a coal seam. Knowledge of these organic structures enables the prediction of the chemical and reactive behaviour of coals. Coal rank is one of the most important parameters used in petrographic studies, measured by the reflectance of vitrinite in a coal sample under a microscope mounted with a photometer (Loison et al, 2014).
Before the existence of petrography, the volatile matter content was initially used to define coal rank. Coals of high volatile matter were classified as of the lower rank, and the low volatile matter coals were of higher rank. This correlation was found to have some discrepancies, as proven by a comparison of the Northern and Southern Hemisphere coals (Loison et al, 2014). Therefore, the petrographic studies of macerals improved the concept of coal rank.

2.1.1 Selection of coals for the carbonization process

The carbonisation process primarily aims to produce metallurgical coke for use at the blast furnaces. In this regard, the coke quality specifications need to be met. This can be achieved through careful selection of coals, operating conditions, as well as the coke oven battery design (Granda et al., 2014). Bituminous coals are preferred in the carbonisation process because they exhibit caking behaviour. When bituminous coals are heated in the absence of air, they soften into a plastic state and become fluid. With continued heating, they swell and then resolidify into coke. Coals that behave in this manner are known as caking coals (Viswanathan, 2017).
For the classification of good coking coals, two laboratory experiments are conducted to determine if the coal or coal blend shows caking capabilities, and the measured properties are

fluidity and dilatometry (Loison et al., 2014). A Geiser Plastometer measures fluidity to determine the coal softening point, maximum fluidity, and re-solidification temperature. Through the temperature stages defined in the plastic state, volume changes do occur and are measured in a dilatometer. Three temperature stages are recorded in a dilatometry test; first, the coal contracts on heating, then swells on further heating, reaching a maximum peak, and eventually contracts on re-solidification. The permanent change in volume is measured as the dilatation of the coal sample.

Coals with high volatile matter are highly plastic and become more fluid on heating, resulting in the coke's weak mechanical structure. Medium to low-volatile matter coals are generally good coking coals; as a rule, coals of volatile matter in the range of 18 – 32% are considered and are normally blended to optimise the cost of producing metallurgical coke. Figure 2-1 below shows the classification of three types of coking coals indicated by point A, B and C, and their fluidity, aromaticity and ring condensation measured (Schobert, 2013). It is illustrated in Figure 2-1 that coals with medium volatile matter (coal C) are the best coking coals based on the moderate fluidity, ring condensation as well as ring condensation and reactivity of the liquid phase.

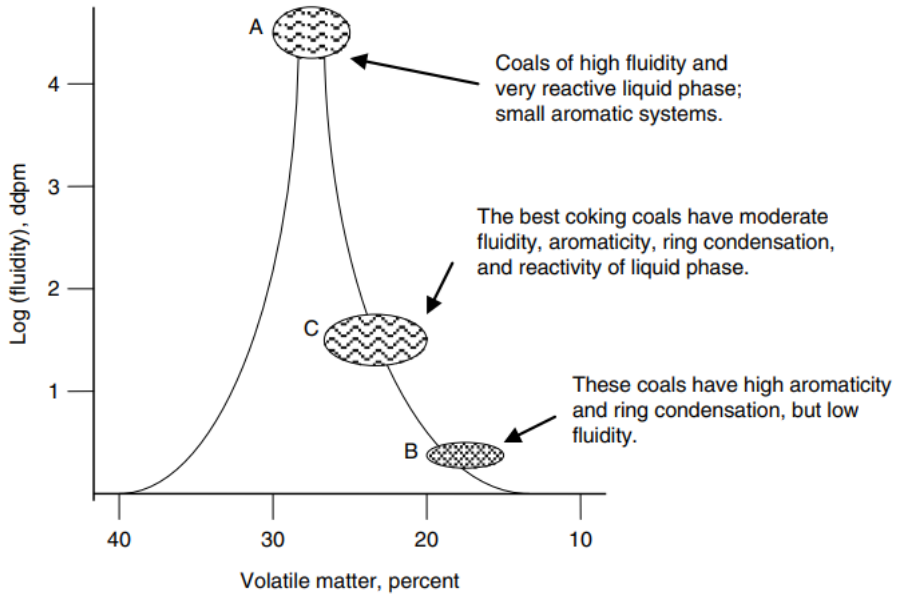

Figure 2-1: Classification of coking coals based on fluidity with aromaticity and ring condensation, ***adapted from***:(Schobert, 2013).

Other parameters of importance are the levels of sulfur, phosphorus, and ash contents in the coal, as the elements are transferred directly into the coke during the carbonisation process and have a negative impact on the blast furnace operation (Díez et al, 2002). Chlorine also gets carried over into the by-products and is very corrosive to the distillation equipment.

2.2 Coal tar production – the coking process

On a molecular level, coal is made up of clusters of condensed aromatic, hydroaromatic, and heterocyclic hydrocarbons linked by aliphatic chains and heteroatomic bridges, which, when heated slowly in the absence of air, produce coke at a yield of 75 wt.% and raw coke oven gas which accounts for 25 wt.% of the coal (Stansberry et al, 1999). Coal tar and moisture are condensed from the raw coke oven gas and sent together with the non-condensable gases to the

by-product plant for separation and further processing. The recovery of these by-products renders the carbonisation process more profitable and essential to the iron and steel-making economy.

2.2.1 Transformation of coal into coke

The first step in the carbonisation process involves the loading of coal with a particle size of about 3,5 mm into a slot-type oven, where oven walls are kept at temperatures between 1080 – 1230 °C by heating flues on the side of the walls.
After charging the coal in an oven, a level bar is used to level the coal charge to a uniform profile. This action leaves a free space above the charge in the oven, and depending on the type of coke to be produced, the charge is left for a specific coking cycle. The typical coking cycle for metallurgical coke is 18 - 20 hours (Díez et al, 2002) . Heat is transferred from the heating flues at the side of the walls through the silica bricks and towards the centre of the coal charge, resulting in a thermal gradient. Due to this, coal transforms different successive layers proceeding toward the center, as depicted in Figure 2-2 below.

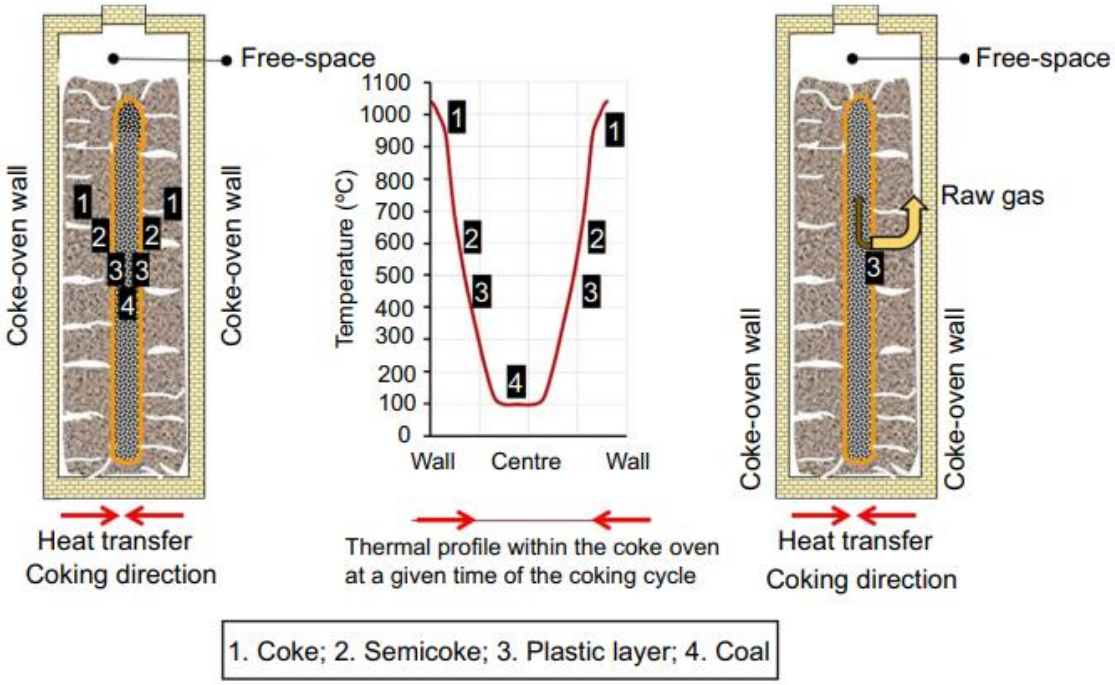

Figure 2-2: A schematic of the coal-coke transformation process in a slot-type oven, ***adapted from***: (Diez & Garcia, 2018).

The high temperatures at the walls increase the rate of coke formation in this area but continually decrease towards the centre. A layer of semicoke, which is a precursor of coke, is formed next to the coke layer. Closer to the semicoke layer is a plastic layer intermediate between coal softening and re-solidifying into the semicoke. At the centre, a coal layer is found and remains until the temperature is high enough to cause any chemical transformations (Tiwari et al, 2014).

Studies on pyrolysis and carbonisation of bituminous coals show that five critical temperature stages define the coal-to-coke transformation and the evolution of volatiles (Diez & Garcia, 2018). The first stage involves drying of coal moisture when the coal charge reaches temperatures of around 100°C, with more distinct changes occurring between 200 to 350 °C. The volatiles evolved in this stage consist of surface functional groups such as carbon oxides from the decomposition of oxygen functional groups, but no significant structural or chemical changes are happening. This is the pre-plastic stage, which prepares the coal charge for the most important step in the process, the plastic stage, which normally takes place between 350 – 550 °C. The chemical and structural changes occurring in the plastic stage are complex; however, there has been good progress made by various researchers toward the understanding of this process. Lewis gave a very good summary of carbonisation chemistry based on the theories developed by researchers in this field (Lewis, 1982). The plastic state is divided into two stages; at temperatures between 350 – 450 °C, the notable physical change is the softening of coal. The softened coal undergoes chemical changes that entail extensive breakage of aliphatic chains, C – C and C – H bond cleavage to form free radicals, molecular arrangement, thermal polymerisation, and aromatic condensation, which involves the formation of aromatic rings by dehydrogenation of saturated rings and recombination reactions. As a result, there is a progressive evolution of gases and aromatic hydrocarbons which constitute primary tar. During the evolution of gases, the plastic mass swells, causing the structure to become porous due to the entrapment of gases. With the rise in temperatures beyond the plastic range, coal solidifies into semicoke at temperatures above 550 °C. At these temperature ranges, there is a gradual evolution of hydrogen and growth of pre-graphitic layers in semicoke, leading to the development of coke. The final stage takes place when the charge reaches temperatures around 800 – 1100 °C, which leads to the consolidation and stabilisation of coke.

2.3 Recovery of by-products

According to various authors, gases evolved at the different stages of the carbonisation process pass through layers of semicoke and migrate towards oven walls and the free space above the coal charge (Diez & Garcia, 2018). The free space creates a secondary reactor where primary tar undergoes secondary pyrolysis, resulting in solid carbon forming that contributes to the amount of insoluble in coal tar and reduces tar yield.
Quantitative analysis of the evolution of raw coke oven gas was carried out at INCAR experimental coking plant in a 6-ton oven with volatile matter sampled at the centre of the ascension pipe (Alvarez et al, 1989). A gas chromatograph with a flame detector was used for qualitative and quantitative study of the gaseous components present. Based on the results of the experiment, hydrogen is the most dominant species available, with concentrations increasing steadily at the beginning of the carbonisation process to about 50-58 % vol in the first 10 hours of the coking cycle. When the coal charge reaches 600°C after 10 hours, the hydrogen concentration shows a steep increase until the end of the carbonisation process. In the same period, methane concentration decreases from 38% vol at the start of the process to 25% vol at the end of the carbonisation cycle. This is attributed to the convergence of the plastic layers, which indicates the end of the plastic stage and the beginning of the semicoke transition to coke. Other gaseous species present (CO_2, C_2H_4, C_2H_6) behave similarly to methane, whereas carbon monoxide shows an increase towards the end of the process.

In the experiments mentioned above, coal tar was recovered from raw coke oven gas and, after that, solubilised in $CHCl_3$. The analysis of coal tar composition was done using GC with a flame ionisation detector measured at different coking times and carbonisation temperatures.

The results show that light aromatic hydrocarbons such as BTX and phenols are recovered at temperature ranges of 100 - 200°C, with less condensed Polycyclic aromatics appearing at coal charge center temperatures of around 400°C. The PACs are most dominated by the naphthalene species, which accounts for about 18% of the fraction, followed by phenanthrene, anthracene, fluoranthene, pyrene, and small amounts of methylnaphthalene.
A further increase in temperature to around 600°C leads to a small percentage recovery of heavy aromatic hydrocarbons that are mostly found in pitch characterisation.
From the study, it can be concluded that coal tar consists of mono and polycyclic aromatic compounds as well as the heterocycles of oxygen, nitrogen, and sulfur compounds, and no aliphatic compounds were detected.

The industrial practice on the recovery of by-products involves direct quenching of raw coke oven gas as it emerges from the ovens through the ascension pipe into the collecting main. The coal tar and ammonia liquor are separated at the gas purification plant, where coal tar is decanted for quality control and handling and, after that, transported to the distillation plant to recover valuable chemical oils.

2.4 Coal tar characterisation

Coal tar is a complex mixture of aromatic compounds condensed from raw coke oven gas; these range from monocyclic aromatic compounds, which are mainly the BTX and the phenol fraction, to polycyclic aromatic compounds. The PACs consist mostly of Polycyclic aromatic hydrocarbons (PAH), which constitute more than 90% of the total tar composition and a small fraction of heterocyclic compounds containing nitrogen, sulfur, and oxygen atoms (Diez & Garcia, 2018). Knowledge of the coal tar composition and its physical properties is of vital importance to the distillation plant for planning, process optimisation, and addressing health issues inherent in the use of coal tar; hence, specific test methods have been developed and applied in industry. A detailed review of ISO standards applied in the industry to characterise pitch and coal tar properties is provided by Raymond, Markus, and Werner.
Conventional methods used in the distillation plants for the characterisation of physical properties of coal tar and pitches are described below, these include solubility in solvents, coking value, density, and as well as rheological properties.

Solubility in solvents: Coal tar normally contains high molecular carbon particles that are formed during secondary pyrolysis of volatile products in the oven-free space which are classified as primary quinoline insoluble particles. These particles are directly transferred to the residue pitch product during distillation and have a negative impact on the application of the product in the manufacturing of graphite electrodes; hence, their classification is important. The solubility of tar in quinoline and toluene solvents are methods used in industry to quantify the content of insoluble particles.

Density and viscosity: coal tar density is an indication of the average molecular weight and boiling point of components present. It is greatly influenced by the severity of cracking in the coke ovens. Density is measured using a hydrometer or a density bottle method and usually ranges from 1100 to over 1200 kg/m³ depending on the coke oven conditions used to produce the tar.
The standards used for coal tar viscosity measurements are ASTM D1665 and DIN 51560.

Simulated distillation: A laboratory distillation at atmospheric pressure is normally carried out at temperatures up to 360°C to quantify the distribution of fractions present in a coal tar sample.

Table 2-1 below shows a typical distribution of different fractions obtained from a laboratory distillation of coal tar.

Table 2-1: The distribution of coal tar oil fractions and pitch residue from a laboratory fractional distillation, ***adapted from***: (Kozlov et al, 2020).

Fraction	Yield (wt. %)	Boiling point (°C)
Phenol	1	≤ 170
Phenol	2,9	170 - 210
Naphthalene	10	210 - 230
Absorbing	6,2	230 - 270
Anthracene	23.9 - 30.9	270 - 360
Pitch	49 - 56	≥ 360

Gas chromatography and mass spectrometry: Gas chromatography coupled with mass spectrometry analytical technique is used to characterise the individual compounds found in coal tar. This information is important for process monitoring and optimisation as well as in classifying the PAHs present as they are known to be mutagens. A typical classification of aromatic compounds found in coal tar using GC-MS analysis is presented in Figure 2-3 below in the order from light aromatic compounds to the heaviest.

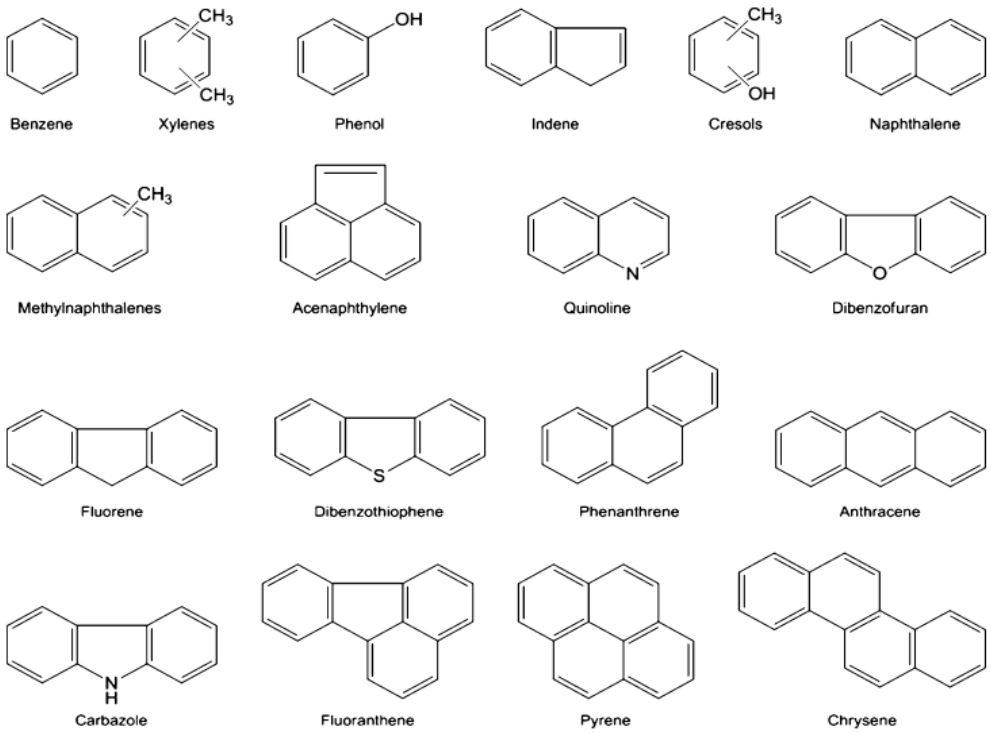

Figure 2-3: Typical aromatic compounds found in coal tar, ***adapted from***: (Granda et al, 2014).

2.5 Distillation Fundamentals

Distillation is a physical process used to separate volatile species from heavy components in a liquid mixture by differences in boiling points (Richardson et al., 1991). It has been reported in the literature that distillation was invented in the city of Alexandria in Egypt by the 1st century AD, where the early applications were in the production of alcoholic beverages and the purification of essential oils from natural products (Review & Werner, 1953).
Despite the introduction of new separation technologies and the fact that distillation is a very energy-intensive process, it is still a widely used process in the chemical and petroleum industries, this is illustrated in Table 2-2 below are various applications of fractional distillation in industry for the manufacturing of various products.

Table 2-2: Applications of the distillation process in various chemical industries, ***adapted from***: (Binay K. Dutta, 2007)

Feed/Components	*Industry/Plant*	*Product*
Crude petroleum	Refinery	Various petroleum products
Ethylene oxide/Water	Petrochemical	Ethylene oxide
Acrylonitrile/Water	—do—	Acrylonitrile
Styrene/Ethylbenzene	—do—	Styrene
Benzene/Ethyl benzene/others	—do—	Ethylbenzene
Propylene/Propane	—do—	Propylene
Ethanol/Water	Fermentation/Distillery	Ethanol
Acetic acid/Acetic anhydride	Acetic anhydride plant	Acetic anhydride
Air	Air separation plant	Nitrogen, Oxygen, Argon
Aniline/Nitrobenzene	Aniline plant	Aniline

2.5.1 Basic operation of a distillation column

This section provides the most basic operation of a distillation process. For a detailed description of the process, a few excellent books are recommended (Coulson & Richardson, 1979), (Henry Z. Kister, 1992), (Henry Z. Kister, 1990), (Binay K. Dutta, 2007).

The distillation process begins with a feed mixture (either in the liquid state, vapour or a combination of both) that needs treatment depending on the goal to be achieved. The purpose of separation can be the recovery of specified components in a mixture or increasing product purity. The feed stream is fed into the column where the separation of individual components in the mixture by mass transfer takes place in between a series of trays or packing stages as shown in Figure 2-4. The feed is eventually split into two separate streams, the low boiling fraction (light product) withdrawn at the top of the column, as well as the high boiling fraction (heavy product) collected at the bottom of the column. The light product consists of highly volatile components that come out as vapour at the top of the column and are directed into a heat exchanger (condenser), where heat is removed, and the product is condensed to a liquid phase. The condensed liquid is collected into a reflux drum that serves two important purposes: the first is for product handling, and the second most critical function is to supply reflux liquid back to the column for improved separation. The basic idea of a reflux stream is to effect equilibrium between the distillate that is rich in high volatile components with the rising vapour which is not so rich in high volatile material due to the difference in composition between the

two phases, the highly volatile components in the reflux liquid transfer to the vapour phase and vice versa for the liquid phase. In turn, the vapour becomes concentrated with highly volatile components, and this also leads to increased demand for vapour from the bottom of the column. The heavy product consists of less volatile components that remain in liquid form and thus are withdrawn in the lower section of the column as the bottom product. A portion of the bottom product passes through a heat exchanger called the reboiler, where heat is supplied to boil off the remaining highly volatile components for improved separation.

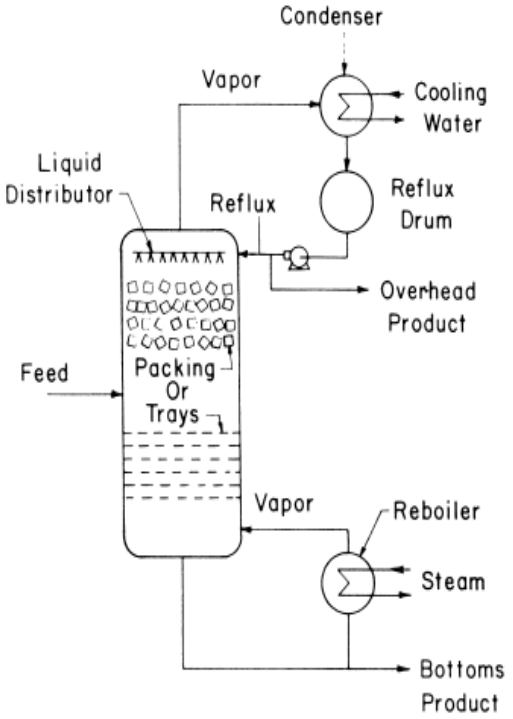

Figure 2-4: A schematic diagram of a distillation column and other auxiliary equipment, ***adapted from***: (Resetarits & Lockett, 2003).

Several parameters need to be defined in the design and controlled during the operation of a distillation process for stable and optimum production. Design variables include the column, diameter, height, number of equilibrium stages (trays or packing), and the dimensions of column internals. These parameters are determined based on the production and product specifications, which in turn determine the operational parameters such as the reflux ratio, reboil ratio, column temperature, and pressure profile.

A detailed review on distillation operation, equipment, and hydraulics is provided in Appendix A. This section is not included in the main literature review as it falls outside the scope of this dissertation. However, it is provided for those interested or requiring a more detailed explanation of distillation processes.

2.5.2 Distillation theory (Vapor - Liquid equilibrium)

Separation of a liquid mixture by distillation is based on the distribution of components between the vapour and liquid phase. Therefore, knowledge of the vapour-liquid equilibrium (VLE) of the mixture is essential to the distillation process (Johann G. Stichlmair et al., 2021). VLE data can be determined through experimentation or suitable predictive methods.

2.5.2.1 Experimental methods for determination of vapor-liquid equilibrium

The experimental methods aim to measure the composition, temperature, and pressure of the liquid and vapour phases in equilibrium. This is achieved by vaporising the liquid mixture in a still pot or boiling flask, followed by condensation of the vapour produced. When equilibrium is reached, samples of the condensate and liquid mixture in the flask are taken and analysed for composition. The experiment is repeated over different liquid mixture compositions to capture the behaviour of VLE for a particular mixture.

The Othmer, still invented by D.F. Othmer in 1928, is the early version of the experimental set-up used to determine VLE data for various mixtures. Other methods were introduced over the years, the Colburn still, Scheeline and Gilliland (Binay K. Dutta, 2007) . However, due to experimental errors ((I) superheating of the liquid due to the incorrect thermometer or thermocouple reading, (II) partial condensation of vapour before it leaves the flask due to heat loss) inherent to the methods mentioned above, a modified version of the Gillespie is the most preferred setup as it is free of these errors. A detailed description of the modified Gillespie method is given in (Kuan Shih Yuan et al., 1963). This process measures the constant pressure equilibrium data and can also be modified to measure constant temperature data. VLE data collected from the experiments is used to construct constant pressure or constant temperature phase diagrams shown in Figure 2-5 below. Phase diagrams are important because, given the thermodynamic state of a mixture, they can help us identify the phases present and the relative composition of the liquid and vapour phases.

In the $T-x-y$ diagram below, x represents the liquid mole fraction, y is the vapour fraction and T_i^{boil} is the boiling point or dew point temperature. The boiling point temperature is the temperature at which the first bubble of vapour starts to form when a liquid mixture is heated, and conversely, for the dew point, a first drop of liquid forms as vapour is condensed.
The bottom line indicated by $T-x_a$ is the boiling point curve, and the top curve labelled $T-y_a$ represents the dew point curve. When a mixture of liquid is heated to a temperature of T_{sys} at constant pressure, a liquid mole fraction x_a is in equilibrium with a vapour fraction of y_a. This result is normally represented by a tie line connecting the saturated liquid concentration to the corresponding equilibrium vapour phase concentration.

The endpoints where both the boiling and dew point curves meet represent the pure component boiling point, with A being the lighter component; it starts boiling at a temperature T_a^{boil} which is lower than the B pure component boiling point T_b^{boil}.

With a few modifications to the experimental setup, a constant temperature diagram represented by $P-x-y$ in Figure 2-5 (b) is plotted. The different phase regions and composition are a function of pressure, and the pure component saturation pressure points are identified in the diagram.

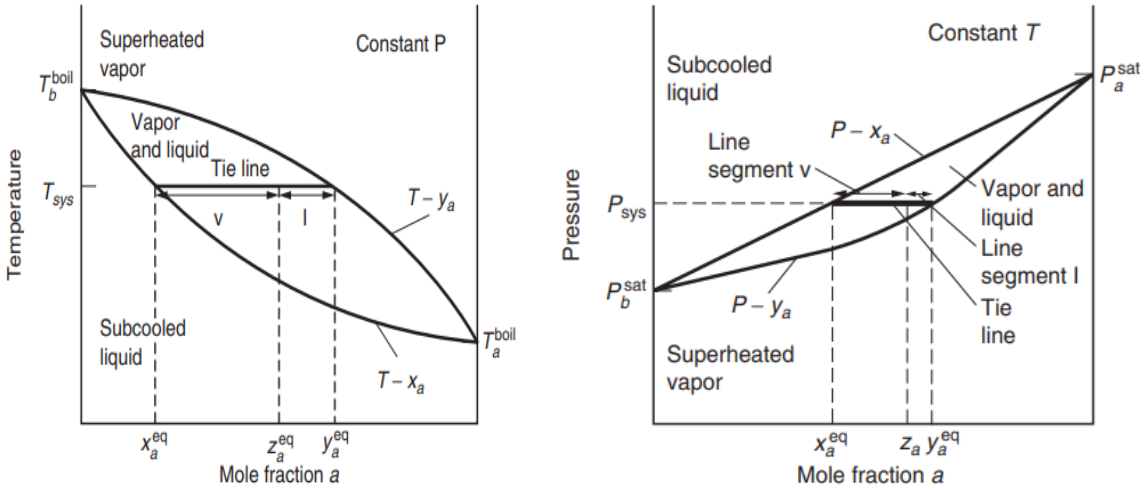

(a) (b)

Figure 2-5: Phase diagrams for a binary mixture (A) – (B) system (a) constant pressure (T-x-y) diagram at 1 atm, (b) constant temperature (P-x-y) diagram, ***adapted from***: (Binay K. Dutta, 2007).

2.5.2.2 Thermodynamic modelling of the VLE system

Establishing a criterion for chemical equilibrium is important when dealing with the distribution of components between phases in a multi-component system. A derived thermodynamic property, known as the chemical potential μ_i, provides the criteria for chemical equilibrium as defined by Equation 2.1.

$$\mu_i^{\alpha} = \mu_i^{\beta} \ldots\ldots 2.1$$

According to equation 2.1, to establish the chemical equilibrium of component i between phases α and β, chemical potentials must be equal. This has to do with the balance between the energetic and entropic effects of the system at a specified temperature and pressure.
As useful as chemical potential is in defining the chemical equilibrium of mixtures, it has mathematical inconveniences in application (Milo D. Koretsky, 2012). A property that is much friendlier mathematically was developed by G.N Lewis, and this is known as fugacity. f_i.

$$f_i^{\alpha} = f_i^{\beta} \ldots\ldots 2.2$$

To determine fugacities for both phases represented in Equation 2.2, a relationship between fugacity and composition between the two phases must be established. This is achieved through the thermodynamic expression below in terms of the variables T, P, and n_i.

$$RT\ ln\left(\frac{f_i}{z_i P}\right) = \int_0^P \left[\left(\frac{\partial V}{\partial n_i}\right)_{T,P,n_i} - \frac{RT}{P}\right] dP \ldots\ldots 2.3$$

Or in terms of variables T, V, and n_i

$$RT\ ln\left(\frac{f_i}{z_i P}\right) = \int_V^{\infty} \left[\left(\frac{\partial P}{\partial n_i}\right)_{T,V,n_i} - \frac{RT}{P}\right] dP - RT\ ln\left(\frac{PV}{RT}\right) \ldots\ldots 2.4$$

Where z_i is either the mole fraction of component i in the vapour (y_i) or liquid phase (x_i) and n_i is the number of moles in the phase considered. The expression $\widehat{\varphi}_i = \left(\frac{f_i}{z_i P}\right)$ is called the fugacity coefficient, and it compares the fugacity of species i to the partial pressure it would have as an ideal gas or liquid. From a molecular perspective, the fugacity coefficient indicates the molecular interactions of a component in a mixture and how it deviates from ideal behaviour if $\widehat{\varphi}_i < 1$ the attractive forces dominate, and conversely if $\widehat{\varphi}_i > 1$ the repulsive forces are stronger.

2.5.2.3 Ideal VLE system

The ideal VLE system works on the assumption that there are no intermolecular interactions in the vapour phase, meaning the vapour phase follows the ideal gas law and the liquid phase behaves as an ideal solution described by the Lewis/Randal reference state (all intermolecular interactions are the same).
Substitution of the ideal gas law in Equation 2.3 results in fugacity of the vapour phase ($\hat{f}_i^{v}$) represented by Equation 2.5.

$$\hat{f}_i^{v} = y_i P \ldots\ldots 2.5$$

With the substitution of the volume additivity relation for ideal liquid mixtures, the liquid phase fugacity equals;

$$\hat{f}_i^{l} = x_i f_i^{o} \ldots\ldots 2.6$$

Where f_i^{o} is the fugacity of pure specie i at system pressure.
Due to the ideal solution and low system pressure assumptions above, the Poynting correction factor is negligible; therefore, the liquid phase fugacity is equal to saturation pressure. Equating Equations 2.5 and 2.6 to satisfy the equilibrium condition stated in 2.2 leads to the expression 2.7.

$$y_i P = x_i P_i^{sat} \ldots\ldots 2.7$$

Equation 2.7 is the Raoults law and can be used to determine the vapour or liquid composition given a set of equilibrium conditions for a mixture of liquid and gas phases.

For a binary mixture of (a – b)

$$y_a P = x_a P_a^{sat} \ldots\ldots 2.8$$

And

$$y_b P = x_b P_b^{sat} \ldots\ldots 2.9$$

Combining Equations 2.8 and 2.9

$$y_a P + y_b P = P = x_a P_a^{sat} + (1 - x_a) P_b^{sat} \ldots\ldots 2.10$$

Solving for vapour mole fraction.

$$y_a = \frac{x_a P_a^{sat}}{x_a P_a^{sat} + (1 - x_a) P_b^{sat}} \ldots\ldots 2.11$$

2.5.2.4 Relative volatility

Description of the ideal VLE system enables the discussion of the concept of relative volatility, which is a parameter that indicates the ease of separation of a component from the mixture. For a binary mixture of components A and B, relative volatility can be defined as the ratio of the concentration of A to B in the vapour phase divided by A to B in the liquid phase.
This parameter can be derived by assuming Raoult's Equation 2.7.

Solving for vapor fraction in equation 2.7

$$y_i = \frac{P_i^{sat}}{P}\, x_i \ldots\ldots 2.12$$

Equation 2.12 relates the composition of equilibrium liquid to its vapour at any pressure and temperature. The equation above is often written as;

$$y_i = K_i x_i \ldots\ldots 2.13$$

Where K_i is the equilibrium value

Relative volatility is defined by;

$$\alpha_{AB} = \frac{K_A}{K_B} = \frac{P_A^{sat}}{P_B^{sat}} = \left(\frac{y_A}{x_A}\right)\left(\frac{x_B}{y_B}\right) \ldots\ldots 2.14$$

Equation 2.14 can also be written as;

$$\alpha_{AB} = \frac{y/(1-y)}{x/(1-x)} = \frac{(1-x)y}{(1-y)x} \ldots\ldots 2.15$$

Solving for vapor fraction;

$$y = \frac{\alpha_{AB} x}{1 + (\alpha_{AB} - 1)x} \ldots\ldots 2.16$$

Figure 2-6 below illustrates the behavior of a vapour liquid mixture at different relative volatility measurements. At relative volatility close to one, the graph shows a more linear behaviour with no distinct separation in concentration between the vapour and the liquid phase.

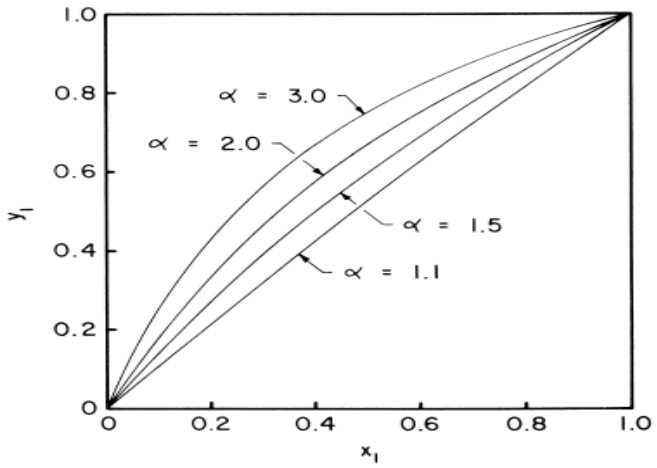

Figure 2-6: Vapour to liquid mole fraction as a function of relative volatility, ***adapted from***: (Resetarits & Lockett, 2003).

Separation of components becomes difficult when relative volatility is close to unity and can form azeotropes (Teja, A. S & Holm. L. J, 2000). An increase in relative volatility leads to an increase in the concentration of more volatile species, as shown in Figure 2-6.

2.5.2.5 Non-ideal systems

Real systems do not follow Raoult's law as they show deviations from ideal behaviour. The deviation from ideal behaviour is attributed to the effect of intermolecular interactions between various species in a mixture. Figure 2-7 shows deviations of mixtures from ideal behaviour; the dotted line in the graphs represents Raoult's law. From a molecular perspective, a negative deviation results from stronger attractive forces holding atoms together, and a positive deviation represents the opposite, where repulsive forces are dominant.

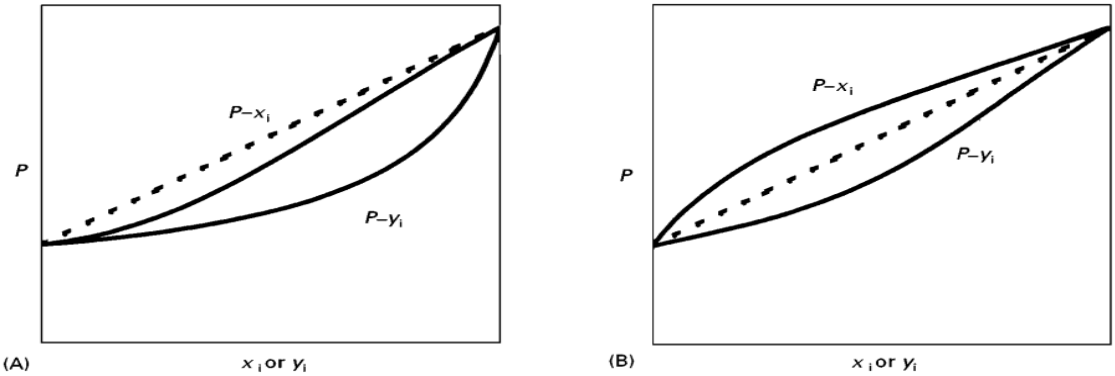

Figure 2-7: Deviation from ideal behaviour, (A) slight negative deviation from Raoult's law, (B) positive deviation from ideal behaviour, ***adapted from***: (Teja. A. S & Holm. L. J, 2000).

Large deviations from ideal behaviour lead to a mixture that does not change in composition on distillation and normally has a boiling point higher or lower than its pure components; this is known as the azeotropes as indicated in Figure 2-8 (Binay K. Dutta, 2007). Two extremes are seen on the P– x and P– y curves as they go through a maximum at the same composition; the same goes for the minima. At the azeotrope, the liquid phase mole fraction is the same as the vapour mole fraction;

$$x_i = y_i$$

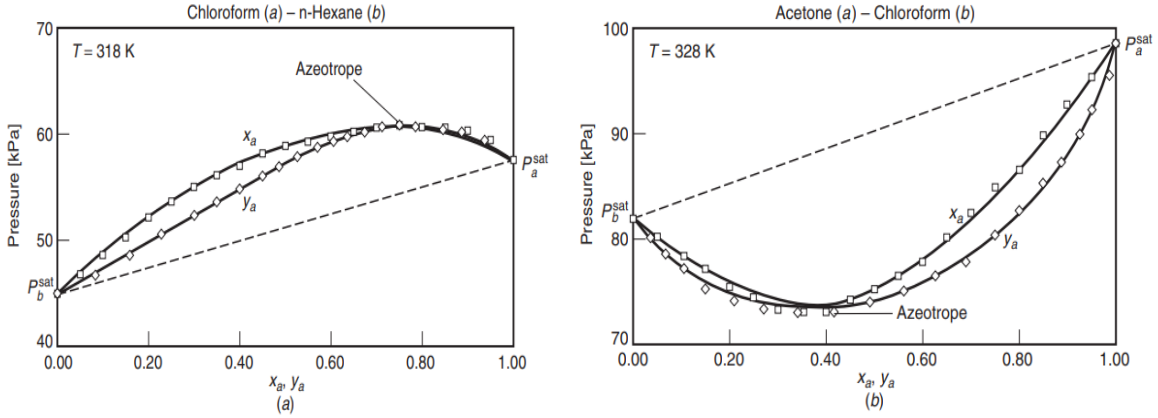

Figure 2-8: P – x – y phase diagrams (a) minimum boiling azeotrope (chloroform – n-hexane), (b) maximum boiling azeotrope (acetone – chloroform), ***adapted from***: (Milo D. Koretsky, 2012).

Deviation from Raoult's law necessitates VLE models that best describe real systems operating away from ideal behaviour. The widely used thermodynamics models are the equation of state that best represents the vapour phase behaviour and partial determination of liquid fugacities and the activity coefficient models used mainly for liquids and solids (C-Y Lu & Peng, 1993). In the calculation of fugacities for a two-phase system, the fugacity coefficient ($\widehat{\varphi}_i$) is used to account for non-ideality in the vapour phase, and the activity coefficient (γ_i)is applied for the liquid phase fugacity as represented by Equations 2.17 and 2.18.

Vapor phase fugacity;

$$\hat{f}_i^v = \widehat{\varphi_i^v}_i y_i P \ldots\ldots 2.17$$

Liquid phase fugacity;

$$\hat{f}_i^l = \gamma_i x_i f_i^o \ldots\ldots 2.18$$

For a vapor-liquid equilibrium system, the combination of Equations 2.17 and 2.18 leads to;

$$y_i \, \hat{\varphi}_i^v \, P = x_i \, \gamma_i^l \, f_i^o \ldots\ldots 2.19$$

Where:

- y_i – vapourmole fraction.
- $\widehat{\varphi}_i^v$ – fugacity coefficient.
- P – total pressure.
- x_i – liquid mole fraction.
- Υ_i^l – activity coefficient.
- f_i^o – fugacity as defined by the Lewis/Randall reference state.

2.5.2.5.1 Equation of state model approach

The equation of state models describes the $P - V - T$ relationship of pure species and mixtures with appropriate mixing rules. In the case of a VLE system, the equations allow us to determine the fugacities of the vapour mixtures and the liquid phase to some extent. The equation of state is represented in two forms: the volume explicit virial equation of state and the pressure explicit cubic equation of state. This review will focus only on the cubic equation state since it gives mathematical simplicity and a good theoretical estimation of properties.

Redlich – Kwong

The Redlich-Kwong model is one of the earliest models of the equation of state, which was developed in 1949 to improve on the Vand der Waals equation of state (Redlich & Kwong, 1949).

The model is represented as follows;

$$P = \frac{RT}{V - b} - \frac{a}{\sqrt{T}V(V + b)} \ldots\ldots 2.20$$

Where:

$$a = \frac{0.42748R^2T_c^{2.5}}{P_c} \ldots\ldots 2.21$$

$$b = \frac{0.08664RT_c}{P_c} \ldots\ldots 2.22$$

- R – 8.314 J/mol.K.
- T_c – Critical temperature.
- P_c – Critical pressure.
- V – Volume.

The Redlich – Kwong model works better in determining vapour phase properties and performs poorly for liquid phase properties and, therefore, is not accurate for use in VLE systems.

Soave – Redlich – Kwong

The Soave model represent a modifed version of the Redlich-Kwong model. The parameter $\frac{a}{\sqrt{T}}$ in the Redlich – Kwong model was replaced with the expression $\alpha(T, \omega)$, which is a function of temperature and accentric factor. West and Eibar applied the Soave model to predict hydrocarbon VLE, and the results were remarkably accurate (Soave, 1972). Another study by Peng et al. confirmed the reliability of the Soave model using the hydrocarbon and non-hydrocarbon binary mixtures. However, the accuracy was found to be lacking in predicting liquid densities in the region closer to the critical point (Robinson et al., 1985).

$$P = \frac{RT}{V-b} - \frac{a\alpha}{V(V+b)} \ldots\ldots 2.23$$

$$a = \frac{0.42748R^2T_c^{2.5}}{P_c} \ldots\ldots 2.24$$

$$b = \frac{0.08664RT_c}{P_c} \ldots\ldots 2.25$$

$$\alpha = (1 + (0.48508 + 1.5517\omega - 0.15613\omega^2)(1 - T_r^{0.5}))^2 \ldots\ldots 2.26$$

Where:

- $\alpha -$ Function of temperature and accentric factor.
- $\omega -$ Accentric factor.
- $P_c -$ Reduced temperature.

Peng - Robinson

The Peng-Robinson equation of state is the most widely used model as it performs better than the Saove model; it accurately predicts the vapor pressure of pure substances and mixtures as well as liquid densities and those of non-polar substances (Ch et al., 1973). The model was developed by modifying the attractive pressure term of the Van der Waals equation.

$$P = \frac{RT}{V-b} - \frac{a\alpha}{V^2 + 2abV - b^2} \ldots\ldots 2.27$$

$$a = \frac{0.45724R^2T_c^2}{P_c} \ldots\ldots 2.28$$

$$b = \frac{0.07780RT_c}{P_c} \ldots\ldots 2.29$$

$$\alpha = (1 + (0.37464 + 1.5422\omega - 0.26992\omega^2)(1 - T_r^{0.5}))^2 \ldots\ldots 2.30$$

2.5.2.5.2 Activity coefficient model approach

The inability of the equations of state to accurately predict the properties of mixtures in a liquid phase motivates alternative models that best describe the behaviour of the condensed phases. Activity coefficient models make use of the excess Gibbs energy expression as a function of composition to calculate the activity coefficient values, which are then used to determine the fugacity in liquid mixtures.
The activity coefficient models are based on the differentiation of the excess Gibbs energy as shown by Equation 2.31 below.

$$\mathrm{RT}\ln\gamma_i = \left(\frac{\partial \mathrm{nG^E}}{\partial \mathrm{n_i}}\right) \ldots\ldots 2.31$$

Various models have been proposed, and the most widely known are presented below in Table 2-3.

Table 2-3 Activity coefficient models for binary pairs, ***adapted from***: (D. Ernest et al., 2011)

Name	Equation for Species 1	Equation for Species 2
(1) Margules	$\log\gamma_1 = Ax_2^2$	$\log\gamma_2 = Ax_1^2$
(2) Margules (two-constant)	$\log\gamma_1 = x_2^2[\bar{A}_{12} + 2x_1(\bar{A}_{21} - \bar{A}_{12})]$	$\log\gamma_2 = x_1^2[\bar{A}_{21} + 2x_2(\bar{A}_{12} - \bar{A}_{21})]$
(3) van Laar (two-constant)	$\ln\gamma_1 = \frac{A_{12}}{[1 + (x_1A_{12})/(x_2A_{21})]^2}$	$\ln\gamma_2 = \frac{A_{21}}{[1 + (x_2A_{21})/(x_1A_{12})]^2}$
(4) Wilson (two-constant)	$\ln\gamma_1 = -\ln(x_1 + \Lambda_{12}x_2) + x_2\left(\frac{\Lambda_{12}}{x_1 + \Lambda_{12}x_2} - \frac{\Lambda_{21}}{x_2 + \Lambda_{21}x_1}\right)$	$\ln\gamma_2 = -\ln(x_2 + \Lambda_{21}x_1) - x_1\left(\frac{\Lambda_{12}}{x_1 + \Lambda_{12}x_2} - \frac{\Lambda_{21}}{x_2 + \Lambda_{21}x_1}\right)$
(5) NRTL (three-constant)	$\ln\gamma_1 = \frac{x_2^2\tau_{21}G_{21}^2}{(x_1 + x_2G_{21})^2} + \frac{x_1^2\tau_{12}G_{12}}{(x_2 + x_1G_{12})^2}$ $G_{ij} = \exp(-\alpha_{ij}\tau_{ij})$	$\ln\gamma_2 = \frac{x_1^2\tau_{12}G_{12}^2}{(x_2 + x_1G_{12})^2} + \frac{x_2^2\tau_{21}G_{21}}{(x_1 + x_2G_{21})^2}$ $G_{ij} = \exp(-\alpha_{ij}\tau_{ij})$
(6) UNIQUAC (two-constant)	$\ln\gamma_1 = \ln\frac{\Psi_1}{x_1} + \frac{\bar{Z}}{2}q_1\ln\frac{\theta_1}{\Psi_1} + \Psi_2\left(l_1 - \frac{r_1}{r_2}l_2\right) - q_1\ln(\theta_1 + \theta_2T_{21}) + \theta_2q_1\left(\frac{T_{21}}{\theta_1 + \theta_2T_{21}} - \frac{T_{12}}{\theta_2 + \theta_1T_{12}}\right)$	$\ln\gamma_2 = \ln\frac{\Psi_2}{x_2} + \frac{\bar{Z}}{2}q_2\ln\frac{\theta_2}{\Psi_2} + \Psi_1\left(l_2 - \frac{r_2}{r_1}l_1\right) - q_2\ln(\theta_2 + \theta_1T_{12}) + \theta_1q_2\left(\frac{T_{12}}{\theta_2 + \theta_1T_{12}} - \frac{T_{21}}{\theta_1 + \theta_2T_{21}}\right)$

Margules equations

The Margules equation is one of the simplest activity coefficient models and results from a power series expansion of the excess Gibbs energy function (Teja. A. S & Holm. L. J, 2000). The parameter A illustrated by equation 1 in Table 2-3 is fit to experimental data for a given binary mixture and is dependent on the temperature and pressure of the system. If the parameter A is determined for a binary mixture and the expression for excess Gibbs energy is given, the activity coefficient for both species can be quantified by application of equation 1.
The limitation posed by the Margule equation is that it cannot model activity coefficients that are not symmetric.

Van Laar model

The Van Laar equation was developed using the Van der Waal equation of state as a basis. It is a two-parameter model that is widely used and can fit many systems very well. The two

parameters, A_{12} and A_{21} in equation 3 are not temperature dependent and need to have the same sign for the model to work over a complete range of compositions. Limitations in the model are the fact that it cannot represent both the minimum and maximum extremes.

Wilson model

Wilson equation is derived from a molecular basis with parameters Λ_{12} and Λ_{21} representing energetic parameters describing the interaction between like and unlike charges (D. Ernest et al., 2011). The Wilson equation is recommended for polar and hydrocarbon compounds; however, it does not take into account the presence of two liquids, meaning it is not used for immiscible systems.

NTRL

The nonrandom two-liquid model was developed in 1968 by Renon and Prausnnitz (Renon & Prausnitz, 1968). The model is also derived from a molecular basis with the energetic τ_{12} and τ_{21} parameters describing the molecular interactions between species, and α is the entropic parameter, which accounts for the non-randomness of the mixture. The NTRL model is favourable for miscible systems and mixtures of organic compounds in water and works well for systems with large deviations from ideality.

UNIQUAC

The universal quasi-chemical theory is normally recommended for polar and non-polar species as well the partially miscible liquids. It is an extension of the Wilson equation and combines the excess Gibbs energy into the combinatorial part that is due to entropic effects and the residual part, which takes intermolecular forces into account.

$$g^E = g^E_{combinatorial} + g^E_{residual} \dots\dots 2.32$$

2.6 Distillation modelling and optimisation

Before the development and use of computers, shortcut methods were applied in the modelling and design of distillation columns, as rigorous models were laborious and took much time to solve. Overdesign was applied to compensate for the error derived from the use of shortcut methods (Ricardo et al., 2015). The rigorous methods provide greater accuracy in the design of complex multicomponent columns and allow for the determination of temperatures, pressure, flows, composition, and heat transfer in every stage. The introduction of computers allowed for the application of rigorous methods in the design of distillation columns; however, there were challenges with the early models that resulted in numerical instabilities since the method involved stage-by-stage calculation and constituted many complex nonlinear equations (Seader et al., 2006). In 1963, the theta method was developed by Holland and proved to be a success in the modelling and design of distillation columns (Holland, 1981).

Shortcut methods are only used in the preliminary design and analysis of distillation columns as they are not accurate enough to model complex multicomponent columns; thus, rigorous methods are the focus of discussion in this section.

2.6.1 Rigorous methods (Stage equilibrium models)

A group of equations known as the MESH (material, equilibrium, summation, and heat) equations are solved to create a model representing the conditions of the distillation column. These equations are developed from the overall mass balance and component mass balance equations, as well as the energy balance and phase equilibrium equations. The minimum specifications for calculation are:

- Column profile pressure.
- Feed flow, composition, and thermodynamic condition.
- Separation requirements.
- Number of stages in the column, and other auxiliary equipment.

MESH equations describe the steady state behaviour of distillation columns and assume the equilibrium stage concept, with no chemical reactions occurring and no entrainment of liquid droplets in the vapour phase. Figure 2-9 below shows an equilibrium stage model for a vapour-liquid phase system with feed conditions (flowrate F_j, temperature T_{Fj}, pressure P_{Fj}, mole fraction $z_{i,j}$ of component i, and overall molar enthalpy h_{Fj}) entering stage j.

MESH equations for stage j in Figure 2-9 are represented below as mentioned before; these are mass and energy balance equations and were developed by Wang and Henke (H. J. Ernest & Seader, 1981).

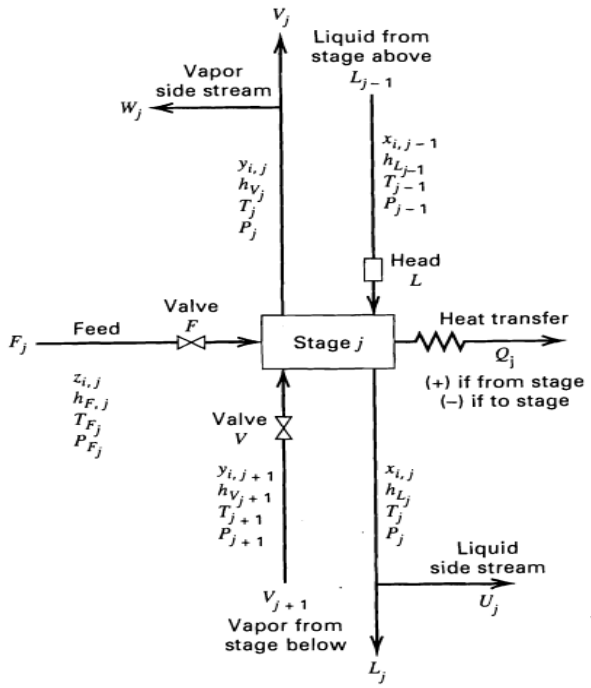

Figure 2-9: An equilibrium stage model, ***adapted from***: (D. Ernest et al., 2011).

Material balance for each component – M equations:

$$M_{i,j} = L_{j-1}x_{i,j-1} + V_{j+1}y_{i,j+1} + F_j z_{i,j} - (L_j + U_j)x_{i,j} - (V_j + W_j)y_{i,j} = 0 \dots \dots 2.33$$

Where:

- L_j – liquid flowrate from stage j.
- $U_j -$ liquid side stream flow rate.
- $W_j -$vapor side stream flowrate.
- $Q_j -$ heat transfer to simulate condenser, reboiler, intercoolers, and winter heaters.
- $F_i -$ Feed flowrate.
- $z_i -$ Feed fraction i.

Phase equilibrium relations – E equations:

$$E_{i,j} = y_{i,j} - K_{i,j}x_{i,j} = 0 \dots \dots 2.34$$

Where:

- $K_{i,j} -$ phase equilibrium ratio.

Summation of mole fractions – mole fraction summation equations:

$$(S_y)_j = \sum_{i=1}^{C} y_{i,j} - 1 = 0 \dots \dots 2.35$$

$$(S_y)_j = \sum_{i=1}^{C} x_{i,j} - 1 = 0 \dots \dots 2.36$$

Energy balance – H equations:

$$H_j = L_{j-1}h_{Lj-1} + V_{j+1}h_{Vj+1} + F_j h_{Fj} - (L_j + U_j)h_{Lj} - (V_j + W_j)h_{Vj} - Q_j = 0 \dots \dots 2.37$$

Total material balance:

$$L_j = V_{j+1} + \sum_{m=1}^{j} (F_m - U_m - W_m) - V_1 \dots \dots 2.38$$

MESH equations above are nonlinear and are normally solved using iterative techniques that involve equation partitioning with equation tearing or linearisation.
Of the early solution models before the introduction of computers were the Lewis – Matheson method as well as the Thiele – Geddes methods, which were initially calculated by hand, stage by stage, equation by equation, and later introduced to computers and proved to be very

unstable. The Lewis–Matheson method requires specifying the number of equilibrium stages with a reflux ratio and feed stage location as well as separation requirements of two key components (Lewis & Matheson, 2023). Iterative variables are the computation of compositions of non-key components in between stages with interstage vapours and liquid flow rates. On the other hand, the Thiele-Gedes method specifications are the number of stages above and below the feed point, the reflux ratio, and the distillate flow rate. The method tear variables are interstage temperatures and flows of vapour and liquid phases (Thiele & Geddes, 1933).

Amundson and Pontinen developed a solution procedure that showed that MESH equations (2.32),(2.33), and (2.37) could be combined and solved by simultaneous linear equations for all stages using equation tearing methods (Amundsoni & Pontinen, 1958). The same tear variables in the Thiele–Geddes method were applied, and the equation sets were easily handled and solved by a computer.

With the success of equation tearing techniques in 1964, Friday and Smith analysed a number of these methods available at the time and realised that no technique is universal to all problem types (Friday & Smith, 1964). For separation problems where feed components have close boiling points (similar volatility), a procedure known as the Boiling Point method is applicable, and for a wide range boiling point, the recommended method is the sum rate method. However, the most widely used methods, especially in simulators, are the Newton–Raphson methods as well as the inside–out methods, which address the intermediate case where BP and SR methods fail to converge and also provide flexibility and are capable of handling a range of separation problems.

2.6.1.1 Bubble point method

The Bubble point method combines material balance equations and phase equilibrium to estimate liquid compositions ($x_{i,j}$) and flows through the application of the Thomas tridiagonal matrix (Friday & Smith, 1964). With the satisfaction of the summation equations, the matrix output variables are used to calculate the column temperature profile by the bubble point equation (bubble temperature as the iteration variable). The bubble point method works best in narrow boiling point cases where feed components have similar or tight volatility values, and the equilibrium condition is ideal, meaning temperatures are not sensitive to composition (H. J. Ernest & Seader, 1981).

2.6.1.2 Sum rates method

The Sum rate method applies to absorbers, strippers, and extractors. It was developed to solve cases where mixtures have a wide boiling point range with the equilibrium ratio-dependent strongly on composition (Friday & Smith, 1964).

The Thomas tridiagonal matrix is still applicable for determining the composition and flows in the liquid phase; however, energy balances are used to estimate stage temperatures through the Newton-Raphson method (Ricardo et al., 2015).

2.6.1.3 Newton – Raphson method

The Newton-Raphson method works best for a broad range of distillation problems as volatility ranges do not affect convergence, and the non-ideal solutions are accounted for (Goldstein & Stanfield, 1964). In this method, the distillation material, energy, and equilibrium equations are grouped by stage and then linearised (Naphtali & Sandholm, 1971). For a distillation problem with f system equations;

$$f(\phi, \eta) = 0 \ldots \ldots 2.39$$

Where:

- $f -$ system equations.
- $\phi -$ dependent variables.
- $\eta -$ independent variables.

To obtain successive corrections to the dependent variables, Equation 2.39 is linearised.

$$f(\phi, \eta) + f_{\phi}(\phi, \eta)\Delta\phi = 0 \ldots \ldots 2.40$$

Solving for change in dependent variables, equation 4.39 becomes;

$$\Delta\phi = -f_{\phi}^{-1}(\phi, \eta) f(\phi, \eta) \ldots \ldots 2.41$$

2.6.1.4 Inside-out method

The model is used mostly in simulators because of its ability to solve separation problems of various types with less computational time, hence its wide application in distillation, absorption, stripping, etc (D. Ernest et al., 2011). In the models described above, too much computational time is spent calculating equilibrium ratios and enthalpies using rigorous thermodynamic models for each iteration step. To solve this problem, Boston and Sullivan in 1974 came up with a method to use a simple approximate model which is empirical to estimate thermodynamic properties used to solve MESH equations (inner loop) and a rigorous model on the outer loop to update parameters in the inner loop (Boston', 1974).

2.6.2 Column efficiency

Column efficiency is an important concept in distillation design. It is normally specified in simulators to determine the actual number of trays required to achieve a specified separation of a feed mixture. Lewis first articulated the concept in 1922, where he defined column efficiency as the ratio of equilibrium stages to the actual number of stages (Lewis. W. K., 1922). In this paper, basic equations based on the equilibrium assumption were derived to estimate the theoretical rate of rectification per stage for a binary mixture. By assuming small changes between equilibrium stages, Equations 2.42 and 2.43 below allow the determination of the required number of stages necessary to effect a certain level of enrichment.

$$\frac{dx}{dn} = y_n - x_n - \frac{V_c}{L_{n+1}}(y_c - y_n) \ldots\ldots\ 2.42$$

On integration of Equation 2.42

$$\Delta n = \int_{x_1}^{x_2} \frac{dx}{y_n - x_n - V_c\left(\frac{y_c - y_n}{L_{n+1}}\right)} \ldots\ldots\ 2.43$$

Where:

- $n -$ number of the plate under consideration.
- $x_i -$ mole fraction of volatile component in liquid.
- $y_i -$ mole fraction of volatile component in vapor.
- $V_c -$ Vapor flow from plate n.
- $L_{n+1} -$ Liquid flow from plate n to n+1.

However, it has always been known that the number of plates in a real column is always higher than the equilibrium number of stages therefore making the theoretical plate concept unsatisfactory. In 1925 Murphree published a paper outlining the method for calculating the number of plates for a mixture of any number of components (Murphree, 1925) . The concept of absorption was applied to the analogy that distillation involves the transfer of material between the vapor and liquid phase, with the less volatile component absorbed in the liquid phase as the less volatile is being liberated. This perspective gives an expression shown by Equation 2.44 for calculating efficiencies for volatile components.

$$y_n = y_n^* - (y_n^* - y_{n-1})e^{-K_g'' A_n P_n t_n} \ldots\ldots 2.44$$

Where:

- $y_n^* -$ value of y in equilibrium with liquid on the nth plate.
- $K_g'' -$ coefficient of material transfer.
- $A_n -$ average area of contact.
- $P_n -$ total pressure of vapor above the nth plate.
- $t_n -$ time of contact between liquid and vapor on the nth plate.

Following the development of local efficiencies derived by Murphree, in 1936 Lewis demonstrated the relationship between plate efficiency and the number of plates required for to achieve a specified separation thereby concluding the traditional methods in column efficiency (Lewis, 1936). Equation 2.45 can be used to estimate the column section efficiency, where is the stripping factor is comprised of the slope of the equilibrium line as well as the liquid and vapor flowrate per active area.

$$\eta_{section} = \frac{\ln\left[1 + \eta_{tray}(\lambda - 1)\right]}{\ln \lambda} \ldots\ldots 2.45$$

Where:

- $\eta_{section}$ – section efficiency.
- η_{tray} – Murphree tray efficiency.
- λ – stripping factor.

Over the years, there have been significant advancements in the development of efficiency methods that are superior to the Murphree tray efficiency method (Taylor & Duss, 2019). The Hausen method takes advantage of the reference states chosen to ensure that efficiency calculated using the mole fraction differences in the liquid state is the same as in the vapor phase whereas the Murphree efficiency uses reference states for phase (Taylor & Duss, 2019)uilibrium (Taylor & Duss, 2019). The generalized Hausen method presented by Standart is considered to be superior to the Murphree efficiency definition. Despite all these improvements, industry engineers still prefer the traditional methods for design and simulation. Most of the new proposed methods are not considered for practical use and it is not known if any of them have been applied in the design of real columns.

Given the views discussed above the current research employs traditional methods in defining column efficiency for simulations carried out as this is still the most widely accepted method in distillation column calculations.

2.6.3 Process Optimisation

This review focuses mainly on the general non-linear optimisation of problem and a limited number of techniques applicable to finding the solutions. The literature on optimisation problems and applicable techniques is vast, and it is impossible to cover everything. In this review, only the necessary theories relevant to the current research are mentioned.

Chemical industries are often faced with the challenge of making the best possible decisions to achieve the optimum performance of a plant or an engineering design project. These decisions include plant profitability, reduction in energy consumption and pollutants as well and increasing valuable product yields. This type of problem encountered in the industry is known as the optimisation problem, and it is often solved using mathematical programming techniques coupled to a physics or statistical model representing process behaviour to capture possible areas of plant operability (Ricardo et al., 2015). For a successful operation or design of a chemical process, engineers need to specify the decision variable that is most important to the plant, and this is known as the objective function. The objective function is often economical as the business focus is more on maximising profits or minimising operational costs. Therefore, the formulation of an objective function will include raw material costs and revenues from selling products as well as costs associated with operating variables such as energy consumption and other utility costs (Pintarič & Kravanja, 2006).

2.6.3.1 Formulation of the optimisation problem

The standard form of the optimisation problem with a single non-linear objective function and constraints is illustrated below.

$$\max or \min f(x) \ldots \ldots 2.46$$

$$s.t.$$

$$h(x) = 0$$

$$g(x) \leq 0$$

$$x_{iL} \leq x_i \leq x_{iU}$$

In the model above, the three functions defined are f, h, g, which represent the objective function, equality constraints, and inequality constraints, respectively. Continuous process variables are represented by a vector variable x (e.g. temperatures, flowrates, pressure, etc.) subject to upper and lower constraints. With d being a vector variable of design parameters such as sizes of process equipment (e.g. diameter, height, area, etc.). And y is a decision variable with a binary vector that shows acceptance or rejection of a solution calculated.

2.6.3.2 Optimisation techniques

Application of the appropriate optimisation technique depends largely on the type of problem at hand defined by the objective function as well as the inherent constraints if there are any specified. The different types of problems encountered in the chemical industry are either linear or non-linear which can be represented mathematically by continuous functions however in some cases it may be required to solve a case that involves discontinuous, integer, and discrete functions. The optimisation techniques that apply to the two situations above are classified according to local (gradient-based) and global optimisation algorithms. Problems involving continuous functions are well handled by the local optimisation algorithm which involves finding the derivative of the function since they are easier to differentiate whereas the discrete variables are complex and difficult to find the resultant derivative, therefore global optimisation algorithms are well suited for these situations.

The sections below describe the different optimisation algorithms, how they apply to different problems and the known advantages and drawbacks thereof.

Gradient-based methods (The local optimisation algorithm)

These are gradient based methods that use the derivative information to solve an optimisation problem to find the optimum solution possible. Local optimisation algorithms are popular mainly because of the advantage they provide over other methods because they are efficient and can handle a large number of variables (Venter, 2010). Despite the good characteristics presented by local optimisation methods there are however some disadvantages which include not having the capacity to handle discrete variables as mentioned above, they are susceptible to noise, and can be very difficult to implement (Venter, 2010).

In an optimsation problem defined in Subsection 2.6.3.1, constraints are defined and a search method is carried out in such a way not to violate these specified conditions. In doing this, the gradient based methods employes a two-step process to attain the optimum point. The first process make use of the gradient information to search for a direction in the search space within the constraints, this is defined by the variable s in Equation 2.47 below. The second step is using this information to move in the direction and an appropriate step size represented by $\lambda^*$is applied to reach the optimum point.

$$X_{i+1} = X_i + \lambda^* s \dots\dots 2.47$$

Where:

- $X_{i+1} -$ is the next point in the search direction.
- $X_i -$ the initial point.
- $s -$ gradient.
- $\lambda^* -$ step length.

The local optimisation method described is also known as the steepest descent method where an initial trial point is moved iteratively along the direction of the steepest descent until the optimum is reached.

If the problem has inequality constraints and the gradient information is available, the Karush – Kuhn – Tucker conditions can be used to find the optimum point. At the optimum point, the gradient of the Lagrangian of each of the inequality constraints must vanish $\lambda_j g_j(x)$. In the case of unconstrained optimisation, the necessary condition is the objective function must vanish at the optimum point.

$$\nabla f(x) + \sum_{j=1}^{m} \lambda_j \nabla g_i(x) + \sum_{k=1}^{p} \lambda_{m+k} \nabla h_k(x) = 0 \dots\dots 2.48$$

The KKT conditions help identify a local optimum but cannot guarantee the achievement of a global optimum (Dutta, 2016a). Newton's technique below demonstrates the application of the KKT condition therefore justifying its importance in optimisation techniques.

Unconstrained methods

Newton's method is an unconstrained gradient-based algorithm derived from a second-order Taylor polynomial series expansion of the objective function.

$$f(x) \approx f(x_i) + \nabla f(x_i)^T (x - x_i) + \frac{1}{2}(x - x_i)^T H(x_i)(x - x_i) \dots\dots 2.49$$

Where:

- $H(x_i) -$ Hessian matrix that contains the second-order partial derivatives of the objective function at x_i.

By differentiating equation 2.49 and setting the result equal to 0 based on the KKT conditions, the resultant equation is given by 2.50 below;

$$x = x_i - H(x_i)^{-1}\nabla f(x_i) \ldots\ldots 2.50$$

The Newton method is proven to be robust and efficient when modified to one-dimensional search as is normally done in practice (Dutta, 2016b).

The most popular methods unconstrained methods widely used in practice are the Fletcher – Reeves and the Fletcher – Goldfarb – Shanno methods. The Fletcher – Reeves method combines the conjugate characteristics with the steepest descent method to achieve both efficiency and reliability (Fletcher & Powell, 1963) . In principle, the technique makes use of conjugate search directions to find the optimum.

BFGS method is part of the variable metric methods that make use of the information from the previous iteration to estimate the new search direction. The BFGS method is much more efficient than the Fletcher – Reeves method on the basis of optimised computer memory storage in approximating the inverse Hessian matrix (Venter, 2010).

Constrained methods

Discussion is only limited to direct search methods as they are more efficient and have become the most popular methods in constrained optimisation. Three direct search methods are mostly encountered in solving constrained optimisation problems are sequential linear programming (SLP), modified feasible directions (MMFD), and sequential quadratic programming (SQP).

The SLP converts the non–linear problem to an equivalent linear approximation of the objective and constraint function. Linear approximations are carried out until convergence to the optimum point. Though easy to construct, the method is sensitive to constraints and may not always find the optimum region. The MMFD method is based on the modification of the original method of feasible directions and it is more robust and quick to find a feasible region in the search space.

The SQP method develops a quadratic approximation of the objective function and a linear approximation of the constraint function. The algorithm finds a search direction by solving the function approximations stated. Once the search direction is obtained, the penalty function is used to determine the step size in the obtained search direction. The process is repeated until convergence.

Non-gradient based methods

Other techniques of importance are the Powell's method and Nealder – Mead simplex algorithms which are also capable of solving non – linear optimisation problems without the use of the gradient information (Powell, 1964), (Nelder & Mead, 1965) .

2.6.3.3 Optimisation problems

There are different classifications of optimisation problems, namely, linear programming problems (LP), non-linear programming problems (NP), and mixed integer non-linear programming problems (MINLP), and the selected mathematical model is dependent on the type of process model and constraints applicable (Pintarič & Kravanja, 2006). The focus of this research is on the distillation process, which is highly non-linear, and therefore, only non-linear programming models are applicable and part of the discussion.

Various optimisation methods have been proposed in the literature, mainly for crude oil process design and operations. Q.Xu *et al*. developed an E3 strategy for the optimisation of crude oil blending and processing, with three objective functions: profit maximisation, minimising carbon dioxide emissions, and reducing furnace energy consumption (Mittal et al., 2011). The developed E3 methodology provides support concerning the decision-making and operation of a refinery process. Dauda Ibrahim proposed an optimization-based design approach using a rigorous simulation model to design a crude oil distillation process by optimising through the MILNP technique, the unit design while accounting for heat recovery opportunities using pinch analysis (Ibrahim et al., 2017). The proposed design is capable of identifying the optimum design unit operations, taking constraints into account. In the research, as mentioned earlier, both authors used the HYSYS simulation environment to model the process units and the relevant process data was generated by running various cases to investigate the influence of independent variables on dependent variables. Lopez C. *et al.* applied metamodels (second-order polynomials) to develop a model that captures process *behaviour* with a combination of an NP optimisation programming model to maximise profits by optimising operational variables (López et al., 2013). Selected operational parameters were crude oil blending, pump around specifications, temperatures, stripping steam, and product flows.

Optimisation problems discussed above apply to distillation modelling as the nature of the process is highly non-linear and therefore requires a suitable optimisation technique to maintain accuracy and to provide a proper representation of reality as these models are used in real-life plant operations to make very crucial decisions.

2.6.3.4 Optimization in process simulators

Simulators such as Aspen HYSYS and Aspen Plus integrate process simulation as well as optimisation simulation (Documentation Team, 2004). The different optimisation methods and associated restrictions specific to the mentioned simulators are summarised in Table 2-4 below.

Most authors prefer an optimisation simulation environment different from process simulation due to the convergence problems and simulation time inherent; however, it is still possible to integrate both methods depending on the complexity of the problem at hand.

Table 2-4: Optimization methods found in simulators, ***adapted from***: (Documentation Team, 2004).

Method	Description	Restrictions
Fletcher-Reeves	Corresponds to the Polak Ribiere modification of the Fletcher-Reeves conjugate gradient scheme	This scheme is efficient for minimization without restrictions. This method does not handle constraints
Quasi Newton	It refers to the method of Broyden-Fletcher-Goldfarb-Shanno	In limited applicability is similar to the Flechter-Reeves method. This scheme is efficient for minimization without restrictions. This method does not handle constraints
		In both limited applicability and is similar to the method Flechter-Reeves
BOX	This method corresponds to a sequential search problem solver with nonlinear objective functions	Handles inequalities constraints, but not equalities. Usually requires a large number of iterations, however it is a fairly robust method
SQP	It is the Sequential Quadratic Programming (SQP) method	Considered one of the most efficient methods to minimize linear and nonlinear problems. Allows equality and inequality constraints
Mixed	This strategy seeks to take advantage of the strength of the BOX method and SQP efficiency. Use an initial assessment with BOX method using a low tolerance, then find the solution with tolerance using SQP	Only allows inequality constraints
Complex	Traditional black boxes method. Only available in Aspen Plus	It does not require derivative calculations. It can handle as inequality constraints and bounds on the optimization variables. Blocks should be used for converging external convergence recycles or design specifications. Requires many iterations to converge

2.7 **Coal tar distillation and current research**

The primary purpose of coal tar distillation is the production of residue pitch, which is an important binder for manufacturing anodes and graphite electrodes in the aluminium and steel industry (Baron et al., 2016). Through the distillation of coal tar, other valuable chemical oils are recovered and play an important role in the carbon chemical industry.

2.7.1 Coal tar distillation and product Fractions

In processing coal tar through the distillation process, light fractions and inherent moisture are initially distilled at temperatures below 170°C. Light oils constitute mainly the BTX (benzene, toluene, and xylenes) fraction, of which, in recent times, their value has become less important due to strong competition from petroleum derivatives (Diez & Garcia, 2018). The BTX fraction is mostly used as a fuel source in the chemical industry, with the xylenes separated and used as the basis for industrial monomers and chemicals.
With further distillation of the dehydrated tar at temperatures between 170 - 230 °C, carbolic oil is produced as the overheard product. The carbolic fraction consists mainly of phenols, which are further processed for the production of polycarbonates. Cresols and Xylenols also form part of the carbolic stream and are important in the preparation of resins, herbicides, and disinfectants.
The most valuable fraction due to its economic interest in the chemical oils recovered from coal tar distillation is the naphthalene oil, which takes place at temperatures 230 - 260°C. It is

the basis of many chemicals in the chemical industry, pharmaceuticals, and construction industry. Separation of naphthalene oil leads to the production of nitrogen bases such as quinoline, isoquinoline, carbazole, and acridine that form part of the wash oil stream. Its main application is in the coke oven industry as a solvent, and it is partly blended with anthracene oil for the production of carbon black (Granda et al., 2014). Anthracene oil is the heaviest fraction recovered from coal tar distillation at temperatures between 300 - 360 °C. The anthracene stream is composed of other aromatic compounds such as acenaphthene, fluorene, phenanthrene, fluoranthene, and pyrene. The main application of this fraction is in the production of carbon black used for the manufacturing of tires, rubbers, and inks, as well as coatings.

Residue pitch is the final product left after all the oils have been distilled from coal tar and accounts for approximately 50 % of the total yield.

2.7.2 Coal tar research and prospects

Environmental challenges that exist due to the use of fossil fuels, as well as the dominance of petroleum-derived products in the chemical industry, have led to the decline in interest in coal-derived products for a very long time; however, recent patterns show marked research development and technological advancement in coal tar and coal tar pitch (Manera et al., 2023). This sudden surge in research interest is driven mainly by the geopolitical sensitivity of the petroleum oil market as well as the limited availability of this resource in other countries. Hydroprocessing research and technological development of low-temperature and medium-temperature coal tar into alternative liquid fuels for transportation is on the rise, as well as the conversion of coal tar pitch into new high-performance carbon materials (Ma et al., 2021). Research of interest due to relevance to the current research is the work done by Romanova *et al.* to obtain naphthalene of purity from coal tar similar to one derived from petroleum through distillation simulation processes (Romanova et al., 2018). Research results show a naphthalene purity of 99.99 wt% and recovery of 90.50 wt%.

Recent research shows that there is still a bright future for coal and coal tar in the energy and chemical industry if various processes used for extraction and recovery are efficient and environmentally friendly.

3 Coal tar distillation model development

The purpose of this research work is to investigate the distribution of coal tar product qualities from a tar distillation plant by developing a distillation simulation model and to search for an optimal plant operating strategy through maximising product revenue sales. To achieve these aims a detailed process description is defined in Section 3.1 to establish the basic operating conditions and the design setup of a plant in investigation. This is followed by the methodology framework used to create the simulation model as well as the optimisation model in Section 3.2. Detailed development of the model is described in Section 3.3, followed by validation methods to ensure the accuracy of the model in representing reality.

3.1 Process Description

A typical process flowsheet for a tar distillation plant is shown in Figure 3-1, which consists of four distillation column systems: the dehydrator, fractionator, creosote column, and flash column.

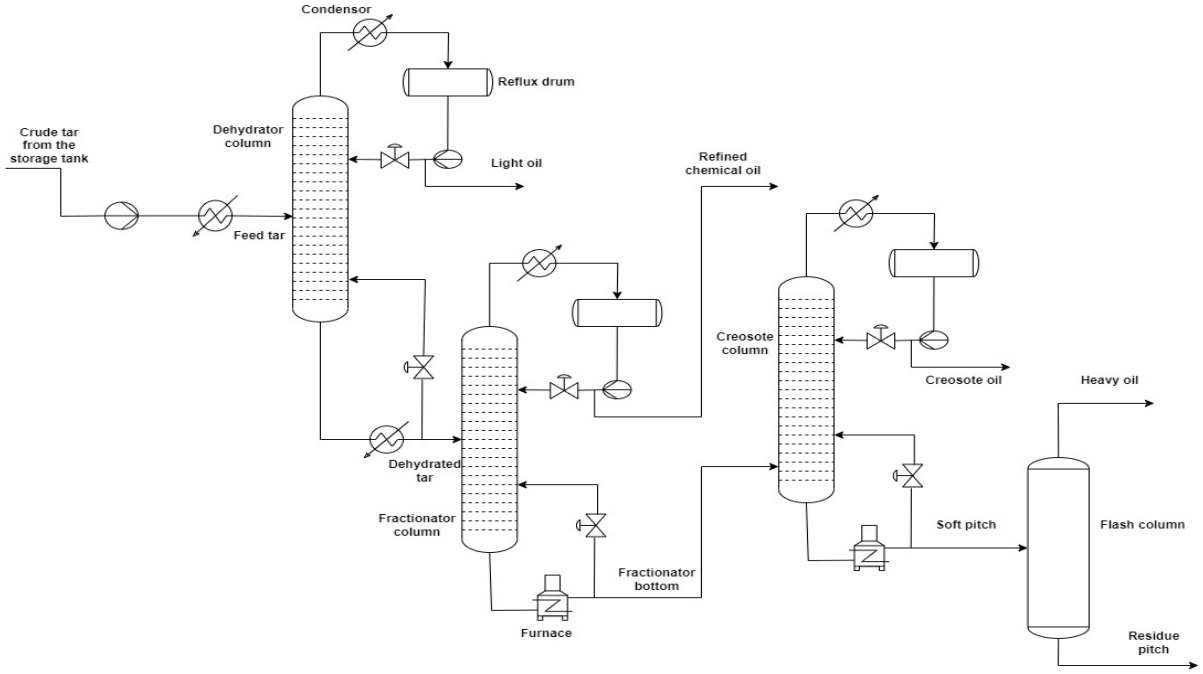

Figure 3-1: Coal tar distillation process

Coal tar feed from the storage tank is passed through a heat exchanger at a rate of 25 t/h to increase the stream temperature from 75 °C to 160 °C before entry into the dehydrator column. The purpose of a dehydrator column is to remove moisture from the tar, and in the process, light oil is produced as the top product, which is mainly the BTX fraction further decanted for the separation of water. A dehydrator column is made up of 7 sieve trays with the top pressure at atmospheric and the bottom temperature setting at 220°C. The dehydrated tar is transferred to the fractionator column, which operates at a top pressure of 60 kPa and consists of 20 bubble tray caps. The distillate recovered is an intermediate product for the naphthalene distillation plant, and it is defined as the refined chemical oil composed mainly of phenols and naphthalene components. A reboiler running on natural gas is applied to heat the bottom stream of the

fractionator to recover some of the light fractions still present for separation efficiency improvement. The bottom product from the fractionator is fed to the creosote column for recovery of creosote oil as the distillate product. The creosote column has 20 valve trays and operates under a vacuum pressure of 50 kPa with a reboiler situated at the bottom. Soft pitch is the bottom product from the creosote column, which can be recovered as an immediate product depending on the type of pitch being produced. For a soft pitch product with a softening point of 55 - 59 °C, further distillation through the flash column is normally not required; however, for pitches with a softening point of 68 - 73 °C as well as hard pitches of 115 - 118°C flash distillation is applied to remove most of the oils still present.

3.2 Methodology

This section describes the methodology framework used to develop a coal tar distillation steady-state simulation model as well as the process optimisation model; both are applied interactively to achieve the aims of this research project. Aspen HYSYS Version 11 program was used to create the process and optimisation models. The Aspen HSYSY simulator has a wide application in process engineering as it provides the tools to create rigorous steady state and dynamic models for plant design and monitoring. Many chemical industries adopt this application because it helps with plant troubleshooting, operational improvement, business planning, and asset management (Giwa & Karacan, 2012).
Figure 3-2 shows the methodology framework used in this research project, which is divided into two parts; the first stage involves coal tar model development followed by the optimisation process.

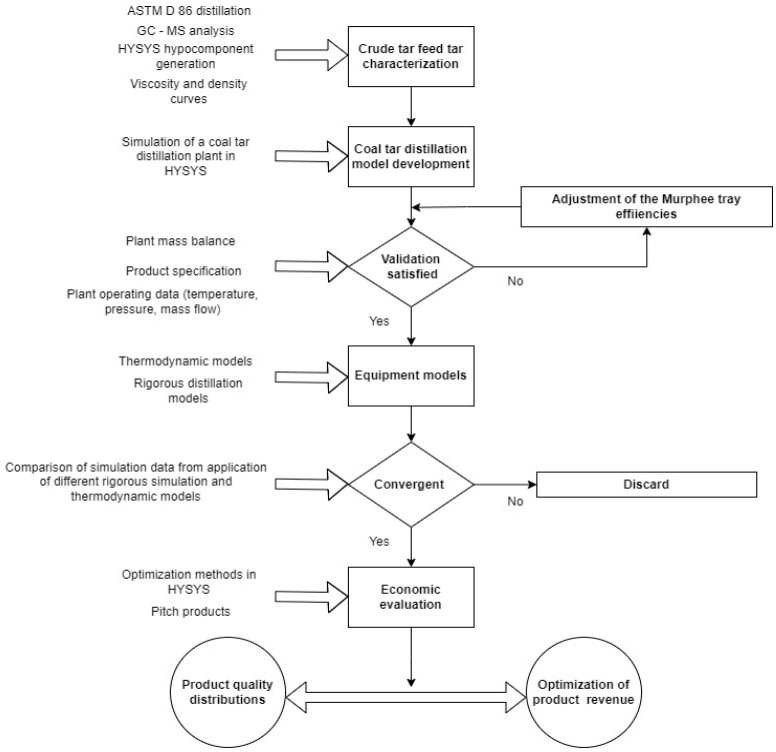

Figure 3-2: Methodology framework.

The first step in the distillation model development is the characterisation of crude tar feed by the distillation method ASTM D86 to extract the oil fractions, followed by GC – MS analysis to identify various aromatic components present. In the current case, plant historical data was collected and combined with hypothetical fractions in HYSYS to complete the feed assay. The ASTM D86 method end boiling point is 360°C, and therefore, fractions above the specified temperature are not distilled and are not identified in GC – MS hence the addition of hypothetical components for a better estimation of the feed stream. The addition of hypothetical components requires the estimation of the density and viscosity curves for an accurate description of the feed, and this was carried out in HYSYS by using historical viscosity and density data from the plant.
The second step consists of selecting a random thermodynamic model and a solution method to create the distillation model in HYSYS. The selection of the appropriate solution method and a thermodynamic model is investigated later, and based on the results, justification of the model is made. Simulation model results are validated with average plant mass balance data, and depending on the deviation, Murphee tray efficiencies are adjusted for each column to match plant data mass balances.

An optimisation model is built in HYSYS for process improvement, considering quality constraints, adjustment of critical process parameters, and product costs of each product produced in the process. The optimisation method applied is justified by computing different cases using each model available in HYSYS, and depending on convergence as well as maximisation of the objective function, an appropriate method is selected.

3.3 Coal tar feed characterisation

Due to the unavailability of laboratory institutions in the country that have the facilities to handle coal tar and perform distillation characterisation experiments, alternative methods were employed to work out the feed analysis for distillation modelling. Feed coal tar data from the reference Tar plant was used, though not complete for the purpose of the distillation modelling to be carried out in the current research. Parameters such as true boiling point, density and viscosity curves as well as the GC – MS are necessary for a full characterisation of the feed material to a distillation process and model. A summary of the data available from the reference plant is illustrated in
Table 3-1

Table 3-1: Summary of data from the reference Tar plant.

Stream	**Parameter**			
	TBP	*GC-MS*	*Density*	*Viscosity*
Coal tar	x	x	x	x
Distillates	x	A	N	x
Pitch product	x	x	A	A

A - available
N - not complete
x - not available

Based on the product GC – MS historical information available, a plant mass balance was performed to back-calculate the feed coal tar fractions. Hypocomponents in HYSYS were generated for heavy pitch fractions to complete the feed assay as this information is not accounted for in the distillate product analysis. For a complete coal tar characterisation, physical properties such as density and viscosity were estimated again from available product

data presented in Appendix B, C, and a compared to coal tar analysis found in various literature. Lastly, the ASTM D86 boiling point curve was also generated from HYSYS coal tar stream analysis to conclude the feed characterisation, further details on the methods applied will be provided in the subsections below.

3.3.1 Mass balance

The primary purpose of a coal tar distillation plant is to produce residue pitch. Therefore, the production data of a hard pitch product with softening point 115 – 118 Mettler and its associated distillate product data were considered for the mass balance calculation. The pitch product mentioned is produced at specific column operating conditions and thus the quality and yields of distillate oils were also assumed and stated in Appendix D, Section 8.4 representing the actual mass balance from the plant.

The average distillate product quality for each pitch product and related distillates over 12 months in 2022 has been collected and is presented in Appendix B, Table 8-1 and Table 8-2. Additionally, a complete mass balance back calculation for 115-118 pitch can be found in Appendix D. Assumptions on the yield of specific distillates were made where specific product fraction data was not available to complete the mass balance and the judgment of an experienced plant laboratory technician also helped in specifying some of the data that is recorded in GC – MS analysis but not captured in the reports. The feed fractions worked out from the mass balance calculations are shown in Table 3-2 below, arranged in the order of light components with low boiling points to the heavier aromatic components boiling at higher temperatures.

Table 3-2: Coal tar feed fractions.

Fractional composition (wt%)	Value
Light fractions	0,029
Tar acids	0,017
Methyl naphthalene	0,011
Naphthalene	0,12
Phenanthrene & Anthracene	0,087
Heavy carbon	0,24
Above 360 °C	0,50

The following two subsections provide a complete analysis of the coal tar feed stream comprising distillation and physical property data. After all the parameters required for characterisation have been determined, the overall coal tar property data is compared to high-temperature coal tar found in literature from three different authors.

3.3.2 Pure component and hypo-component generation in HYSYS

The fractional composition in Table 3-2 is represented as an aggregate of several aromatic hydrocarbon species; for instance, the light fraction composition is a combination of the BTX

components (benzene, toluene, and xylene) with tar acids made up mainly of phenols cresols, and the indene fractions, etc. Methyl naphthalene is captured as a sum of 1 and 2 – methylnaphthalene followed by heavy carbons, which are components with boiling points above 230°C as indicated by *Maloletnev et al.* in the characterisation of chemical distillate fractions of coal tar (Maloletnev et al., 2014).

The mass balance estimation above considered 115 – 118 M distillate product data for the back calculation of feed fractions, and based on the plant operating conditions a temperature a temperature just below 360 °C is applied therefore coal tar fractions above 360°C are not captured hence hypocomponents in HYSYS were created to classify components in the boiling temperature range above 360 °C.

3.3.3 Coal tar viscosity, density, and ASTM D86 Curves

Hypocomponent generation in HYSYS requires an estimation of the viscosity and density data to have a more accurate representation of the feed assay. By applying the assumption that pitch products are recovered at temperatures above 360°C, the hypo-components specified are the main components of pitch products, and therefore, the available viscosity and density data for pitches in Appendix C can be used to generate viscosity curves and estimate densities for hypocomponets generated. The Brookfield DVE viscometer is used in the plant to determine pitch product viscosity at two different temperature points. The selected temperature ranges for hard pitch 115 – 118 Metler is 140°C and 160°C, with the expected viscosity values measured equal to 18000 cP and 4200 cP, respectively. In determining the density of the two pitch products, the ASTM D3142 method is applied, and the expected values for 115 – 118 Mettler pitch is 1300 kg/m^3 and 1200 kg/m^3 for 68 – 73 Ring and ball pitch product.

The average viscosity and density data records for the two pitch products from the reference tar distillation plant were collected and used in HYSYS to generate the viscosity curves for specified hypocomonents and the estimated coal tar viscosity and density curves are presented in Appendix E, Figure 8-5 and Figure 8-6 respectively.

Below is a comparison of the coal tar density estimate determined from the various methods described above with three other coal tars used by three different authors in their research as illustrated in Table 3-3. The estimated coal tar density used in the current study is 0,84% heavier in comparison to the ones used in previous studies as indicated in Table 3-3, with a viscosity difference of 2 cP units based on the data published by author 3.

Table 3-3: A comparison of coal tar physical property data.

Parameter	**Unit**	**Current research**	**Author 1** (Kozlov et al., 2021)	**Author 2** (Maloletnev et al., 2014)	**Author 3** (Perruchoud et al., 2016)
Density at 20°C	kg/m³	1,19	1,18	1,18	1,18
Viscosity at 160°C	cP	12	-	-	<10

These differences in parameters can be attributed primarily to the Coke battery operations as well as the coal blends for each manufacturing process as they are different hence the slight differences can be expected. The quinoline insoluble content for the coal tar used in this study is 6,4 % as stated Table 3-4 representing the full analysis of coal tar in the current research study and the one in Kolmakov is at 3 % which proves that the coking conditions are more intense for the production of tar used in the current research hence the high viscosity as well as the density estimate.

Table 3-4: Full characterisation of the coal tar feed stream.

Property	Value
Density at 20°C, kg/m³	1194
Viscosity at 160°C, cP	12
Quinoline Insolubles, %	6,40
Moisture, %	5,70
Fractional composition, wt %	
Light fractions	0,029
Tar acids	0,017
Methyl naphthalene	0,011
Naphthalene	0,12
Phenanthrene & Anthracene	0,087
Heavy carbon	0,24
Above 360 °C	0,50

From (Kozlov et al., 2020) and many other sources it is well known that coal tar pitch constitutes 50% of the original coal tar distilled and the other half is the distillate products. In light to this fact, the boiling point curve for coal tar must have a cut point of 50% at temperatures above 360°C and this is consistent with the ASTM boiling point curve generated in HYSYS for the coal tar in the current study illustrated in Figure 3-3. The 50% cut point is at an estimated temperature of 370°C.

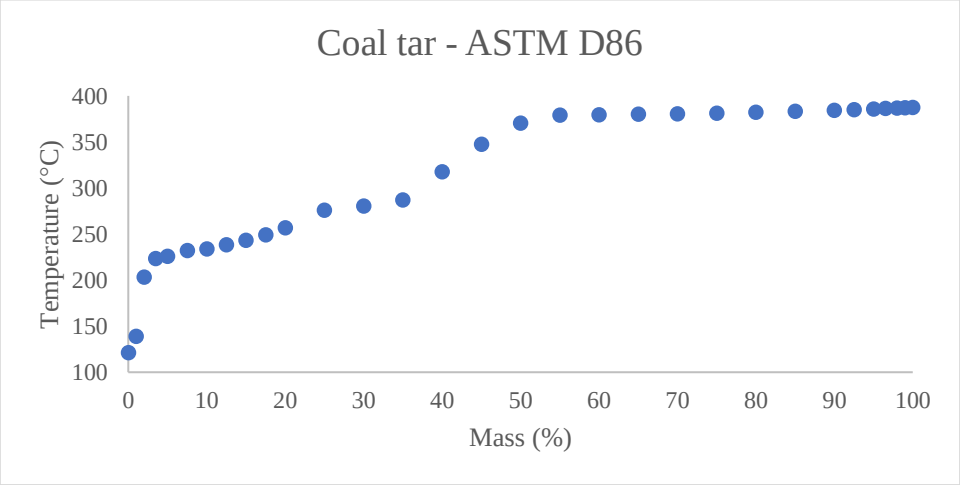

Figure 3-3: Coal tar TBP curve simulation.

3.4 The Distillation Model

The process that follows defining the feed stream composition and physical property data is the selection of a random fluid package before entering the simulation environment in HYSYS. The NRTL activity coefficient model was selected for the initial simulation and later compared with Peng Robinson for the determination of the best-suited fluid package for the process being modelled. The second step in model development was the selection of a solution method. The inside-out method was chosen as it is the most widely used model in distillation simulation, given the fact that it can solve problems of various types and has short computational times.

The production capacity of the coal tar distillation process considered is 25 t/h, with a total of four distillation stages to produce five different products supplied to the carbo-chemical and aluminum industries. The system configuration created in HYSYS is shown in Figure 3-4 below with initial column conditions specifications in Table 3-5.

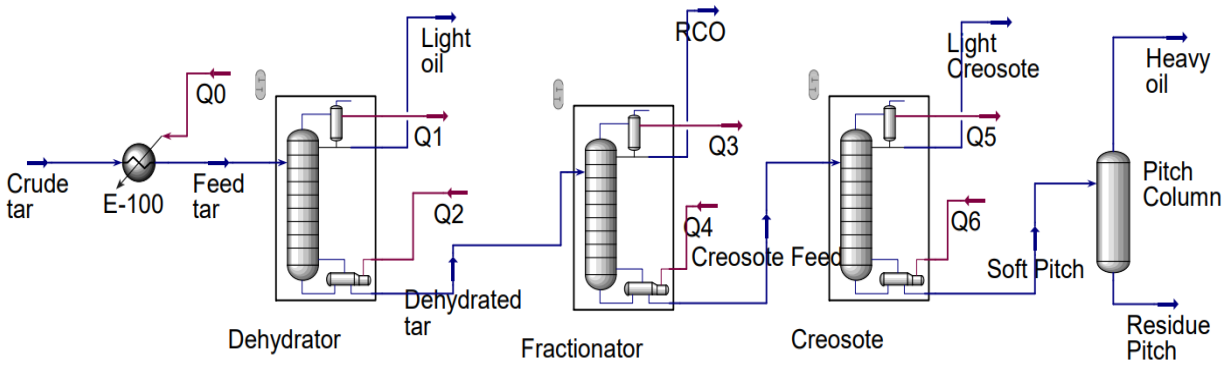

Figure 3-4: Coal tar distillation model in HYSYS environment.

The selection of the initial operating conditions in Table 3-5 below is based on the actual plant operating data when running the production process for 115 – 118 Mettler pitch product with associated distillates. More detailed data on process operating conditions for the two pitch products under consideration are shown in Appendix J, Table 8-11 and Table 8-12.

Table 3-5: Initial simulation conditions.

Column	Dehydrator	Fractionator	Creosote	Vacuum
Top pressure (kPa)	100	60	50	17
No. of trays	7	20	20	-
Top temperature (°C)	-	-	-	-
Bottom temperature (°C)	220	300	350	-

Distillate qualities are defined based on specific aromatic compounds present for each product and certain compositional standards are required to consider a product in correct specification. However, in the initial case, actual plant conditions and product qualities are simulated to ensure the model gives a better representation of the plant.

Defining the product pitch softening point in HYSYS is a challenging task as this parameter is not available. Therefore, this particular problem motivated a search for an alternative variable that has a direct relationship to the softening point and can be used in HYSYS to characterise

residue pitch quality. The section below addresses the reasoning and procedures followed to characterise pitch products.

3.4.1 Softening Point Calculation

In a paper published in 1977, George R. Romovacek investigated the influence of quinoline-insoluble solid particles in pitch on the preparation and baking of carbon blocks (Romovacek, 2013). This research addressed one of the concerns pitch customers had on the influence of QI on viscosity and softening point. The study was carried out by analysing about 150 pitches with QI content between 8 – 20% and softening points 100 – 120 °C. Based on the results of this study, it was realised that an increase in QI had a direct impact on viscosity and softening point in pitch. On another note, it was discovered that there is a good correlation between viscosity and softening points as illustrated by the viscosity-temperature graph in Figure 3-5 below.

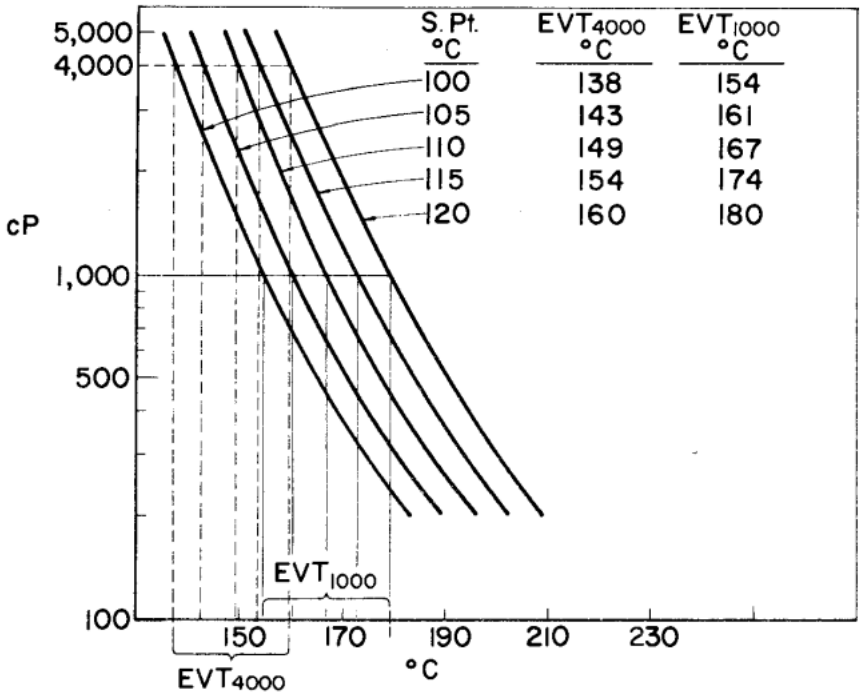

Figure 3-5: Viscosity - temperature relation for pitches of increasing softening points, ***adapted from***: (Romovacek, 2013).

For a better clarification and interpretation of the results, an equiviscous temperature is defined, which is the temperature point where different pitch samples have the same viscosity values. In this case, the 1000 cP and 4000 cP were the viscosity levels chosen, and the equiviscous temperatures were measured for all the 150 pitch samples. Equiviscous temperature increases with the pitch softening point, as displayed by the parallel viscosity-temperature curves in Figure 3-5. The following correlations were established to calculate equiviscous temperature given the pitch softening point determined by the Mettler method (Romovacek, 2013).

EVT at 1000 cP viscosity;

$$EVT_{1000} = 32.3 + 1.231 \times Softening\ point \ldots\ldots 3.1$$

EVT at 4000 cP viscosity;

$$EVT_{4000} = 26.2 + 1.117 \times Softening\ point \ldots\ldots 3.2$$

The results above allow us to make the inference that the softening point is essentially a temperature of equal viscosity determined by the softening point method. Therefore, we can use viscosity as an alternative parameter to characterise a specific pitch product softening point using equiviscous temperatures. From the reference tar distillation plant, viscosity-temperature measurements are done for a hard pitch of 115 – 118 Mettler at 140°C and 160°C temperature levels, and on average, the viscosity values are 18000 cP and 4200 cP, respective. This means that hard pitch quality criteria in HYSYS will be set for the mentioned viscosity values, which translates to a pitch softening point of 115 – 118 Mettler. For a softer pitch of 68 – 73 RB softening point, the average viscosity values are 400 cP and 240 cP at temperatures 140°C and 120°C.

3.4.2 Viscosity – temperature correlation

Residue pitch product stream temperature is usually at temperatures above 360°C, thereby making it difficult to assess the quality of the product produced when running the HYSYS simulation model. For instance, the quality criteria for 115 – 118 Mettler pitch is the viscosity values at specified temperatures of 160°C and 140°C; therefore, with stream temperatures at random values, product quality cannot be predicted. To address this problem, viscosity correlation models were used to simulate product characteristics at specific temperatures. The Twu and Bulls viscosity blending model was applied to get a viscosity correlation at temperatures required by the pitch quality criteria (Al-Besharah et al., 1987).

$$\ln\ln(\nu + 0.7) = m \ln T + b \ldots\ldots 3.3$$

Where:

- ν – viscosity in centistoke.
- T – absolute temperature.
- $m\ and\ b$ – constants for a particular oil.

The viscosity blending model is incorporated in HYSYS, which is used to estimate the viscosity curve for a material stream of different components.

3.5 Thermodynamic Model Selection

Simulations must represent actual plant situations and provide users with solutions approximate to reality. In building process simulations, the selection of thermodynamic models is important in the sense that the behaviour of components present in a mixture must be well captured by describing the possible interactions between components as well as the relationships between certain groups of parameters to give a good representation of real plant conditions.

3.5.1 The Decision Tree Model

Eric Carlson from Aspen Technology developed a procedure for selecting an appropriate thermodynamic property model by summarising some of the main parameters in a decision trees model, as shown in Figure 3-6 below (Carlson, 1996).

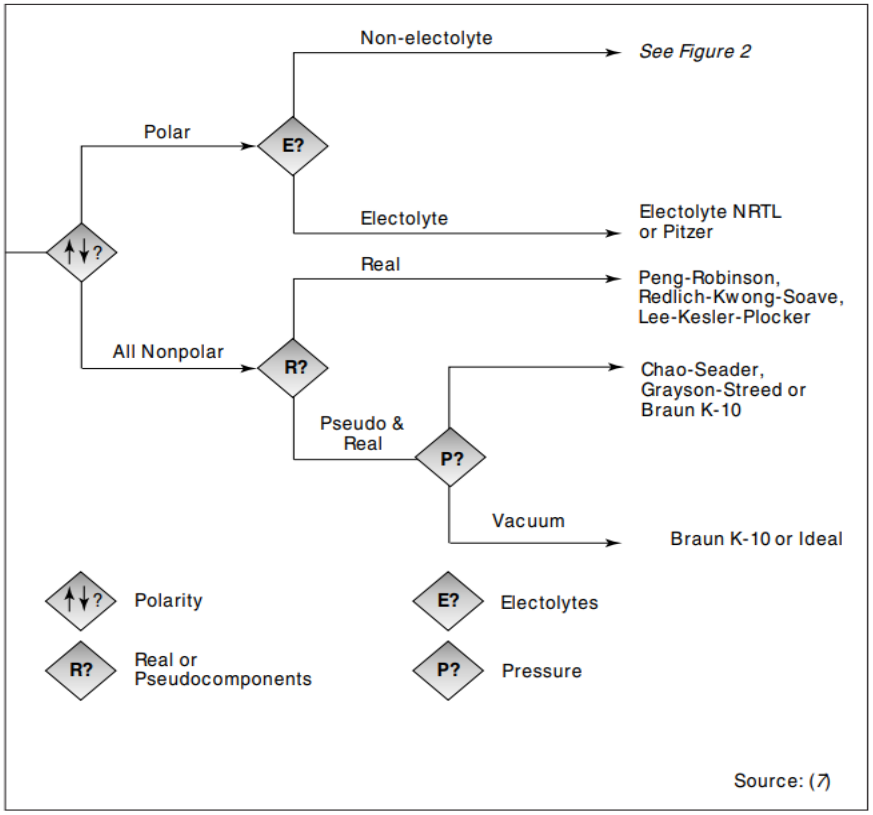

Figure 3-6: Procedure for the property model selection; First step, ***adapted from***:(Carlson, 1996).

The first step involves identifying polarity in molecules since it is an important parameter affecting interactions between substances. If the polar path is chosen, the second step includes the evaluation of whether the components under study are electrolytic, which requires the application of ionic equilibrium. For polar non-electrolytic substances, the decision tree continues as illustrated in Figure 3-7 below.

Based on a procedure laid out by Carlson, there are, in general, five main steps in selecting the proper representation of physical properties:

1. Select a suitable physical property method.
2. Validate the physical properties.
3. Describe components not available in the database and missing parameters.
4. Obtain experimental data.
5. Estimate the missing parameters.

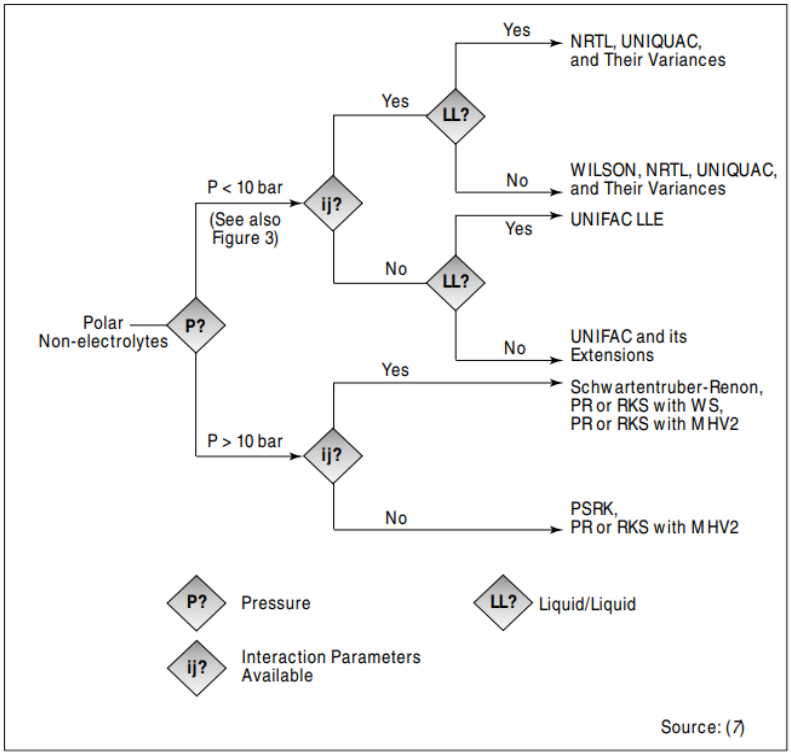

Figure 3-7: Procedure for polar non-electrolytic substances, ***adapted from***: (Carlson, 1996).

The selection of an appropriate physical property model is performed for the coal tar simulation model by applying the methods mentioned above. In our case, the coal tar feed stream specified consists of polar molecules such as acenaphthene, carbazole, cresols, pyrene, fluoranthene, and quinoline (Casal et al., 2008). Thus, the polar non-electrolytic path is chosen, followed by operating conditions where system pressure is less than 10 bar with interaction parameters available and no liquid-liquid equilibria because the mechanism of the distillation process is based on the vapour–liquid equilibrium. According to the path chosen based on the Carlson method, the thermodynamic property models most suitable for the coal tar distillation case are Wilson, NRTL, and UNIQUAC activity coefficient models paired with the equation of states such as the ideal gas or Redlich – Kwong to represent the vapour phase.

3.5.2 Fluid Package Simulation Experiments

The method above requires validating generated VLE data from the HYSYS distillation simulation with experimental information to ensure that the selected property model best represents reality. However, due to the lack of experimental VLE data from the reference plant and in the literature, an alternative approach was taken to run a simulation experiment to evaluate the performance of the chosen thermodynamic models. The decision parameter selected is the heavy key component fraction (naphthalene) in the distillate with the adjusted variable being the reflux ratio and the boil-up ratio held constant at 0,50. Physical property data such as density, enthalpy, and heat capacity were also investigated for two different thermodynamic models. The first test involved the verification and justification of the activity coefficient models suggested by the decision tree above by running the distillation simulation on the first column in the flowsheet at different reflux ratios and column-top pressures

applicable to the system in the study. The results from this test are illustrated in Figure 3-8 below. Suppose there are no deviations in the heavy in the distillate from the Wilson as well as the NRTL model. In that case, the decision tree model is justified, meaning the two thermodynamic models are suitable for the simulation of a coal tar distillation plant.

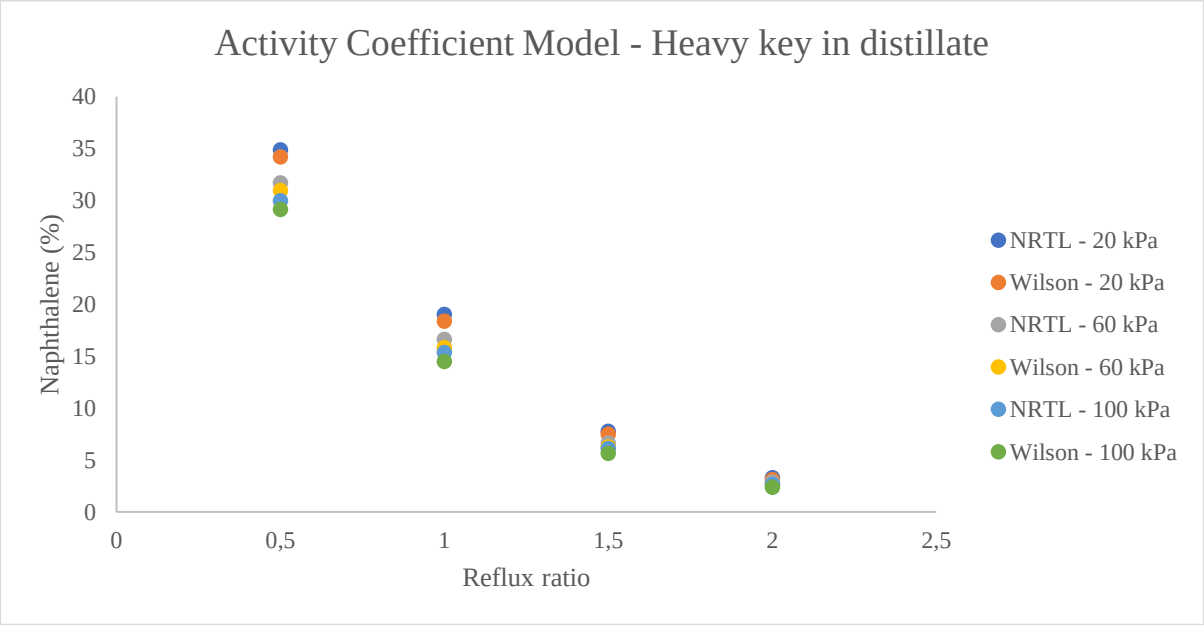

Figure 3-8: Activity coefficient model evaluation.

Evaluation of the Wilson and NRTL thermodynamic models represented by the results in Figure 3-8 shows that the two model predictions of the heavy key distillate fraction are the same for both at different column pressures and reflux ratios. The top pressure plays a significant role in the distillate product distribution because, at low pressures, the heavy key distillate fraction is slightly higher than with operation at higher pressures. However, as the reflux ratio increases, the heavy key distillate fraction converges to a value of 2,4 %, which is the same for both models at different pressures.

The operation of the coal tar distillation system under study is at vacuum pressure, which causes a significant impact on the interaction between molecules. This enables us to assume that the ideal or cubic equations of state can, to some degree, be used to model the thermodynamic behaviour of the system; however, results must be validated to test the idea and to ensure that accuracy is maintained.

The second test involves the comparison of the NRTL activity coefficient model to the Peng-Robinson equation of state using conditions similar to the ones in the first test.

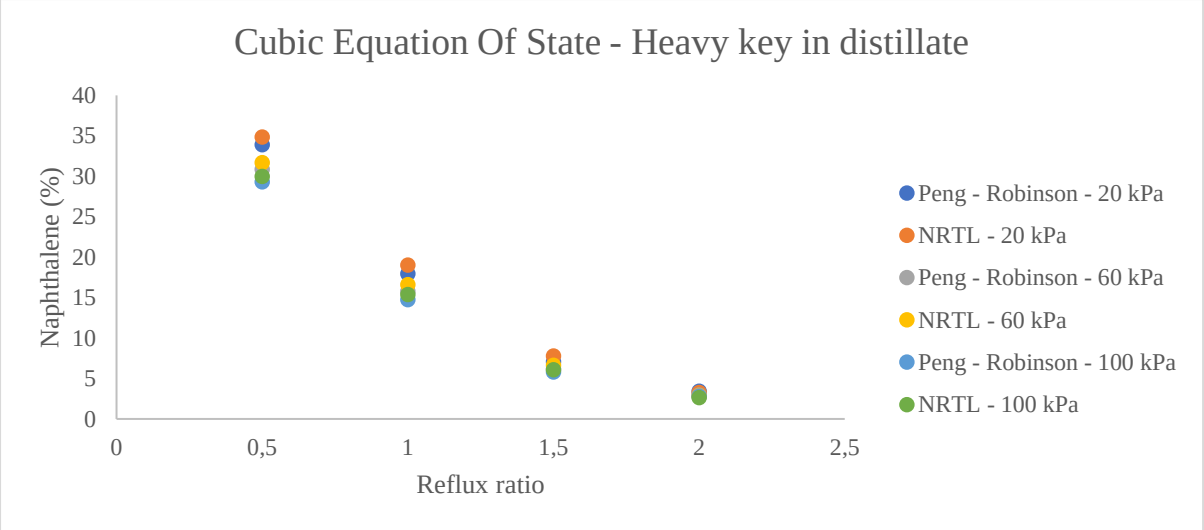

Figure 3-9: Comparison between the activity coefficient model and the cubic equation of state.

Based on the results from the second test shown in Figure 3-9, the behaviour of the system is the same as in the first test, and there is no significant variation in heavy key in distillate fraction prediction represented by the Peng-Robinson cubic equation of state and the NRTL activity coefficient model. Furthermore, the coal tar physical property data is computed using HYSYS stream analysis to further investigate the performance of the two thermodynamic models from the second test.

3.5.3 HYSYS stream analysis – Physical property evaluation

Physical property evaluations were performed in HYSYS stream analysis by investigating the two fluid packages for further validation of the cubic equations of the state and compared with activity coefficient models chosen from the decision tree model. A performance comparison between the NRTL and the Peng-Robinson models is presented in Figure 3-10 to Figure 3-12.

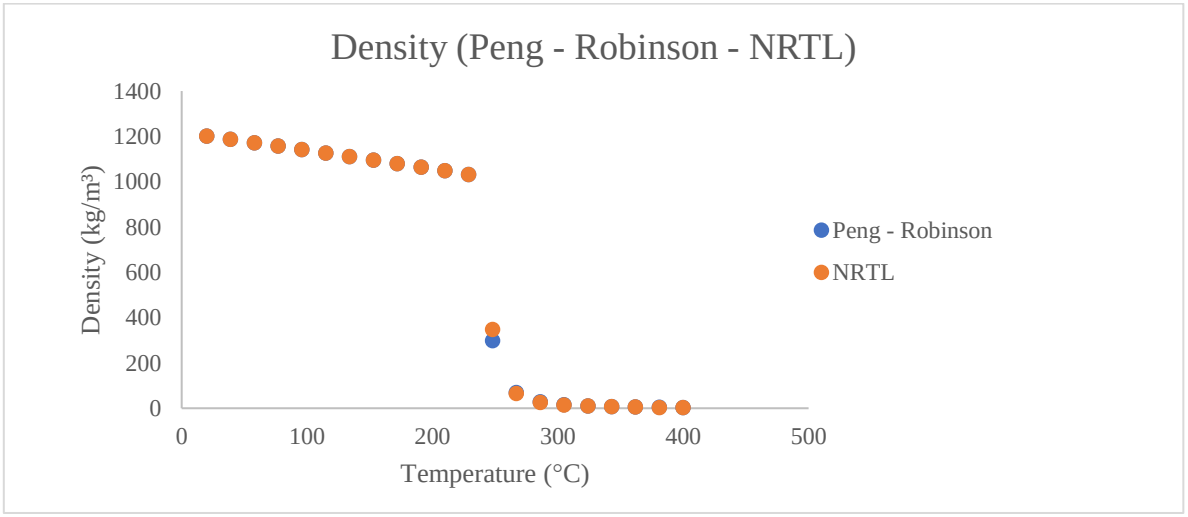

Figure 3-10: Density variation with temperature at constant pressure (100kPa).

With pressure held constant at 100 kPa, the coal tar density decreases with an increase in temperature, exhibiting a linear change up to a temperature of 229 °C where phase change starts to occur. The change is accompanied by a significant drop in density from a temperature of 229°C to 267°C. The density results in Figure 3-10 are consistent with general coal tar density values at low temperatures (Baron et al., 2016). Of high importance is the comparison of the density behaviour generated from the application of the Peng-Robinson equation of state fluid package as well as the NRTL activity coefficient model. Based on the results, the prediction is similar, and there are no apparent deviations from the two models.

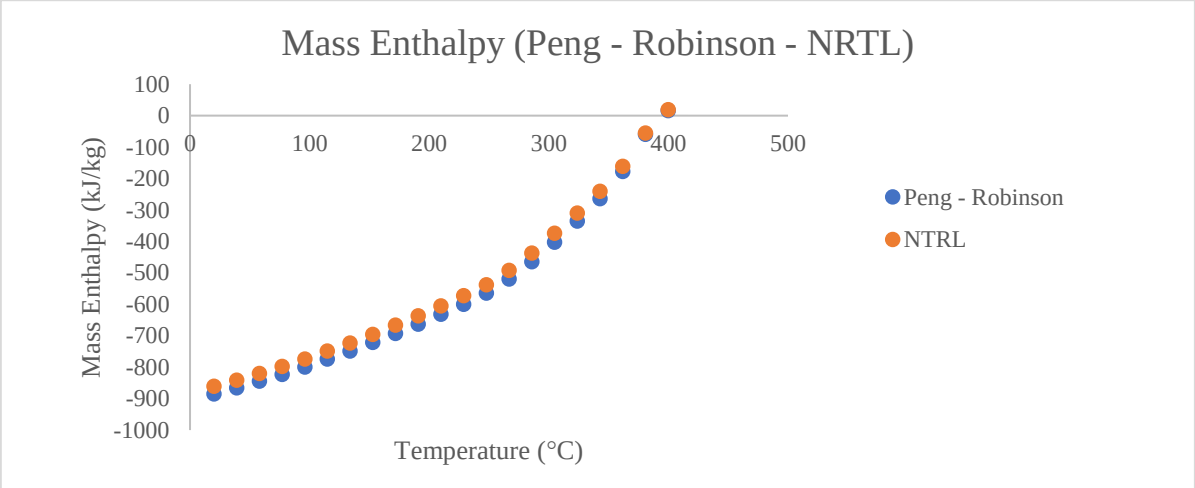

Figure 3-11: Temperature - Enthalpy change with temperature at constant pressure (100 kPa).

Figure 3-11 and Figure 3-12 represent the enthalpy and heat capacity of the coal tar feed stream to confirm the property predictions made using the equation of state and the activity coefficient model. The enthalpy and heat capacity predictions are similar to the two models as the results show no deviations between the two properties.

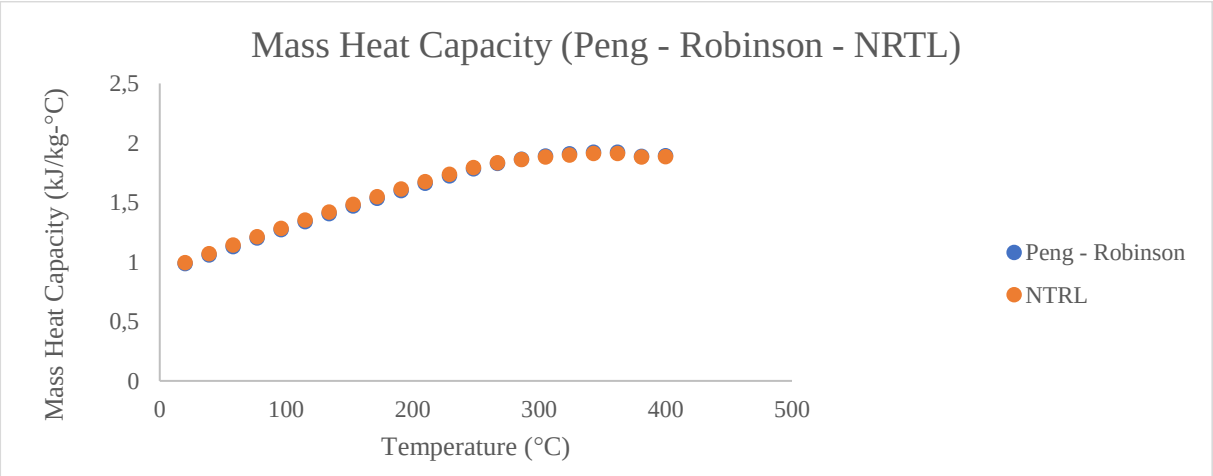

Figure 3-12: Heat capacity - temperature relation at constant pressure (100 kPa).

3.5.4 Suitable property model – Coal tar simulation

Distillation simulation experiments were considered in the selection of an appropriate thermodynamic model mainly because there was no experimental data VLE data to confirm fluid package predictions. The decision tree proposed by Eric Carlson was used to choose the most likely thermodynamic model based on the nature of molecular interactions of species present in the stream being analysed. The heavy key product distribution at various reflux ratios in the HYSYS distillation simulation was used to compare the behaviour of the NRTL and Wilson thermodynamic activity coefficient models proposed by the Carlson decision tree model.

Analysis of the system conditions motivated the investigation into the application of an equation of state and how its behaviour in comparison to the initially suggested activity coefficient model performs. In addition, physical properties predictions were investigated, and the results showed that the equation of state predictions is close to the activity coefficient model at system conditions with density values verified with the data in the literature as well as from the reference plant.

Based on the distillation simulation experiments to investigate the heavy key product distributions as well as the property data predictions from the selected activity coefficient model in comparison to the equation of state, the Peng-Robinson equation of state was chosen as the appropriate thermodynamic model for the coal tar distillation model development. The physical property data predicted are similar to those in literature, and compared to thermodynamic models, the cubic equations of states are easier to use.

3.6 Solution Method Selection

A more detailed review of the solution methods was given in the literature review 2.6.1, and based on this information, it was established that the Newton-Raphson method, as well as the Inside method, are the most widely used methods for solving a broad range of distillation problems however the inside out method provides better computational time. Therefore, it was the model selected for the current study on coal tar simulation.

3.7 Validation

The model validation process is a success when the reference plant mass balance and product qualities are replicated in a distillation steady state simulation by application of process conditions specified to produce 115 – 118 Mettler pitch residue. In the development of the initial mass balance calculation, product quality information was used; however, yields were assumed based on the knowledge and judgment of an experienced production planner due to the unavailability of consistent plant product flow rate recordings. This necessitated the application of a mass balance reconciliation process between the calculated values and the estimations from a steady-state HYSYS distillation simulation described above to have a more practical model consistent with reality. The adjusted model was tested by simulating the production of a different pitch product to evaluate if the quality distributions similar to those

found in the reference plant can be achieved with the application of the 68 – 73 Ring and Ball pitch process conditions.

Plant mass and energy balances are often not accurate due to inherent gross and random errors in measurements, which are a result of process faults and instrument disturbances (Crowe et al., 1983). Data reconciliation is a weighted least square method used in process engineering to deal with mass and energy problems by ensuring conservation laws are obeyed and errors between measured values are minimised (Crowe, 1986). The availability of simulators with optimisation functions has made it much easier to solve these problems since the process units with mass balance equations are built in, and the optimisation can be made by specifying an objective function and process constraints as well as adjustable parameters (Piccolo et al., 1996). There are two types of data reconciliation problems based on process behaviour, namely, linear and non-linear data reconciliation. In the distillation case, non–linear data reconciliation methods are applied due to the nature of the process. Shown below is a formulation of the non–linear reconciliation problem to minimise an objective function, which is the sum of the weighted least square variables such that conservation laws and constraints are met.

Choose x:

$to\ min$

$$[(y-x)^T Q^{-1}(y-x)] \dots\dots 3.4$$

$such\ that$

$$h(x) = 0\ and\ g(x) \geq 0 \dots\dots 3.5$$

Where:

- $y -$ measured/calculated value.
- $x -$ reconciled value.
- $Q -$ inverse of the variance of a measured variable.
- $h(x) -$ set of equality constraints representing the model.
- $g(x) -$ set of inequality constraints in the process.

In our case, the flow rates based on assumed yields of all five product streams were selected as the objective function set as the sum of the square differences multiplied by the factor denoting the importance of certain variables, as shown by Equation 3.6 below.

$$\min\left[\sum_{i=1}^{5}\left(\frac{y_i - x_i}{V}\right)^2\right] \dots\dots 3.6$$

Where V is the variance of the square standard deviation assumed to be 5,0 % between measured or calculated values with constraints placed on selected product qualities defined inTable 3-6, adjusted parameters were column top and bottom temperatures as well as the

Murphee tray efficiencies to achieve the separation level required and the reflux and reboil ratios.

Table 3-6: Adjusted process conditions for mass balance reconciliation.

Column	**Adjusted process conditions**		
	Reflux ratio	*Boil up ratio*	*Overall stage efficiency*
Dehydrator	0,062	0,30	0,52
Fractionator	0,11	0,38	0,49
Creosote	2,9	3,0	0,86
Flash	-	-	-

The simulation was set up to find the minimum value of the sum of least squares between the calculated and model flow rates by adjusting the Murphee tray efficiencies and other operational parameters mentioned above, as well as considering the quality constraints. The overall objective function was reduced from a value of 3812 to 712,2 which is an indication that the function worked and the objective was achieved. Adjusted Murphee tray efficiencies for each column changed from 100% in the initial simulation development to values indicated in Table 3-6 to achieve the separation level specified for the product qualities. The resultant mass balance with adjusted flow variables is illustrated in Appendix D, Table 8-6.

According to the simulation results, only the RCO and heavy oil stream had flow rate deviations less than 5,0 %, and the rest of the three streams had larger deviations; this result is shown in Table 3-7 below. The possible reason for such high deviations on the other three streams can be a function of an incorrect assumption in the initial mass balance owing to the fact that the product qualities specified are actually out of spec, as has been the problem that the plant is dealing with and the yields assumed are based on what is expected from the plant and not the reality of the current situation. However, this is one of the goals of this research project, which is to have a proper analysis of the current situation and improve on it to get the correct quality specifications required by the plant.

Table 3-7: Product flowrate comparison between calculated and reconciled values.

Stream	**Stream flow (t/h)**	
	Actual	*Reconciled value*
Crude tar feed	25	25
Light oil	1,0	2,3
RCO	4,0	3,9
Light creosote	6,0	6,7
Heavy oil	1,5	1,6
Residue pitch (115-118 M)	13	11

Quality parameters were selected based on what the reference plant considered in their service level agreement with their customers. A summary of the important parameters considered in

terms of quality specification are listed in Table 8-7 and Table 8-8 in Appendix G and presented in such a way that the actual plant measurements derived from GS – MS analysis mass balance calculations are compared with the desired quality base. This data was used to validate the quality predictions from the simulated process model in the production of 115 – 118 M pitch and distillates. Based on the results presented in Table 3-8, there are no significant deviations when comparing the actual measured product quality results from the plant for each product and the simulation results. The detailed simulation results are available in Appendix H, Table Table 8-9 showing composition of light oil and RCO with the pitch quality and light creosote density performance indicated in Figure 8-10 and Figure 8-11.

Table 3-8: Comparison between actual and steady-state simulation product quality values (115 - 118 M).

Product	**Unit**	**Quality parameter**		**In Range**
		Actual	Model	
Light oil	%			
Naphthalene		43 ± 2,9	48	0,046 % deviation
Light fraction				
RCO	%			
Naphthalene		44 ± 6,1	44	Yes
Light creosote	kg/m³			
Density		1125 ± 51	1147	Yes
Residue pitch (115 - 118 M)				
Viscosity	cP			
Viscosity @ 160 °C		3686 ± 446	3523	Yes
Viscosity @ 140 °C		-	-	-

Process conditions applied in the production of 68 – 73 RB pitch, which differ from the production of the 115 – 118 M pitch, were used in validating the steady state distillation simulation model created in HYSYS with adjusted Murphee tray efficiences, which represents the reference plant operations and can be optimised to ensure product qualities are improved to meet customer demands. A detailed summary of the process conditions for the manufacturing of both pitch products is represented in Appendix J, Table 8-11 and Table 8-12. In applying 68 – 74 RB conditions product quality characteristics predicted by the simulation model were compared to available quality data to ensure the efficacy of the model. The results illustrating the comparison between the actual quality data as well as the model predictions are shown below in Table 3-9 below. All the quality parameters predicted are in range and matching the plant current standards.

Table 3-9: Comparison between actual and steady-state simulation product quality values (68 - 73 RB).

Product	Unit	Quality parameter		In Range
		Actual	Model	
Light oil	%			
Naphthalene		41 ± 2,6	41	Yes
Light fraction		-	43	
RCO	%			
Naphthalene		46 ± 6,1	47	Yes
Light creosote	kg/m³			
Density		1123 ± 34	1154	Yes
Residue pitch (68 - 73 RB)				
Viscosity	cP			
Viscosity @ 150 °C		235 ± 46	237	Yes
Viscosity @ 170 °C		109 ± 19	124	Yes

The naphthalene quality parameter in both pitch products is out of specification for the light oil product when compared to the standard required by customers, which is supposed to be below 8,0 %; however, the simulated values are similar to what is produced in the plant. The refined chemical oil is an intermediate product for the naphthalene plant, and based on plant standards, the values in both simulations and actuals are lower than what is normally expected, which should be greater than 55%. On the other hand, the other three products, which are the light creosote, heavy oil, and the residue pitch, are all within limits for the production of both pitch products in simulation as well as the actual values from the plant; this is indicated in Table 3-8 and Table 3-9 above.

The coal tar plant distillation model was developed in this section with the purpose of evaluating the overall performance of a distillation plant in producing two pitch products of specific softening points and viscosity, given the coal tar feed composition. A structured procedure was followed in developing the simulation model, which included the collection of raw product GC – MS data from the reference plant to back-calculate the feed composition by applying the mass balance concept. To verify the calculated mass balance in HYSYS by application of specific conditions required for the manufacturing of a pitch product with a softening point of 115 – 118 Mettler and performing data reconciliation to adjust and correct the assumed flowrates. The Murphee tray efficiencies were adjusted for each column to fit the product quality data. And finally validating the steady state distillation simulation model by using process conditions required to produce a pitch product of 68 – 73 Ring Ball softening point to replicate product quality results obtained in the actual manufacturing of the product.

3.8 Optimisation

Optimisation methods play a significant role in the industry regarding decision-making and business profitability. In the current research project, it was decided that an optimisation model

be used to come up with the best possible operating strategy for the coal tar distillation plant by maximising product revenue and ensuring that product qualities are within specifications. The HYSYS original optimiser model was chosen as the optimisation method for the developed coal tar distillation process.

The selected objective function is the sum of product revenues with the process constraints placed on each product's qualities and process conditions (e.g., reflux ratio, reboil ratio, etc.) as adjusted variables.

$Objective\ function$;

$$\max \sum_{i=1}^{n} Q_i C_i \ldots\ldots 3.7$$

Where:

- $Q_i -$ product flowrate (t/h).
- $C_i -$ product cost (R/t).

$Process\ constraints$;

$$z_i \leq u_i \ or \ z_i \geq u_i \ldots\ldots 3.8$$

- $z_i -$ quality parameter specified in the spreadsheet.
- $u_i -$ product quality parameter.

$Adjusted\ parameters$;

$$Lower\ bound \leq A_j \leq Upper\ bound \ldots\ldots 3.9$$

- $A_j -$ process variable.

Equations 3.7 to 3.9 above show a simple mathematical representation of the strategy applied by HYSYS original optimiser to achieve maximum product revenue whilst keeping product qualities within required limits. This procedure was used to investigate optimum conditions to produce the two pitch products 115 – 118 M and 68 – 73 RB and associated distillate fractions.

4 Results and Discussion

This section describes the application of the steady-state coal tar distillation model developed. By first establishing the base conditions along with the associated quality distributions. Furthermore, a sensitivity analysis is performed to study the quality distribution of the light oil, RCO, and Creosote distillates, assisting in establishing an operational philosophy for the process. Finally, this section is concluded by presenting optimized conditions for improved plant operation.

4.1 Establishing the base conditions

A detailed procedure was laid out in Section 3 for the development of a coal tar distillation simulation model, which involved the establishment of the reference plant mass balance and feed composition by back-calculation using product quality data available. The column process conditions, such as the average pressure and temperature specifications to produce 115 – 118 Mettler softening point pitch, were used to replicate the plant mass balance in the HYSYS distillation simulation. Murphee tray efficiencies were adjusted for each column to fit product quality data with distillate rates reconciled through HYSYS original optimiser to minimise the weighted least squares between the plant mass balance as well as the simulation mass balance.

The developed simulation model with adjusted Murphee tray efficiencies was validated by simulating the production of a pitch product with softening points 68 – 73 Ring and ball using plant conditions specific to the production of the mentioned pitch product. In achieving the product and distillate quality associated with the manufacturing of the pitch product, the model validation was a success. In the process described above, base conditions in terms of process parameters, product yields, and qualities were established. The base distillate and pitch yields from the distillation simulation using plant conditions are represented in Table 4-1 below.

Table 4-1: Base product yields in the production of two pitch products with different softening points.

Stream	Yield (%) 115 - 118 M	Yield (%) 68 - 73 RB
Crude tar feed	-	-
Light oil	9,3	6,5
RCO	16	19
Light creosote	27	9,6
Heavy oil	6,2	0,18
Residue pitch	42	65

The 115 – 118 M is a hard-pitch residue with a yield of 42 %, as indicated by the simulation results, and the soft-pitch residue 68 – 74 RB is at a yield of 65 %. The difference between the two pitch products agrees with reality, as the hard pitch distillation process is intense, with the aim of driving out most of the distillate fractions to achieve a higher softening point value. The soft pitch process is not that severe in terms of operating temperatures applied as more

distillates are still available and recovered in the pitch, hence the higher yield when compared to the hard pitch product (Kozlov et al., 2021).

The statement made above is also consistent with the distillate yields produced from the manufacturing of the two pitch products. Higher distillate yield fractions are achieved from the hard pitch production process. Low yields are obtained from the soft pitch process, as indicated in Table 4-1. The light oil distilled in hard pitch is 2,8 % higher in yield than the light oil in soft pitch. In comparison, the refined chemical oil yield is 3,4 % less, and the light creosote as well as the heavy oil yields are 17 % and 6,1 % higher respectively.

The coal tar distillation model is developed in such a way that the reference plant actual performance is represented, given the process conditions applied. As mentioned in the model development section, the product quality distribution was mainly adjusted by changing the Murphee tray efficiencies. According to the quality performance results from the distillation model in Table 4-2 below, the light oil and RCO quality parameters do not meet the plant specifications, and this is the actual reality in the reference plant.

Table 4-2: Distillate fraction quality specifications.

Product	**Unit**	**Quality parameter**		**Requirement**	**Specification met**
		115 - 118 M	68 - 73 RB		
Light oil	%				
Naphthalene		48	41	< 8,0	No
RCO	%				
Naphthalene		44	47	> 55	No
Light creosote	kg/m³				
Density		1147	1154	> 1125	Yes

The naphthalene content in light oil is higher than the specification in RCO, less than what is required by normal operating standards. However, the light creosote density quality parameter meets the specification.

4.2 Column operating conditions

The initial column operating conditions, which are similar to the actual plant operation for both the production of 115 – 118 M and 68 – 73 RB pitch and related distillates, were shown in Section 3, Table 3-5 and Appendix J, Table 8-11 and Table 8-12.

This section examines the control operating conditions used in practical plant operation to achieve the desired product quality distribution by running the 115 – 118 M process conditions using the developed and validated HYSYS coal tar distillation model. Since the study is based on a reference tar distillation plant, a limited number of variables are chosen in line with the plant operation. For this purpose, the variables used are the column reflux and boil-up ratio; though not measured in the plant, these parameters are known to affect the column top and

bottom temperatures, which are the parameters monitored in practice. The selected control variables are first investigated for consistency with known distillation principles and then later used to study the impact on the distillate qualities.

4.2.1 Process Control Parameters

Figure 4-1 below shows the effect of an increase in reflux ratio to the dehydrator column top temperature at a constant boil-up ratio of 0,010. Based on the results, the column top temperature is reduced by an increase in reflux ratio, however, at a certain point stability is reached where there is minimal change in temperature regardless of any further increase in the reflux ratio.

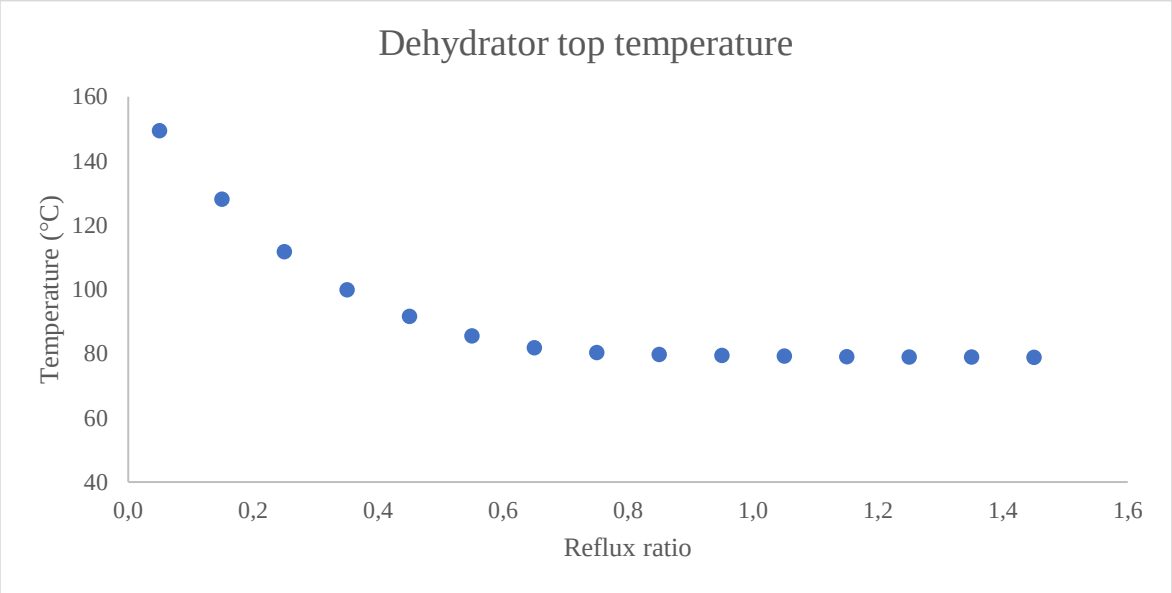

Figure 4-1: Dehydrator top temperature variation with reflux ratio at a constant boil-up ratio of 0,010.

The purpose of a reflux stream in the distillation process is to effect equilibrium between the rising vapour that is not so rich in high volatile components when compared to the reflux liquid; thus, through the mass transfer process, low volatile components get into the liquid stream, and the high volatile to the vapour stream. Because the reflux liquid is normally at a lower temperature than the rising vapour stream, heat transfer is also effective, resulting in a drop in column top temperature (Resetarits & Lockett, 2003). This method is applied in industry to reduce the column top temperatures and improve product quality. The primary benefit of a reflux stream is shown in the product distribution section.

The distillation column bottom temperature is also important in increasing vapour flow rates and reboil some of the light components that are still present in the liquid product, thereby improving product qualities. Figure 4-2 below illustrates the effects of the boil-up ratio on column bottom temperatures; a linear relationship is observed. In general, an increase in boiling up ratio at a constant reflux ratio increases the column bottom temperature as more vapour is

generated and not enough downflowing liquid to cool and provide transfer of components (Binay K. Dutta, 2007). Process controllers apply this strategy to gain an advantage in product qualities as well as the general control and stability of the column.

The results described in this section justify the parameters chosen in practical plant situations to control the top and bottom temperatures; however, the impact of both the reflux and boil-up are not only limited to temperature but also influence qualities, which is the primary application, as illustrated in the following section.

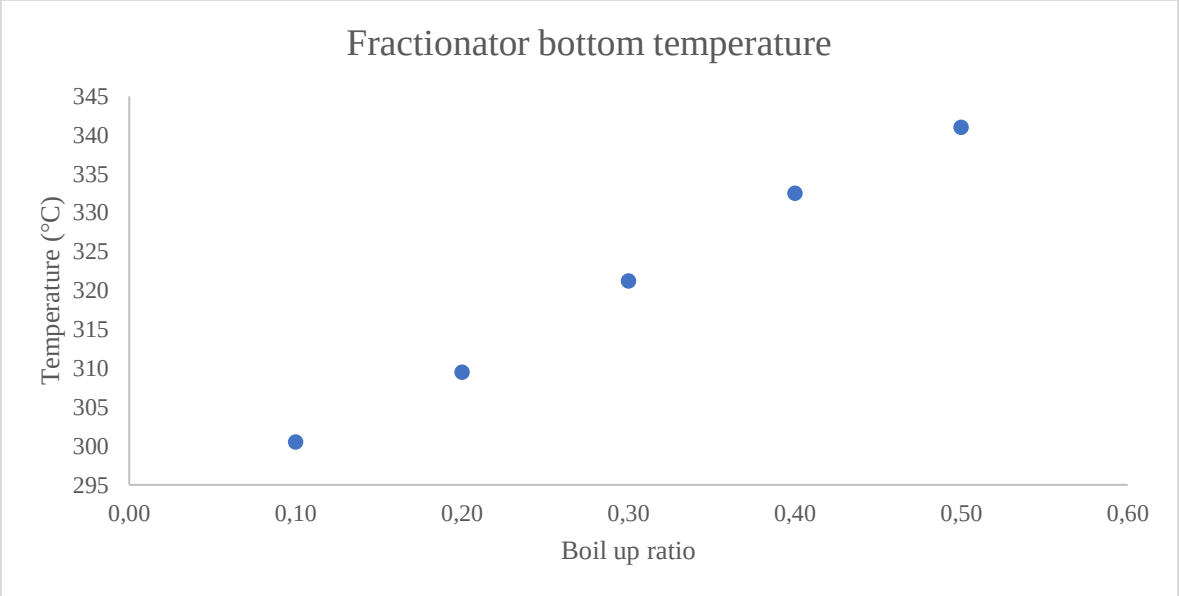

Figure 4-2: Effect of an increasing boil-up ratio on fractionator column bottom temperature at a constant reflux ratio of 0,30.

4.2.2 Product Quality Distribution

Selected quality parameters for the three distillate fractions; light oil, RCO, and creosote, are investigated for the manufacturing of 115 – 118 M pitch and distillates to study the influence of process control parameters on quality distributions.

The effect of a reflux ratio and top temperature on the naphthalene distribution in the light oil stream was studied at a constant boil-up ratio of 0,25, and the result is shown in Figure 4-3 below. The reflux ratio range of 0,050 to 1,45 at a step rate of 0,10 was used. Based on the results illustrated in Figure 4-3, the naphthalene fraction in light oil shows a decline with an increase in reflux ratio and the distillate rate also follows a similar behavior. The target naphthalene content in light oil is a value less 8% which is achieved at a reflux ratio greater than 0,95 according to the result in Figure 4-3, reducing the distillate rate even further to below 0,8 t/h. The changes in reflux ratio can be related to column top temperatures as discussed in Figure 4-1 with the column top temperature profile presented in Appendix L, Figure 8-14. Following this reasoning, the column top operating temperature should be kept below 103 °C to achieve a naphthalene content within specification for light oil (below 8%).

As explained in Section 4.2.1, the primary purpose of a reflux stream is to improve distillate quality through equilibrium mass transfer; hence, in this case, an increase in reflux ratio, which is shown by a drop in column top temperature and an improvement in light oil product quality.

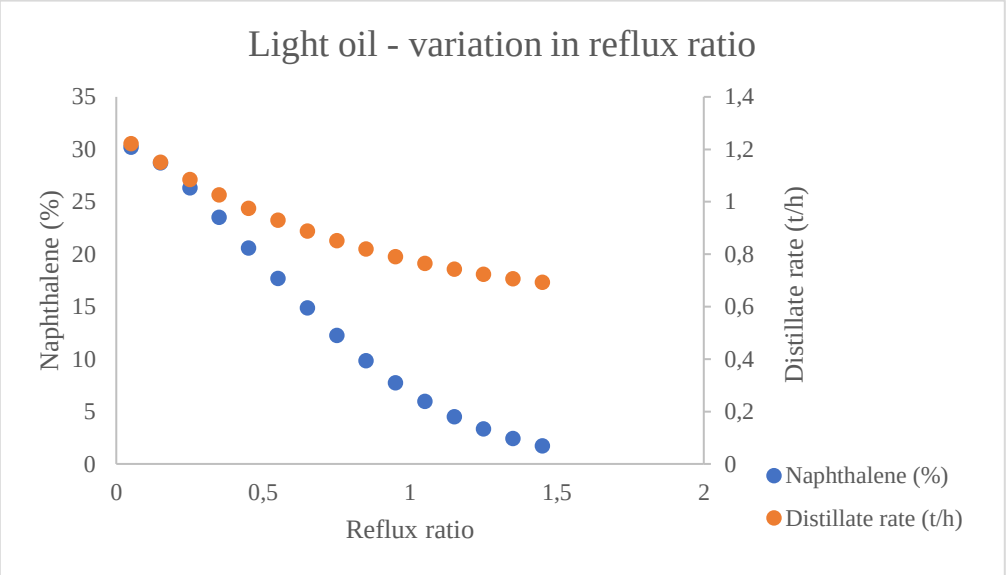

Figure 4-3: Naphthalene distribution in light oil stream with variation in top temperature at a constant boil-up ratio of 0,25.

The effect of boil-ratio changes from 0,01 to 1,49 at a step rate of 0,02 is shown in Figure 4-4 below at a constant reflux ratio of 0,95. The corresponding temperature profile is also presented in Appendix L, Figure 8-15. The boil-up ratio has an opposite effect compared to the reflux ratio, such that the distillate rate and the naphthalene content in light oil rise with an increase in the boil-up ratio.

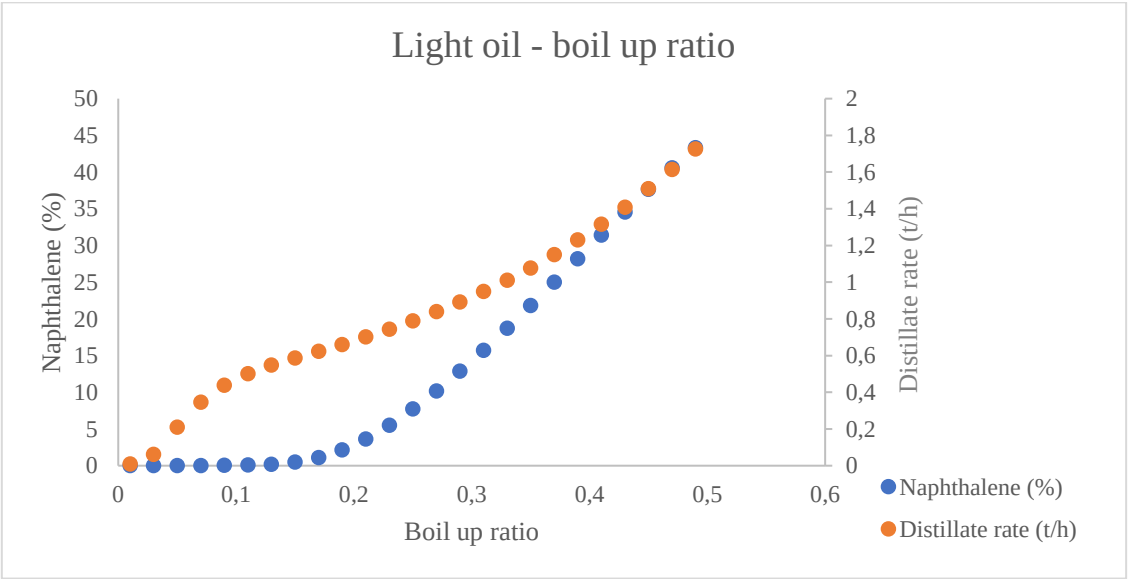

Figure 4-4: Naphthalene distribution in light oil with changes in boil up ratio at at constant reflux ratio of 0,95.

Light oil product is not a high value product in the reference plant and not much attention is given however maintaining good quality is crucial to avoid financial losses and being able to keep customer satisfaction.

With the RCO stream from the fractionator being the intermediate product for the recovery of naphthalene in the downstream processes, it is required that a higher yield is achieved for increased production rates as well as for stable operations and minimum energy requirements. In investigating the influence of operational parameters on the RCO quality, a boil-up ratio in the range of 0,10 to 0,50 at a step rate of 0,10 was applied. From Figure 4-5 below, it can be seen that a change in boil-up ratio from 0,10 to 0,30 had no significant influence on the naphthalene content; however, with an increase from 0,30 to 0,40 there was a notable drop from 58 % to 55 % and with a further reduction to 47 % at a boil up ratio of 0,50. In this case, low boil-up ratios are preferable unless accompanied by an increase in reflux ratio.

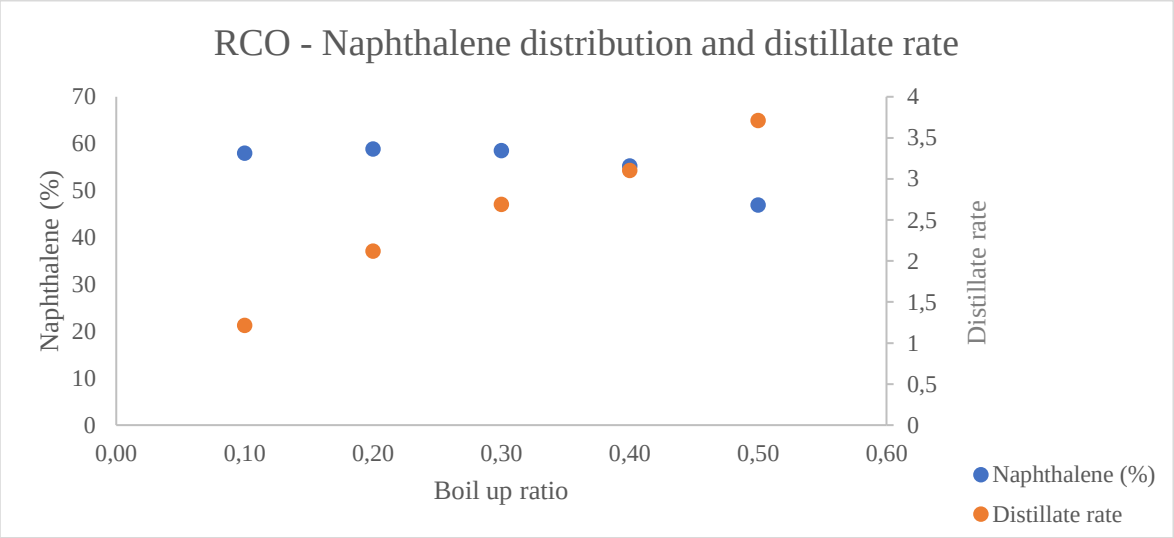

Figure 4-5: RCO stream naphthalene content variation with a boil-up ratio at a constant reflux ratio of 0,80.

There is a high value placed on the RCO distillate from the reference plant and the focus is not only based on the content of naphthalene but also the distillate rate or yield achieved. Figure 4-5 shows the RCO distillate rate on the secondary axis where it is demonstrated that an increase in boil-up ratio positively influences the amount of RCO recovered. However, the increase in the distillate rate is accompanied by a drop in naphthalene content and this creates a more complex situation for production teams to try and balance the two parameters.

The RCO analysis above warrants a further investigation into the RCO stream to check the possibility of maintaining high naphthalene contents whilst also improving the yield or the product distillate rate. A graph depicting the influence of the reflux ratio from 0,10 to 0,80 with the boil-up ratio held constant at 0,40 as this was the value showing optimum results between distillate rate and naphthalene content is presented in Figure 4-6 below. The general behaviour is such that an increase in reflux ratio increases the naphthalene content in the RCO distillate stream however this is accompanied by a decrease in the distillate rate with the two graphs intersecting at a reflux ratio of 0,70 with the resulting naphthalene content at 53% and a distillate rate of 3,2 t/h. This result gives a clearer view of the fractionator operation and what are the possibilities in terms of making decisions concerning quality and yield.

The fractionator operation as described above is concluded by assessing the related temperature profile of the column as indicated in Appendix L, Figure 8-16, and Figure 8-17. At column temperatures below 213°C and bottom temperature of 330°C, the two temperature operating points give a naphthalene content above 55% which meets the requirements specified by the plant.

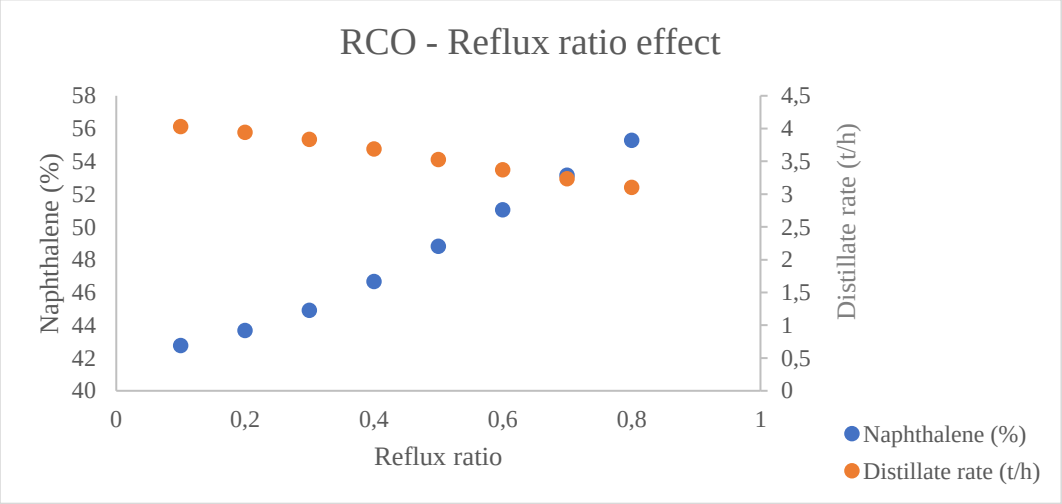

Figure 4-6: Impact of reflux ratio distribution of naphthalene and distillate rate in RCO.

The creosote column is very crucial in not only producing the creosote oil and managing the distillate quality, it is also used as a last control stage for the residue pitch quality depending on the type to be manufactured. Process conditions are intense for a hard pitch to remove most of the oils still present and less intense for the production of soft pitches. A reflux ratio variation of 1,5 to 3,0 at a step rate of 0,50 was chosen to study the impact of the reflux ratio condition on the light creosote density parameter at a constant boil-up ratio of 3,8. A linear relationship is observed as shown in Figure 4-7 below; mass density declines with an increase in reflux ratio from the creosote column. The stipulated density parameter for a light creosote product is a minimum of 1125 kg/m³, of which the results above show values in excess. A linear decline is also seen with regards to the distillate rate, from above 9 t/h at a 1,5 reflux ratio to 7,5 t/h at a reflux ratio of 3.

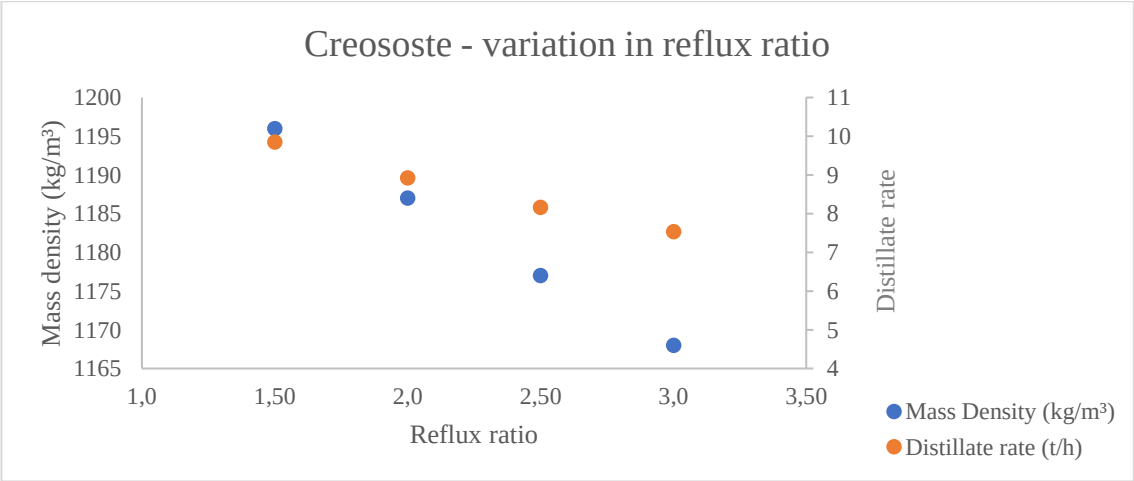

Figure 4-7: Influence of increasing reflux ratio to product density parameter at a constant boil-up ratio of 3,8.

4.3 Optimisation

After the establishment of the base conditions is the optimisation question to improve product quality and increase plant revenue. The optimisation process was developed in HYSYS using the original optimiser method by identifying the product revenue as the objective function with product qualities as constraints and adjustable parameters as process conditions applicable; the details of this process were described in Section 3.8.

4.3.1 Product quality and yield optimisation

Quality constraints on the light oil and RCO products are the naphthalene fraction as specified in Table 4-2 to achieve the customer requirements. Product mass density is the quality parameter for the light creosote oil with residue pitch viscosity used as a substitute for softening point characterisation. The column reflux and boil-up ratio were the adjustable parameters, and the selected objective function was the product revenue, which is calculated as the sum of the product distillate rate multiplied by the cost of each product. Product costs were taken as the values specified for the financial year 2022 from the reference plant, product cost data is shown in Appendix M, Table 8-17.

The quality constraints in the optimisation process were set up in such a way that the customer requirements are met as indicated in Table 4-2 and Table 4-3 under the requirements section.

Table 4-3: Comparison between base and optimal distillate qualities for the production of 115 - 118 M pitch.

Product	Unit	Base quality value	Optimised quality value	Requirement
Light oil	%			
Naphthalene		48	5,8	< 8,0
RCO	%			
Naphthalene		44	67	> 55
Light creosote	kg/m³			
Density		1147	1130	> 1125
115 - 118 M Pitch	cP			
Viscosity @ 160 °C		3523	4212	4200
Viscosity @ 140 °C		-	18110	18000

Through the optimization process, the naphthalene fraction in the light oil distillate was reduced from 48% to 5.8%, meeting the standard specification. The naphthalene content in RCO increased from 44% to 67%, which is beneficial for downstream processes. More naphthalene products can be recovered, and separation is easier with lower energy inputs. The light creosote, as well as the pitch product, are well within the required limits.

Obtaining good quality products to ensure customer satisfaction is important in the industry; however, the business has to make profits to sustain the operations and make good investor returns, therefore, how much product is being generated is also one of the parameters that are important in plant operations. Product yield is one of the basic parameters applied at the plant level to make a judgement of the plant performance. Based on the results in Table 4-4, the hard

pitch yield increased by 8,0 %, as well as the light creosote oil, which saw an increase of 14 %. The hard pitch yield of 49 % is consistent with the experimental study done by (Kozlov et al., 2021) and it is also general information in coal tar distillation to expect a yield of 50 % as mentioned in (Granda et al., 2014), (Baron et al., 2016).

Table 4-4: Product distillate comparison between base and optimised yields in the 115 – 118 M pitch production.

Product	Unit	Base yield	Optimised yield	Change
Light oil	**%**	9,3	0,34	-8,9
RCO	-	16	8,8	-6,9
Light creosote	-	27	40	14
Heavy oil	-	6,2	0,82	-5,4
115 - 118 M Pitch	-	42	50	8,0

According to the product cost information in Appendix M, these are valuable products because their price is high, and more production leads to increased revenues; hence, the optimiser search led to positive yield increases. The light oil distillate was reduced drastically by 9,0 %, this might be based on the low pricing of the product and the quality constraint. Like RCO and heavy oil, the product yields decreased by 6,9 % and 5,4 %, respectively.

Table 4-5: Comparison between base and optimal distillate qualities for the production of 68 - 73 M pitch.

Product	Unit	Base quality value	Optimised quality value	Requirement
Light oil	%			
Naphthalene		41	3,7	< 8,0
RCO	%			
Naphthalene		47	68	> 55
Light creosote	kg/m³			
Density		1154	1133	> 1125
68 - 73 RB Pitch	cP			
Viscosity @ 150 °C		237	274	280
Viscosity @ 170 °C		124	140	140

A similar approach used in the optimisation of the 115 – 118 M pitch production and associated distillates was applied to the 68 – 73 RB pitch process to maximise product revenue. The distillate qualities changed from out-of-specification values from the reference plant to within the required limits after optimisation of the process, as indicated in Table 4-5.

Optimisation of the 68 – 73 RB pitch process also led to the reduction of the light oil as well as the RCO product yields by 6,5 % and 4,9 %, respectively, as shown in Table 4-6. However, the pitch yield increased slightly by 3,1 % in comparison to the base pitch yield.

Table 4-6: Product distillate comparison between base and optimised yields in the 68 – 73 RB pitch production.

Product	Unit	Base yield	Optimised yield	Change
Light oil	**%**	6,5	0,024	-6,5
RCO	-	19	14	-5
Light creosote	-	9,6	17	7,4
Heavy oil	-	0,18	0,59	0,41
68 - 73 RB Pitch	-	65	68	3,0

4.3.2 Maximum product revenue

A total coal throughput of 25 t/h at a utilisation rate of 95 % was considered for the calculation of total revenue. In addition, the product split ratio based on the market demand as specified by the reference coal tar distillation plant was 57 % production of 115 – 118 M pitch and distillates with 43 % owing to the manufacturing of 68 – 73 RB pitch product. The procedure followed is illustrated below.

Total coal tar throughput:

$$25\frac{t}{h} \times 24\ hours \times 365\ days\ \times 0{,}95 = 208050\ tons\ per\ annum$$

115 – 118 M:

$$0{,}57\ \times 208050 = 118588{,}5\ tons\ per\ annum$$

68 – 73 RB:

$$0{,}43\ \times 208050 = 89461{,}5\ tons\ per\ annum$$

Detailed product revenue calculations, including product costs, are available in Appendix M.

Based on the optimisation of the product revenue calculated by maximising the objective function, the total product revenue to produce 115 – 118 M pitch increased from a base value of R 500 million to R 515,3 million per annum, which is a benefit of R 15,3 million per annum. Optimisation of the soft pitch 68 – 73 RB process showed a rise in product revenue sales from R 806 million to R 832 million per annum, which calculates to a benefit of R 26 million per annum.

The overall benefit of optimising the coal tar distillation plant based on the production of two pitch products mentioned above as per market demand is R 41,3 million per annum.

4.3.3 Comparison between initial and optimum conditions

In the production process of the 115 – 118 M pitch represented in Table 4-7, the first two columns, which are the dehydrator and the fractionator, show a reduction in the boil-up ratio

followed by an increase in the reflux ratio when comparing the initial condition and the optimum conditions. The boil-up ratio for the dehydrator was reduced by 86% with a drastic increase in reflux ratio of 0,062 to 1,3 from the initial condition, which led to lower column top temperatures than what it was operated for previously. The same is seen for the fractionator column, where the boil-up ratio decreased by 32 % with an increase in reflux ratio to achieve the maximum naphthalene recovery possible. These results are consistent with the conditions established in Section 4.2.2 on quality distributions. An improvement in light oil quality requires an increased reflux ratio or low column top temperature, and to obtain a good naphthalene recovery in RCO, a low boil-up ratio should be applied in the process.

Table 4-7: Change in operational parameters from initial to optimum conditions for 115 - 118 M pitch process.

Variable	**Dehydrator**		**Fractionator**		**Creosote**		**Flash column**	
	Initial	*Optimum*	*Initial*	*Optimum*	*Initial*	*Optimum*	*Initial*	*Optimum*
Reflux ratio	0,062	1,3	0,11	0,80	2,9	2,1	-	-
Boil up ratio	0,44	0,06	0,38	0,26	0,06	3,8	-	-
Top temperature (°C)	159	96	267	188	314	290	367	391
Bottom temperature (°C)	246	178	330	285	386	394	367	392
Top pressure (kPa)	-	-	-	-	-	-	18	18

The creosote column condition behaviour was different from the first two, which showed an increase in boil-up ratio and a reduction in reflux ratio by 29 %. Lastly, the flash column had no significant changes regarding pressure; however, an increase in top and bottom temperature was noted.

Table 4-8: Change in operational parameters from initial to optimum conditions for 68 - 73 RB pitch process.

Variable	**Dehydrator**		**Fractionator**		**Creosote**		**Flash column**	
	Initial	*Optimum*	*Initial*	*Optimum*	*Initial*	*Optimum*	*Initial*	*Optimum*
Reflux ratio	1,2	3,6	1,5	3	1	3	-	-
Boil up ratio	0,50	0,010	0,80	0,80	0,010	0,80	-	-
Top temperature (°C)	151	86	220	188	283	252	327	360
Bottom temperature (°C)	247	163	339	309	327	336	327	359
Top pressure (kPa)	-	-	-	-	-	-	25	18

In the production of soft pitch 68 – 73 RB and related distillate products, it can be seen from Table 4-8 that the dehydrator column changes are similar to the 115 – 118 M, however, the increase in reflux and reduction in the boil-up ratio are significant which resulted in a drop in both the top and bottom temperatures. The fractionator boil-up ratio stayed constant, and the reflux ratio doubled to recover more naphthalene in the distillate stream. A higher reflux ratio that is three times the initial value, as well as a decrease in boil-up ratio for the operation of a creosote column, is required for optimum results, with the flash column resulting in a 28 % decrease in pressure and an increase in operating temperatures.

5 Conclusion

The byproduct coal tar recovered from the coke oven batteries is still one of the most valuable sources of chemical products in the carbo-chemical industry and also plays an important role in the production of binder pitch for the manufacturing of electrodes in the aluminium industry. A coal tar distillation model consisting of four vacuum distillation columns was developed in the current research to study the process behaviour coupled with an optimiser to improve the distillate yields by maximising the overall product revenue.

The reference plant chosen for this study is an old coal tar distillation plant with limited data records and measurements of process variables; therefore, a plant mass balance was completed using available product data to produce a hard-pitch product with a softening point of 115 – 118 Mettler and associated distillates. The calculated mass balance was then adjusted and corrected through the mass balance reconciliation method in HYSYS by adjusting the Murphee tray efficiencies for each column to fit the product data. The developed simulation model was validated by running operating conditions specified for a pitch with a low softening point of 68 – 73 Ring and ball, thus, the product quality requirements were met. Therefore, through this process, base conditions were established, which were the starting point for optimisation.

Control variables selected for this study are the reflux ratio and boil-up ratio, which are monitored through column top temperature and bottom temperature as done in the coal tar distillation plant used for this study. The consistency of this control method was evaluated by simulating the influence of the selected parameters on product qualities. Based on the results, it was established that the dehydrator column has to operate at lower boil-up ratios when compared to the initial values and high reflux ratios to maintain light oil product quality below 8,0 % naphthalene content to meet the standard requirement and the fractionator column requires low boil up rate in comparison to the initial simulation for the recovery of naphthalene in the RCO to be above 55 %. Basically, the actual operation of the two columns mentioned above is more intense as the top and bottom temperatures are maintained at higher than what is required based on the current feed conditions. The mentioned product qualities of the two products were not within the quality standards from the reference plant, hence the attention given when compared to the rest of the columns. Through the quality distribution study carried out in Section 4.2.2 an operational philosophy for the coal tar distillation process focusing mainly on managing the quality of distillates from the three columns (dehydrator, fractionator, and creosote) was established.

The product revenue was selected as the objective function for the optimisation process, with product qualities as constraints and the reflux as the boil-up ratio as adjustable parameters. The first optimisation process was carried out for the hard pitch with softening points 115 – 118 M, and all product qualities were within specifications after optimisation of the process with a maximum revenue benefit of R 15,3 Million per annum, which is 3,1 % higher than the initial value. In achieving the maximum revenue benefit, the pitch product yield increased from 42 % to 49 %, with the light creosote yield also showing a positive yield by an increase of 14 %. This result is attributed to the financial value of the two products as they are more expensive; hence, the optimiser search increased their yields.

From (Kozlov et al., 2021), (Granda et al., 2014), and (Baron et al., 2016) it is mentioned that the general yield for pitch in coal tar distillation plant is 50%, therefore the optimisation process

got closer to what is expected theoretically from the process. This is also a well known fact from the operation of an actual coal tar distillation plant.

The changes in operational conditions were more intense in the optimisation simulation of a softer pitch product 68 – 73 RB and the distillates; however, the operational philosophy was the same as in the hard pitch production. The dehydrator column operational reflux ratio doubled from the initial value with a significant reduction in the boil-up ratio, which resulted in a naphthalene content of 3,6 % in the light oil stream. As with the fractionator column, the reflux ratio was also doubled with the boil-up ratio constant; this resulted in an increased recovery of the naphthalene content in RCO to 68 %, which is 0,69 % higher than in the production of a hard pitch. The pitch yields were not that significant at a 3,1 % increase; however, due to the high cost of a soft pitch product, an overall revenue benefit of R 26 million (3,2 % increase from the non-optimised condition) per annum was realised from the optimisation of the distillation process.

6 Recommendations

From the research proposal, it was initially planned that a full coal tar characterisation would be performed using the recommended standard distillation technique ASTM D1160 suggested for vacuum distillation; however, due to the unavailability of laboratories with facilities to perform these tests in the country, it was decided to use the limited data available. International laboratories were consulted, but due to high prices, it was decided not to go ahead with the tests. This data would have been beneficial in the sense that a full fractional composition can be specified in the simulation modelling to give more accurate behaviour and output predictions. However, we did manage to get by with a more laborious task of collecting past data even though not enough to build a proper model, process engineering techniques were applied to make it work. In the future, it would be more beneficial to perform the vacuum distillation tests and get a proper representation of the feed material.

The feed conditions were kept constant in the current work, with the temperature and flow rate not varied. This does not give a full spectrum of conditions normally encountered in real plant situations. Optimisation by adjusting feed conditions must be investigated to evaluate whether a potential benefit can be realised.

The current work did not consider the process energy balance; it would be interesting to also gain knowledge on the process overall energy consumption and strategies to minimise it.

Similar studies based on a much more modern coal tar distillation plant should be done. Enough process data and qualities can really help improve the quality of the models developed and provide much better insights as more control variables can be studied on how they influence the process and what advantages are available.

7 References

Al-Besharah, J. M., Salman, O. A., & Akashah, S. A. (1987). Viscosity of Crude Oil Blends. In *Ind. Eng. Chem. Res* (Vol. 26). https://pubs.acs.org/sharingguidelines

Alvarez, R., Barriocanal, / C, Canga, C. S., Canga, J. S., Diez, M. A., Gayol, / O M, & Miyar, E. A. (1989). Coke Oven Gas Control by One-Line Gas Chromatography. *Chromatographia, An International Journal for Separation Science*, *27*, 611–616. https://doi.org/https://doi.org/10.1007/BF02258988

Amundsoni, N. R., & Pontinen, A. J. (1958). Multicomponent Distillation Calculations on a Large Digital Computer. *Industrial & Engineering Chemistry*, *50*(5), 730–736. https://doi.org/https://doi.org/10.1021/ie50581a025

Baron, J. T., Mckinney, S. A., & Wombles, R. H. (2016). Coal Tar Pitch-Past, Present, and Future. *Essential Readings in Light Metals*, *4*, 177–181. https://doi.org/https://doi.org/10.1007/978-3-319-48200-2_25

Bennett, D. L., & Kovak, K. W. (2000). Optimize distillation columns. *Chemical Engineering Progress*, *96*(5), 19–34. www.aiche.org

Binay K. Dutta. (2007). *Principles of Mass Transfer and Separation Processes*. PHI Learning Private Limited.

Boston', J. F. (1974). A New Class of Solution Methods for Multicomponent, Multistage Separation Processes A new class of methods which does not possess. In *The Canadian Journal of Chemical Engineering* (Vol. 52).

Carlson, E. C. (1996). Don't gamble with physical properties for simulations. *Chemical Engineering Progress*, *92*(10), 35–46.

Casal, M. D., Díez, M. A., Alvarez, R., & Barriocanal, C. (2008). Primary tar of different coking coal ranks. *International Journal of Coal Geology*, *76*(3), 237–242. https://doi.org/10.1016/j.coal.2008.07.018

Ch, I. E. J., Plevan, R. E., Quinn, J. A., Ch, A. I. E. J., Rhodes, F. H., Bridges, C., Robb, I. D., Alexander, A. E., Rosano, H., Lamer, V. K., Springer, T. G., Plgford, R. L., Van Stralen, S. J. D., & Nether, ! (1973). A New Two-Constant Equation of State. In *Int. J. Heat Mass Transfer* (Vol. 19). https://pubs.acs.org/sharingguidelines

Coulson, J. M. (John M., & Richardson, J. F. (John F. (1979). *Chemical engineering*. Pergamon Press.

Crowe, C. M. (1986). Reconciliation of Process Flow Rates by Matrix Projection Part II: The Nonlinear Case. *AIChE Journal*, *32*(4), 616–623. https://doi.org/https://doi.org/10.1002/aic.690320410

Crowe, C. M., Campos, Y. G., & Hrymak, A. (1983). Reconciliation of Process Flow Rates by Matrix Projection Part I: Linear Case. *AIChE Journal*, *29*(6), 881–888. https://doi.org/https://doi-org./10.1002/aic.690290602

C-Y Lu, B., & Peng, D. (1993). Prediction of Point Efficiency for Sieve Trays in Distillation. In *I & EC Research* (Vol. 32).

Díez, M. A., Alvarez, R., & Barriocanal, C. (2002). Coal for metallurgical coke production: predictions of coke quality and future requirements for cokemaking. In *International Journal of Coal Geology* (Vol. 50, Issues 1–4). https://doi.org/https://doi.org/10.1016/S0166-5162(02)00123-4

Diez, M. A., & Garcia, R. (2018). Coal tar. In *New Trends in Coal Conversion: Combustion, Gasification, Emissions, and Coking* (pp. 439–487). Elsevier. https://doi.org/10.1016/B978-0-08-102201-6.00015-7

Documentation Team, A. (2004). *HYSYS ® 2004.2 Operations Guide*. http://www.aspentech.com

Dutta, S. (2016a). Multivariable Optimization with Constraints. In *Optimization in Chemical Engineering* (pp. 119–156). Cambridge University Press. https://doi.org/10.1017/cbo9781316134504.007

Dutta, S. (2016b). Optimization of Unconstrained Multivariable Functions. In *Optimization in Chemical Engineering* (pp. 86–118). Cambridge University Press. https://doi.org/10.1017/cbo9781316134504.006

Ernest, D., Henley, J., & Seader, J. D. (2011). *Separation Process Principles: Chemical and Biochemical Operations* (3rd ed.). John Wiley & Sons, Inc.

Ernest, H. J., & Seader, J. D. (1981). *Equilibrium-stage separation operations in chemical engineering*. John Wiley & Sons, Inc.

Fletcher, R., & Powell, M. J. D. (1963). A rapidly convergent descent method for minimization. *The Computer Journal*, *6*(2), 163–168. https://doi.org/https://doi.org/10.1093/comjnl/6.2.163

Franck, H.-G., & Stadelhofer, J. W. (1988). Industrial Aromatic Chemistry. In *Industrial Aromatic Chemistry*. Springer Berlin Heidelberg. https://doi.org/10.1007/978-3-642-73432-8

Friday, J. R., & Smith, B. D. (1964). *An Analysis of the Equilibrium Stage Separations Problem-Formulation and Lonvergence*.

Giwa, A., & Karacan, S. (2012). Simulation and optimization of ethyl acetate reactive packed distillation process using Aspen HYSYS. *TOJSAT*, *2*(2). www.tojsat.net

Goldstein, R. P., & Stanfield, R. B. (1964). Mathematics of Diffusion. In *Sterba, M. J., Hydrocarbon Process. Petrol. Refiner* (Vol. 63, Issue 74). Oxford University Press. https://pubs.acs.org/sharingguidelines

Granda, M., Blanco, C., Alvarez, P., Patrick, J. W., & Menéndez, R. (2014). Chemicals from coal coking. In *Chemical Reviews* (Vol. 114, Issue 3, pp. 1608–1636). https://doi.org/10.1021/cr400256y

Henry Z. Kister. (1990). *Distillation Operation*. McGraw-Hill Education.

Henry Z. Kister. (1992). *Distillation Design*. McGraw-Hill, Inc.

H'ng, S. X., Ng, L. Y., Ng, D. K. S., & Andiappan, V. (2021). Optimising of vacuum distillation units using surrogate models. *IOP Conference Series: Materials Science and Engineering*, *1195*(1), 012050. https://doi.org/10.1088/1757-899x/1195/1/012050

Holland, C. D. (1981). *Fundamentals of multicomponent distillation*. McGraw-Hill.

Ibrahim, D., Jobson, M., & Guillén-Gosálbez, G. (2017). Optimization-Based Design of Crude Oil Distillation Units Using Rigorous Simulation Models. *Industrial and Engineering Chemistry Research*, *56*(23), 6728–6740. https://doi.org/10.1021/acs.iecr.7b01014

I.C. Lewis. (1982). Chemistry of Carbonization. In *Carbon* (Vol. 20, Issue 6). https://doi.org/https://doi-org/10.1016/0008-6223(82)90089-6.

Johann G. Stichlmair, Harald Klein, & Sebastian Rehfeldt. (2021). *Distillation: Principles and Practice* (2nd ed.). John Wiley & Sons.

Kozlov, A. P., Cherkasova, T. G., Frolov, S. V., Subbotin, S. P., & Solodov, V. S. (2020). Innovative Coal-Tar Products at PAO Koks. *Coke and Chemistry*, *63*(7), 344–350. https://doi.org/10.3103/S1068364X20070054

Kozlov, A. P., Cherkasova, T. G., Subbotin, S. P., Solodov, V. S., & Pimonov, A. G. (2021). Dependence of the Softening Temperature of Coal Pitch on the Conditions of Coal-Tar Distillation. *Coke and Chemistry*, *64*(2), 73–79. https://doi.org/10.3103/S1068364X21020022

Kuan Shih Yuan, James C. K. Ho, Benjamin C. -Y. Lu, & A. K. Koshpande. (1963). Vapor-Liquid Equilibria. *Journal of Chemical and Engineering Data*, *8*(4), 549–559. https://doi.org/https://doi-org/10.1021/je60019a024

Kumar Gupta, A., Sen, S., Kumar, R., Ramna, R. V, Kumari, S., Dhakate, S., & Gupta, A. K. (2021). Effect of Process Parameter on Coal Tar Distillate Products. *American Journal of Chemical and Biochemical Engineering*, *5*(2), 55–60. https://doi.org/10.11648/j.ajcbe.20210502.13

Lewis. W. K. (1922). The Efficiency and Design of Rectifying Columns for Binary Mixtures. *Industrial & Engineering Chemistry*, *14*(6), 492–496. https://doi.org/https://doi.org/10.1021/ie50150a010

Lewis, W. K. (1936). Rectification of Binary mixtures. *Industrial & Engineering Chemistry*, *28*(4), 399–402. https://doi.org/https://doi.org/10.1021/ie50316a005

Lewis, W. K., & Matheson, G. L. (2023). *Studies in Distillation Design of Rectifying Columns for Natural and Refinery Gasoline* (Vol. 11). UTC. https://pubs.acs.org/sharingguidelines

Li, J.-K., Feng-Hua, W., & Hua-Ling, S. (2009). The 6 th International Conference on Mining Science & Technology Differences in coal consumption patterns and economic growth between developed and developing countries. *PROEPS*, *1*, 1744–1750. https://doi.org/10.1016/j.pro

Liau, L. C. K., Yang, T. C. K., & Tsai, M. Te. (2004). Expert system of a crude oil distillation unit for process optimization using neural networks. *Expert Systems with Applications*, *26*(2), 247–255. https://doi.org/10.1016/S0957-4174(03)00139-8

Loison, Roger., Foch, Pierre., & Boyer, A. (2014). *Coke : quality and production* (2nd ed., Vol. 2). Elsevier, 2014.

López, D. C., Hoyos, L. J., Mahecha, C. A., Arellano-Garcia, H., & Wozny, G. (2013). Optimization model of crude oil distillation units for optimal crude oil blending and operating conditions. *Industrial and Engineering Chemistry Research*, *52*(36), 12993–13005. https://doi.org/10.1021/ie4000344

Ma, Z. H., Wei, X. Y., Liu, G. H., Liu, F. J., & Zong, Z. M. (2021). Value-added utilization of high-temperature coal tar: A review. In *Fuel* (Vol. 292). Elsevier Ltd. https://doi.org/10.1016/j.fuel.2020.119954

Maloletnev, A. S., Gyul'Maliev, A. M., & Mazneva, O. A. (2014). Chemical composition of the distillate fractions of coal tar from OAO Altai-Koks. *Solid Fuel Chemistry*, *48*(1), 11–21. https://doi.org/10.3103/S0361521914010066

Manera, C., Fragoso, H. P., Agra, A. A., Flores, B. D., Osório, E., Godinho, M., & Vilela, A. C. F. (2023). Systematic mapping of studies on coal tar and pitch over the last five decades (1970–2023). *Chemical Engineering Research and Design*, *196*, 427–450. https://doi.org/10.1016/j.cherd.2023.06.063

Milo D. Koretsky. (2012). *Engineering and Chemical Thermodynamics* (2nd ed.). John Wiley & Sons.

Mittal, V., Zhang, J., Yang, X., & Xu, Q. (2011). E3 Analysis for crude and vacuum distillation system. *Chemical Engineering and Technology*, *34*(11), 1854–1863. https://doi.org/10.1002/ceat.201100242

Murphree, E. V. (1925). Rectifying Column Calculations. *Industrial & Engineering Chemistry*, *17*(7), 747–750. https://doi.org/https://doi.org/10.1021/ie50187a044

Naphtali, L. M., & Sandholm, D. P. (1971). *Multicomponent Separation CaIcuIations by Linearization*.

Nelder, J. A., & Mead, R. (1965). A simplex method for function minimization. *The Computer Journal*, *7*(4), 308–313. https://doi.org/https://doi.org/10.1093/comjnl/7.4.308

Perruchoud, R. C., Meier, M. W., & Fischer, W. (2016). WORLDWIDE PITCH QUALITY FOR PREBAKED ANODES. *Essential Readings in Light Metals*, *4*, 167–176. https://doi.org/https://doi.org/10.1007/978-3-319-48200-2_24

Piccolo, M., Douglas, P. L., & Lee, P. L. (1996). Data reconciliation using AspenPlus. *Developments in Chemical Engineering and Mineral Processing*, *4*(3–4), 157–182. https://doi.org/https://doi.org/10.1002/apj.5500040303

Pintarič, Z. N., & Kravanja, Z. (2006). Selection of the economic objective function for the optimization of process flow sheets. *Industrial and Engineering Chemistry Research*, *45*(12), 4222–4232. https://doi.org/10.1021/ie050496z

Powell, M. J. D. (1964). An efficient method for finding the minimum of a function of several variables without calculating derivatives. *The Computer Journal*, *7*(2), 155–162. https://doi.org/https://doi.org/10.1093/comjnl/7.2.155

Redlich, O., & Kwong, J. N. S. (1949). On the Thermodynamics of Solutions. *Chemical Reviews*, *44*(1), 233–244. https://doi.org/https://doi.org/10.1021/cr60137a013

Renon, H., & Prausnitz, J. M. (1968). Local compositions in thermodynamic excess functions for liquid mixtures. *AIChE Journal*, *14*(1), 135–144. https://doi.org/https://doi.org/10.1002/aic.690140124

Resetarits, M. R., & Lockett, M. J. (2003). Distillation. In *Encyclopedia of Physical Science and Technology* (pp. 547–559). Elsevier. https://doi.org/10.1016/B0-12-227410-5/00182-4

Review, A. E. A. W., & Werner, A. E. A. (1953). *Maney Publishing International Institute for Conservation of Historic and Artistic Works* (Vol. 1, Issue 2). http://www.jstor.orgURL:http://www.jstor.org/stable/1505051

Ricardo, J., López, G., Luis, J., Zapata, G., Leguizamón, A., Gerardo, R., & Niño, R. (2015). *Process Analysis and Simulation in Chemical Engineering* (1st ed.). SpringerCham. https://doi.org/https://doi.org/10.1007/978-3-319-14812-0

Richardson, J. F., Harker, J. H., Backhurst, J. R., & Coulson, R. ’. (1991). *Chemical Engineering Particle Technology and Separation Processes Volume 2 Fifth Edition*. www.elsorier.com

Robinson, D. B., Peng, D.-Y., Chung, S. Y.-K., & Robinson, D. B. (1985). The development of the Peng-Robinson equation and its application to phase equilibrium in a system containing methanol. In *Fluid Phase Equilibria* (Vol. 24).

Romanova, N. A., Leont’ev, V. S., & Khrekin, A. S. (2018). Production of Commercial Naphthalene by Coal-Tar Processing. *Coke and Chemistry*, *61*(11), 453–456. https://doi.org/10.3103/S1068364X18110078

Romovacek, G. R. (2013). Influence of solid particles in pitch on the preparation and baking of the carbon blocks. *Essential Readings in Light Metals*, *4*, 225–231. https://doi.org/https://doi.org/10.1007/978-3-319-48200-2_29

Schobert, H. (2013). Carbonization and coking of coal. In *Chemistry of Fossil Fuels and Biofuels* (pp. 415–434). Cambridge University Press. https://doi.org/10.1017/cbo9780511844188.024

Seader, J. D., Henley, E. J., & Wiley, J. (2006). *Separation Process Principles Second Edition*. http://www.wilev.com/eo/permissions.

Soave, G. (1972). Equilibrium constants from a modified Redkh-Kwong equation of state. In *Chemical Engineering Science* (Vol. 27). Pergamon Press.

Stansberry, P. G., Zondlo, J. W., & Stiller, A. H. (1999). *CHAPTER 7 C o a1-D erive d Carbons*. https://doi.org/10.1016/B978-0-08-042683-9.50009-1

Sundholm, J., Valia, H., Kiessling, F., Richardson, J., Buss, W., Worberg, R., Schwarz, U., Baer, H., Calderon, A., & DiNitto, R. G. (1999). *Chapter 7, Manufacture of Metallurgical Coke and Recovery of Coal Chemicals*.

Taylor, R., & Duss, M. (2019). 110th Anniversary: Column Efficiency: From Conception, through Complexity, to Simplicity. *Industrial and Engineering Chemistry Research*, *58*(36), 16877–16893. https://doi.org/10.1021/acs.iecr.9b02378

Teja. A. S, & Holm. L. J. (2000). Vapour - Liquid Equilibrium: Theory. *Chemical Engineering*, *68*(639), 644.

Thiele, E. W., & Geddes, K. L. (1933). Computation of Distillation Apparatus for Hydrocarbon Mixtures. *Industrial & Engineering Chemistry*, *25*(3), 289–295. https://doi.org/https://pubs.acs.org/doi/10.1021/ie50279a011

Tiwari, H. P., Sharma, R., Kumar, R., Mishra, P., Roy, A., & Haldar, S. K. (2014). A review of coke making by-products. In *Coke and Chemistry* (Vol. 57, Issue 12, pp. 477–484). Allerton Press Incorporation. https://doi.org/10.3103/S1068364X14120072

Venter, G. (2010). Review of Optimization Techniques. *Encyclopedia of Aerospace Engineering, Wiley & Sons Ltd.*, 2–12. https://doi.org/doi: 10.1002/9780470686652.eae495

Viswanathan, B. (2017). Coal. In *Energy Sources* (pp. 81–111). Elsevier. https://doi.org/10.1016/B978-0-444-56353-8.00004-6

Yanagi, T. (1990). Inside a trayed distillation column. *Chemical Engineering*, *97*(11), 120–129.

8 Appendix

8.1 Appendix A: Distillation equipment and the tray performance characteristics

8.1.1 Distillation equipment

It has been reported that the average distillation columns in petroleum and refinery operations are in the order of 1 – 4 m in diameter and 15 – 50 m tall (Resetarits & Lockett, 2003). Columns as big as 15 m in diameter and 100 m in height have also been reported; however, there are not many of them around the world, as larger columns are more expensive and difficult to construct.

Below is a summary of the distillation column and other important auxiliary equipment.

8.1.1.1 The shell

The column shell material is selected based on the corrosiveness of the fluid medium to be processed, the temperature, and the operating pressure. In most cases, carbon steel is the typical material of construction. However, more expensive materials such as stainless steel, titanium, nickel, and ceramic are used whenever corrosive fluids are encountered (Henry Z. Kister, 1992).

Another important parameter in the column design is the shell thickness, which is a function of operating pressure and height. A prescribed method for shell thickness determination is the ASME section VIII standard vessel design code. A high number of trays inside the column requires an increase in height, and this necessitates a thicker shell for proper support and stability so that wind forces do not destroy the column.

Distillation columns are normally supported on concrete foundations. The support should be strong enough to withstand the column weight, liquid load, and wind forces. The seismic factor is also considered in the design since wind stresses are high at the lower parts of the column; hence, most shells are made thicker at the bottom.

8.1.1.2 Inside the column

A single pass tray arrangement is illustrated in Figure 8-1. This shows how the distillation process takes place inside the column. Liquid dispersion flows from the upper tray as gas bubbles through it and overflows past the outlet weir down the downcomer area to the next tray below. For high-pressure operations, multi-pass trays are used to avoid fluid flow problems associated with vapour velocities, such as the entrainment of liquid particles in the up-flowing gas. The downside of multi-pass trays is that they are expensive and difficult to construct. At low-flow operations, packing is normally used to promote vapour-liquid contact. The known types of packing are dumped as well as structured packing. In this process, the liquid is introduced through distributors, which causes trickling down of streams through packings. Packing distillation is not covered in this review; detailed readings on this topic can be found in reference (Bennett & Kovak, 2000).

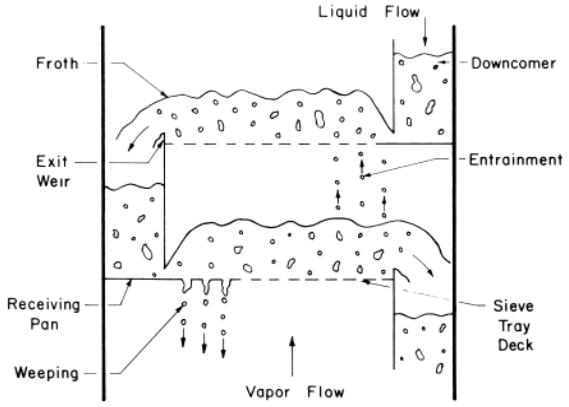

Figure 8-1: A schematic representation of a single pass distillation tray, ***adapted from***: (Resetarits & Lockett, 2003).

A tray is the heart of the distillation process as it serves two very important functions: as vapour comes into contact with the liquid, a gas-liquid dispersion is formed, and the tray holds the dispersion. Mass transfer occurs on the tray; therefore, the performance of the process depends on the tray dynamics.

There are different types of trays available in the market; the three most common ones are discussed below.

8.1.1.3 Distillation trays

The bubble cap tray is one of the oldest trays used in distillation. However, it is not in great use in the industry nowadays unless high liquid flow rates are required (Binay K. Dutta, 2007). A bubble cap tray consists of a cap and a riser bolted onto the tray floor, with the cap bolted onto the riser. The riser allows vapour passage from the bottom through the cap openings in this arrangement. An assembly of a bubble cap tray is shown in Figure 8-2 (a). The material of construction is usually carbon steel; however, any material of choice can be used depending on the column environment.

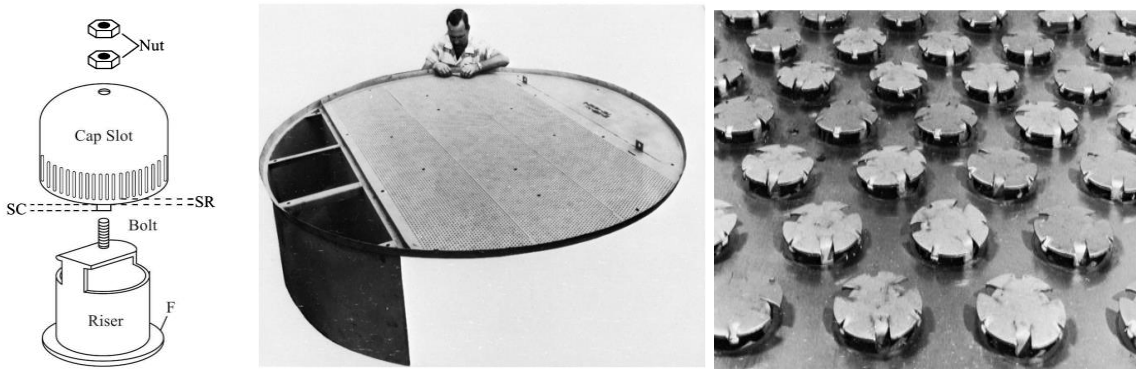

(a) (b) (c)

Figure 8-2: (a) Mechanical assembly of a bubble cap, (b) Sieve tray, (c) Valve tray, ***adapted from***: (Binay K. Dutta, 2007).

A sieve tray is still widely used in industry as it is cheap and easy to construct. Sieve trays have punctured holes or perforations to allow gas to bubble through the liquid. Smaller holes increase the tray capacity to hold more froth and reduce weeping as well as entrainment of liquid droplets into the vapour phase (Yanagi, 1990).

A new class of trays in the market is the valve trays, which provide a variable area for gas-liquid contact depending on flow conditions inside the column. Valve trays consist of disk guides that slide up and down from the tray floor fitted with a circular disk. As gas flow increases, the disk is raised automatically from the tray floor, and its height depends on the gas throughput. At low vapour flow rates, the circular disk settles down to prevent the weeping of liquid droplets, thereby improving the performance of the distillation process. The benefits of valve trays are that they have a high turndown ratio, do not get blocked easily, offer low-pressure drop, and come at a reasonable price (Binay K. Dutta, 2007).

8.1.1.4 Downcomer and the Outlet Weir

The downcomer plate provides a guide for liquid-gas dispersion from one tray to the one below it, with the weir plate bolted onto the downcomer plate for maintaining the required depth of the dispersion on the tray. As the froth overflows from the outlet weir into the downcomer passage, gas bubbles disengage, and a clear liquid flows down to the next tray. The downcomer must allow enough residence time for the disengagement of gas bubbles; 3 – 5 seconds is normally applied in design; however, higher residence times are required for foaming liquids necessitating larger downcomer areas (Henry Z. Kister, 1992).

8.1.2 Tray performance characteristics

The gas-liquid dispersion on a tray shows three different characteristics, as illustrated in Figure 8-3, and all depend on the flow rate of the rising vapour and the downflowing liquid. The spray action becomes dominant at high gas flow rates as the high velocities disintegrate the liquid into droplets. These droplets can be carried over to the next upper tray, causing the accumulation of liquid and, thus, flooding. At low vapour flow rates and high liquid flow, the gas bubbles are slow to rise through the dispersion and are thereby sheared by the fast-moving liquid. The mixture of liquid with slow-rising bubbles has the appearance of an emulsion.

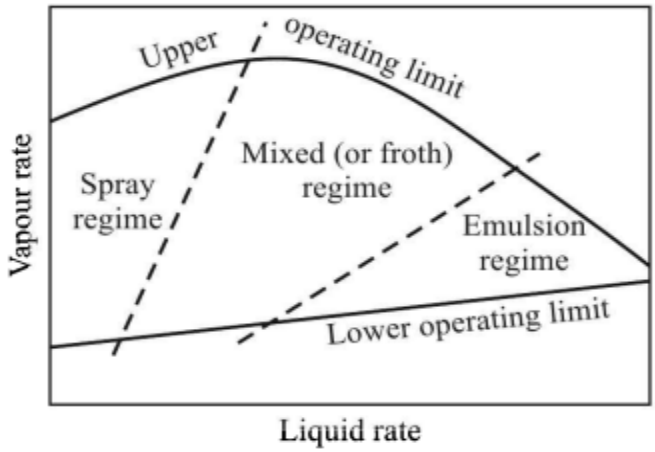

Figure 8-3: Flow regimes of a sieve tray, ***adapted from***: (Yanagi, 1990).

The preferred regime of operation is between the spray and emulsion, known as the froth or mixed regime. The gas velocity is low enough not to cause carry-over of droplets but at the same time high to prevent the formation of an emulsion.

8.2 Appendix B: Distillate product qualities

Table 8-1: GC - MS analysis for 115 - 118 M pitch distillates.

	115 - 118 Pitch				
Distillate	**GC - MS Analysis**				
	Light fractions	Tar acids	Methyl naphthalene	Naphthalene	Phenanthrene & Anthracene
Light oil	-	-	0	43	0
RCO	9,82	4,59	7,11	43,6	7,56
LCO	0	0	-	6,9	26
HO	0	0	0	0	21,5

Table 8-2: GC - MS analysis for 68 - 73 RB pitch distillates.

	68 - 73 Pitch				
Distillate	**GC - MS Analysis**				
	Light fractions	Tar acids	Methyl naphthalene	Naphthalene	Phenanthrene & Anthracene
Light oil	-		0	41	0
RCO	7,65	4,12	9,06	46	10,4
LCO	0	0	-	11,5	26
HO	0	0	0	0	26

8.3 Appendix C: Pitch Quality Data

Table 8-3: 115 - 118 M pitch quality parameters.

Sample Date	Tank	Product	Viscosity 160°C	MIT	QI (%, m/m)	Relative density of pitch	Softening Point
2022/01/11	PT6	115_118M	3168	36,52	12,098	1,326	115,1
2022/02/24	PT6	115_118M	3680	0,18	11,848	1,326	115
2022/03/23	PT6	115_118M	3680	38,06	11,848	1,326	115
2022/04/27	PT6	115_118M	4864	37,79	11,777	1,325	117,3
2022/05/14	PT6	115_118M	4096	38,37	11,523	1,324	115
2022/06/27	PT6	115_118M	3552	35,64	11,771	1,325	115
2022/07/18	PT6	115_118M	3008	35,35	11,83	1,322	115,3
2022/08/23	PT7	115_118M	3584	40,13	13,285	1,314	116,1
2022/09/16	PT6	115_118M	3584	36,12	13,853	1,322	115,1
2022/10/26	PT6	115_118M	3466	39,76	12,796	1,316	115,7
2022/10/26	PT6	115_118M	3466	39,76	12,796	1,316	115,7
2022/11/24	PT6	115_118M	4096	37,02	12,753	1,317	116,7
2022/12/26	PT6	115_118M	3680	40,53	14,079	1,316	115,7
			Avg				**Avg**
			3686,462				115,5923077
			Std. dev				**Std. dev**
			446,1425				0,702152228

Table 8-4: 68 - 73 RB pitch quality parameters.

Sample Date	Tank	Product	150°C	170°C	QI %	Relative density of pitch	Ring and Ball SP
2022/12/28	T9	68_73RB	259	112	9,906	1,29	71
2022/12/19	T9	68_73RB	227	105	10,124	1,288	68,5
2022/12/09	T7	68_73RB	233	99	10,435	1,293	70
2022/12/05	T9	68_73RB	233	102	10,523	1,29	70,5
2022/11/28	T7	68_73RB	297	124	11,697	1,29	73
2022/11/17	T9	68_73RB	252	101	12,893	1,29	68,5
2022/11/16	T7	68_73RB			11,642	1,29	68
2022/11/09	T7	68_73RB			9,173	1,293	68,5
2022/10/25	T9	68_73RB	307	134	10,38	1,289	72
2022/10/07	T9	68_73RB	236	99	9,344	1,292	70,5
2022/09/30	PT6	68_73RB	252	108,8	9,012	1,294	72
2022/09/15	T9	68_73RB	252	112	10,494	1,29	72,5
2022/09/14	PT6	68_73RB	344	147	10,374	1,291	71,5
2022/09/12	T7	68_73RB	246	125	11,552	1,293	71,5
2022/09/05	T7	68_73RB	208	96	9,847	1,291	70
2022/08/29	T7	68_73RB	345	156	12,349	1,29	72,5
2022/08/11	T7	68_73RB	205	99	10,681	1,289	69

Sample Date	Tank	Product	150°C	170°C	QI %	Relative density of pitch	Ring and Ball SP
2022/08/10	T9	68_73RB	233	115	11,38	1,29	71,5
2022/07/30	T7	68_73RB	310	137	11,244	1,295	73
2022/07/27	T9	68_73RB	208	108	11,249	1,294	71
2022/07/11	T9	68_73RB	192	102	13,014	1,288	70
2022/07/11	PT7	68_73RB	250	124	13,84	1,29	70,5
2022/06/17	T9	68_73RB	240	108	11,728	1,295	71
2022/06/07	T9	68_73RB	194	98	11,498	1,29	70,5
2022/06/02	PT6	68_73RB	246	115	11,546	1,292	72,5
2022/05/31	T9	68_73RB	192	96	11,776	1,295	68,5
2022/05/30	T7A	68_73RB	204	99	11,873	1,287	71
2022/05/30	T7A	68_73RB	204	99	11,873	1,287	71
2022/05/06	PT6	68_73RB	352	153,6	11,97	1,297	71,5
2022/05/06	PT6	68_73RB	352	153,6	11,97	1,297	71,5
2022/05/05	T9	68_73RB	220	124	11,404	1,296	69,5
2022/05/03	T7	68_73RB	230	105	12,043	1,292	69,5
2022/04/22	T9	68_73RB	211	108	11,839	1,288	70
2022/04/15	T9	68_73RB	201	92	11,345	1,294	71
2022/04/11	T9	68_73RB	195	89,6	10,883	1,295	70
2022/04/07	T7A	68_73RB	156	83	12,044	1,29	68,5
2022/03/21	T7A	68_73RB	208	102	11,603	1,296	70
2022/03/11	T9	68_73RB	176	89,4	11,099	1,293	69
2022/03/04	T9	68_73RB	173	89,6	11,277	1,298	68,5
2022/03/02	PT6	68_73RB	256	122	11,354	1,292	68
2022/02/25	T9	68_73RB	182	86	9,811	1,295	70,5
2022/02/18	T9	68_73RB	192	96	11,465	1,294	70
2022/02/12	T7	68_73RB	176	89,6	11,038	1,292	68
2022/02/07	T9	68_73RB	227	140	12,591	1,292	70,5
2022/01/31	T602	68_73RB	209	105	11,438	1,294	73
2022/01/25	T7	68_73RB	211	105	10,634	1,292	68
2022/01/22	T9	68_73RB	201	92	10,073	1,289	71
2022/01/18	T9	68_73RB	246	115	12,062	1,291	72,5
2022/01/13	T9	68_73RB	160	80	11,103	1,291	73
2022/01/10	T602	68_73RB	224	112	12,082	1,297	69,5
2022/01/04	T9	68_73RB	217	99	10,64	1,29	71,5
2022/01/04	T9	68_73RB	217	99	10,64	1,29	71,5
2022/01/03	T602	68_73RB	211,7	99,2	11,544	1,289	70,5
			Avg	**Avg**			
			230,837	108,8314			
			Std. dev	**Std. dev**			
			47,0265	18,29721			

8.4 Appendix D: Comparison between Actual and Simulated mass balance (115 – 118 M pitch product and distillates).

The following assumptions were made to complete the plant mass balance. This data is based on information received from an experienced production planner who performs mass balances on a daily basis to calculate production figures and do stock planning.

Assumptions:

- Light oil yield – 4 %.
- RCO yield – 16 %.
- Light fractions are only present in light oil and RCO.
- Light creosote yield – 24 %.
- Heavy oil yield – 6 %.

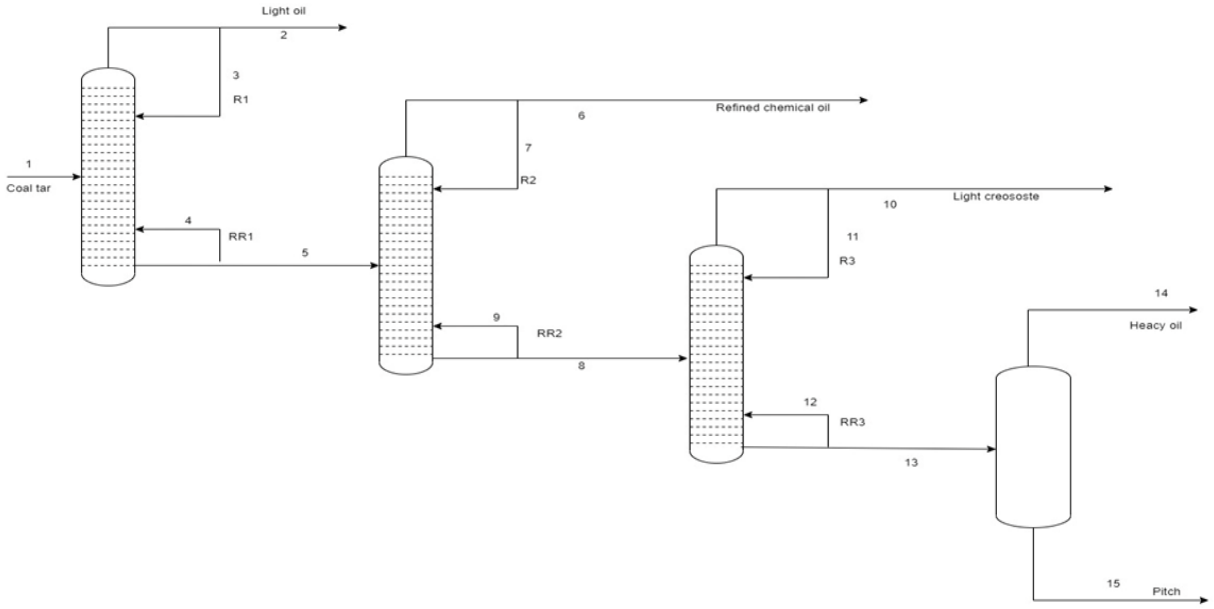

Figure 8-4: Coal tar distillation process flow diagram.

Table 8-5: Actual plant mass balance for the production of 115 - 118 M pitch and distillates.

Stream No.	Description	Composition							
		Light fractions	Tar acids	M Naphthalene	Naphthalene	P&A	Heavy carbon	Residue	Total
1	Coal tar	0,029	0,017	0,011	0,1146	0,087396	0,241	0,500	1
2	Light oil	0,320	0,250	0	0,43	0	0	0	1
3									0
4									0
5	Dehydrated	0,0164	0,0077	0,0119	0,1014	0,0910	0,2508	0,5208	1
6	RCO	0,0982	0,0459	0,0711	0,436	0,0756	0,2732	0	1
7									0
8	Fract bottom	0	0	0,0000	0,0345	0,0941	0,2464	0,6250	1
9									0
10	LCO	0	0	0,0000	0,0690	0,2600	0,6710	0	1
11									0
12									0
13	Soft pitch	0	0	0	0	0,0230	0,0644	0,8929	1
14	Heavy oil	0	0	0	0	0,2150	0,7850		1
15	Pitch	0	0	0	0	0	0	1	1

Table 8-6: Simulation mass balance for the production of 115 - 118 M Pitch product.

	Unit	Crude tar	Feed tar	Light oil	Dehydrated tar	RCO	Creosote Feed	Light Creosote	Soft Pitch	Heavy oil	Residue Pitch
Vapour Fraction		0	0	0	0	0	0	0	0	1	0
Temperature	*C*	70	160	111,3154	295,5007	209,4051	354,4262	281,9611	385,5661	366,6411	367,0692
Pressure	*kPa*	350	335	95	100	60	105	55	55	18,35	38,35
Molar Flow	*kgmole/h*	134,8526	134,8526	21,62887	113,2237	26,82128	86,40245	37,30081	49,10164	6,385771	42,71587
Mass Flow	*kg/h*	25000	25000	2318,778	22681,22	3917,745	18763,48	6699,975	12063,5	1562,583	10500,92
Liquid Volume Flow	*m3/h*	21,20463	21,20463	2,413828	18,7908	3,699181	15,09162	5,794573	9,297049	1,205722	8,091326
Heat Flow	*kJ/h*	-1,8E+07	-1,5E+07	1420014	-12000000	2779444	-13000000	5909683	-20000000	-2088244	-17000000

8.5 Appendix E: Coal tar viscosity and density curves - Simulation

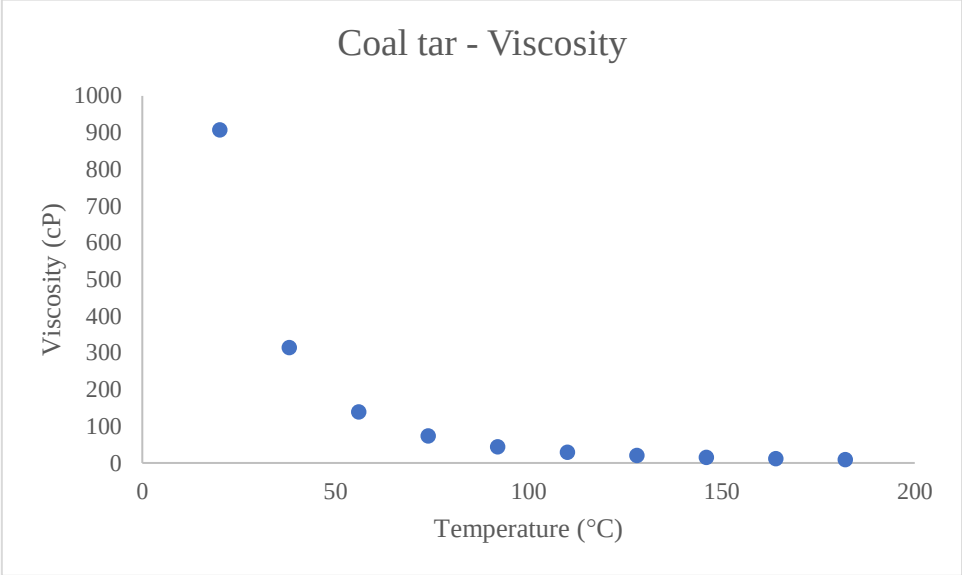

Figure 8-5: Simulated coal tar viscosity curve.

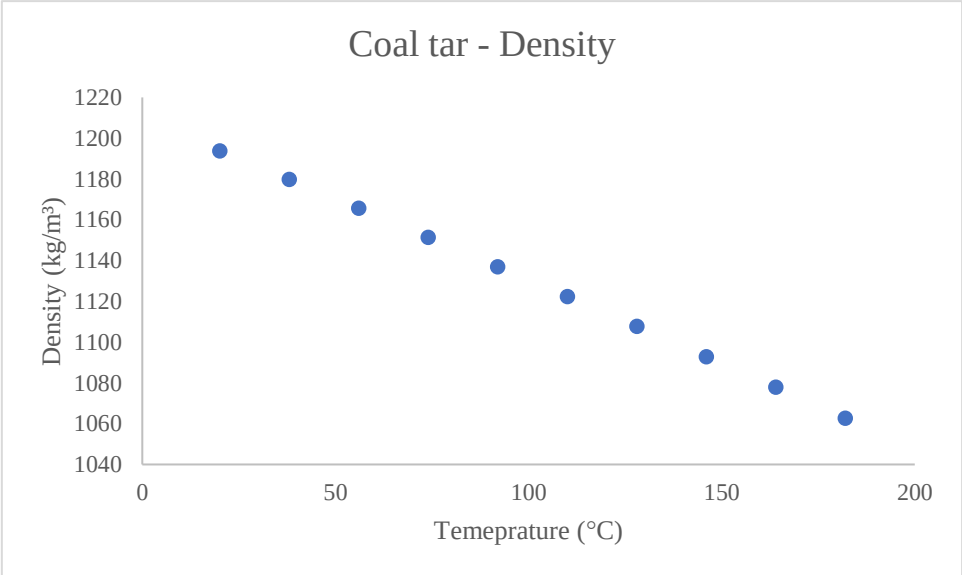

Figure 8-6: Simulated coal tar density curve.

8.6 Appendix F: Comparison of coal tar physical properties with different fluid packages.

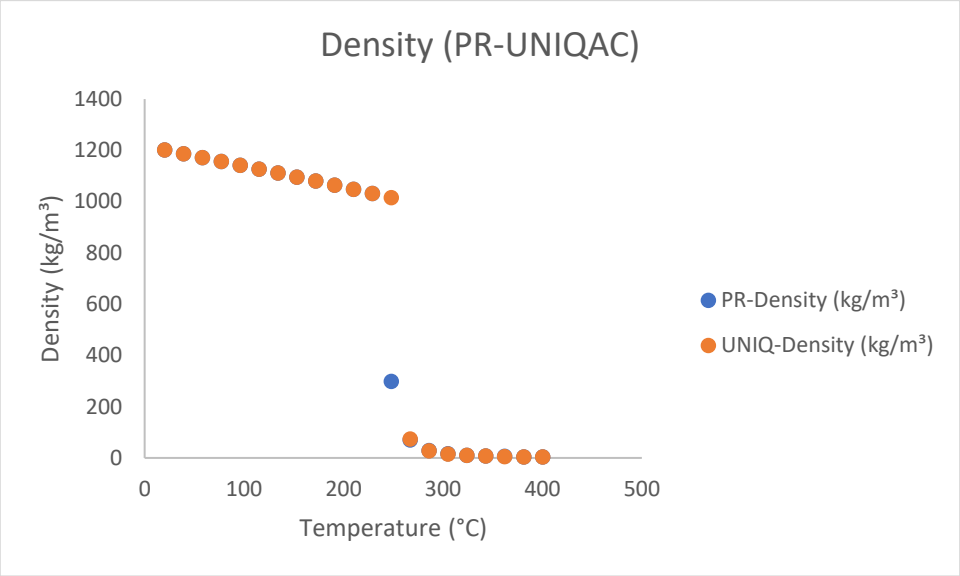

Figure 8-7: Coal tar density data comparison between Peng - Robinson and UNIQUAC fluid package.

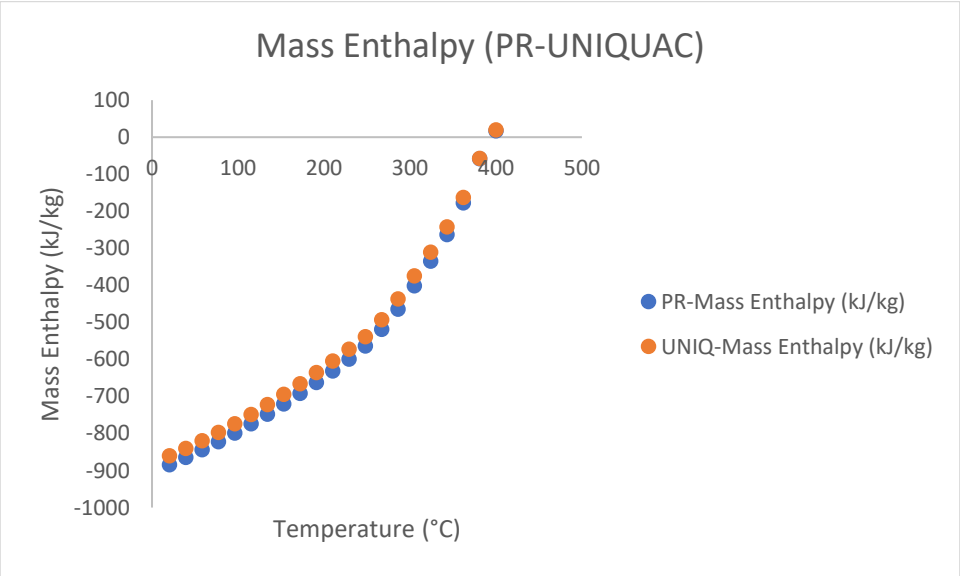

Figure 8-8: Mass enthalpy comparison between Peng - Robinson and UNIQUAC fluid package.

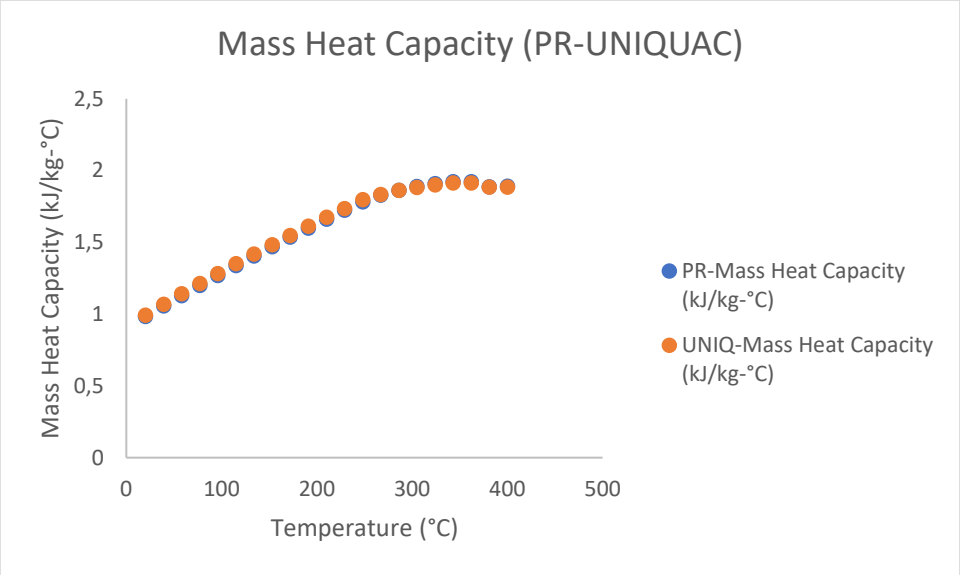

Figure 8-9: Heat capacity comparison between Peng-Robinson and UNIQUAC fluid package

8.7 Appendix G: Reference product plant quality specifications.

Table 8-7: Comparison between base quality value and requirement in production of 115 - 118 M Pitch.

115 - 118 M Pitch

Product	Unit	Base quality value	Requirement
Light oil	%		
Naphthalene		48	< 8
RCO	%		
Naphthalene		43,59	> 55
Light creosote	kg/m³		
Density		1147	> 1125
115 - 118 M Pitch	cP		
Viscosity @ 160 °C		3522,75	4200
Viscosity @ 140 °C		-	18000

Table 8-8: Comparison between base quality value and requirement in production of 68 - 73 RB Pitch.

68 - 73 RB Pitch

Product	Unit	Base quality value	Requirement
Light oil	%		
Naphthalene		40,58	< 8
RCO	%		
Naphthalene		46,6	> 55
Light creosote	kg/m³		
Density		1154	> 1125
68 - 73 RB Pitch	cP		
Viscosity @ 150 °C		237,33	280
Viscosity @ 170 °C		124,26	140

8.8 Appendix H: Product Composition – Simulation results.

Table 8-9: Product quality distributions in 115 - 118 M process.

Product Composition					
Component	***Light oil***	***RCO***	***Creosote***	***115 - 118 M***	***Heavy oil***
Benzene	0,267394	1,27E-03	4,15E-14	5,15E-32	8,28E-30
Toluene	1,98E-02	3,04E-04	6,35E-13	0	0
p-Xylene	5,05E-03	2,01E-04	1,42E-11	8,42E-30	7,33E-28
m-Xylene	2,85E-03	1,15E-04	8,57E-12	5,33E-30	4,63E-28
o-Xylene	4,95E-03	2,62E-04	6,23E-11	1,33E-28	1,04E-26
Phenol	8,19E-02	1,21E-02	9,86E-08	4,27E-24	2,55E-22
Indene	7,22E-03	1,74E-03	1,56E-07	1,17E-22	5,34E-21
m-Cresol	3,14E-03	1,32E-03	6,29E-07	1,76E-21	7,13E-20
p-Cresol	2,01E-03	7,17E-04	1,49E-07	1,30E-22	5,85E-21
o-Cresol	1,49E-03	3,90E-04	3,12E-08	1,34E-23	6,45E-22
Naphthalene	0,486639	0,435932	5,77E-03	1,48E-15	3,94E-14
Quinoline	1,61E-02	2,51E-02	1,93E-03	5,18E-15	1,11E-13
1-M-Naphtln	1,14E-02	2,18E-02	3,83E-03	4,48E-14	8,26E-13
2-M-Naphtln	1,59E-02	2,29E-02	1,63E-03	4,10E-15	8,76E-14
Acenaphthene	3,80E-02	0,142935	0,127507	2,36E-10	2,66E-09
DiBZoPyrrole	2,82E-05	2,30E-03	1,55E-02	4,85E-06	1,59E-05
DiBenzoFuran	2,54E-02	0,130144	0,153121	7,90E-10	7,95E-09
Phenanthrene	1,16E-03	4,54E-02	0,219323	6,43E-06	2,67E-05
Anthracene	3,61E-04	1,42E-02	6,99E-02	2,45E-06	1,00E-05
Fluorene	9,12E-03	5,34E-02	7,11E-02	7,88E-10	7,36E-09
Fluoranthene	4,91E-05	1,75E-02	0,220398	9,26E-03	1,83E-02
Pyrene	8,97E-06	4,04E-03	3,41E-02	2,13E-02	3,34E-02
NBP[1]360*	2,44E-05	6,36E-03	6,72E-02	1,23E-02	2,11E-02
NBP[1]400*	5,16E-05	5,96E-02	8,70E-03	0,957189	0,927146

Table 8-10: Product quality distributions in 68 - 73 RB process.

Product Composition					
Component	***Light oil***	***RCO***	***Creosote***	***68 - 73 RB***	***Heavy oil***
Benzene	0,383217	5,84E-04	5,12E-17	2,03E-21	2,82E-19
Toluene	2,85E-02	1,60E-04	1,02E-15	4,77E-19	4,54E-17
p-Xylene	7,35E-03	1,20E-04	2,97E-14	6,00E-17	4,12E-15
m-Xylene	4,15E-03	6,92E-05	1,81E-14	3,73E-17	2,55E-15
o-Xylene	7,22E-03	1,64E-04	1,49E-13	4,66E-16	2,84E-14
Phenol	0,117697	9,76E-03	3,87E-10	3,48E-12	1,52E-10
Indene	1,01E-02	1,51E-03	8,23E-10	1,05E-11	3,51E-10
m-Cresol	3,71E-03	1,35E-03	4,53E-09	8,45E-11	2,38E-09
p-Cresol	2,47E-03	7,28E-04	9,64E-10	1,51E-11	4,70E-10
o-Cresol	2,02E-03	3,60E-04	1,69E-10	2,22E-12	7,58E-11
Naphthalene	0,405754	0,466002	7,86E-05	2,39E-06	4,43E-05
Quinoline	7,61E-03	2,86E-02	5,30E-05	2,29E-06	3,28E-05
1-M-Naphtln	4,12E-03	2,74E-02	2,01E-04	9,74E-06	1,19E-04
2-M-Naphtln	8,75E-03	2,59E-02	4,09E-05	1,59E-06	2,29E-05
Acenaphthene	4,62E-03	0,22494	0,125389	1,11E-02	7,83E-02
DiBZoPyrrole	6,95E-07	7,10E-05	1,39E-02	6,68E-03	1,14E-02
DiBenzoFuran	2,04E-03	0,156871	0,236895	2,28E-02	0,139532039
Phenanthrene	3,10E-05	2,98E-03	0,257322	8,03E-02	0,179870703
Anthracene	9,66E-06	9,10E-04	8,08E-02	2,58E-02	5,68E-02
Fluorene	6,17E-04	5,12E-02	0,125718	1,34E-02	7,61E-02
Fluoranthene	1,53E-06	1,34E-04	9,13E-02	9,98E-02	9,52E-02
Pyrene	3,08E-07	2,19E-05	1,49E-02	3,04E-02	2,32E-02
NBP[1]360*	7,31E-07	5,07E-05	2,88E-02	3,45E-02	3,00E-02
NBP[1]400*	2,65E-06	1,30E-04	2,45E-02	0,675368448	0,309439782

8.9 Appendix I: Pitch Characterisation – Simulation results

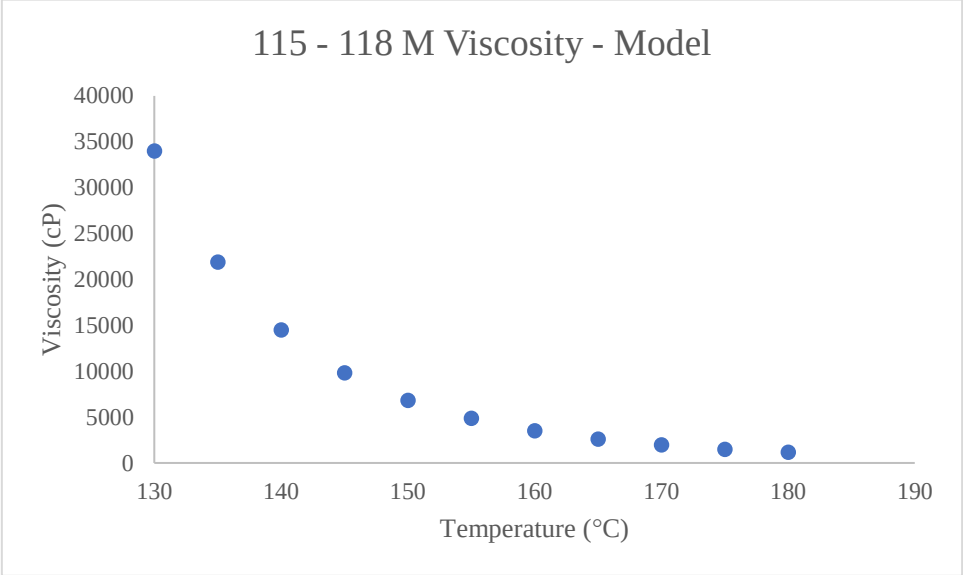

Figure 8-10: 115 - 118 M Pitch viscosity curve.

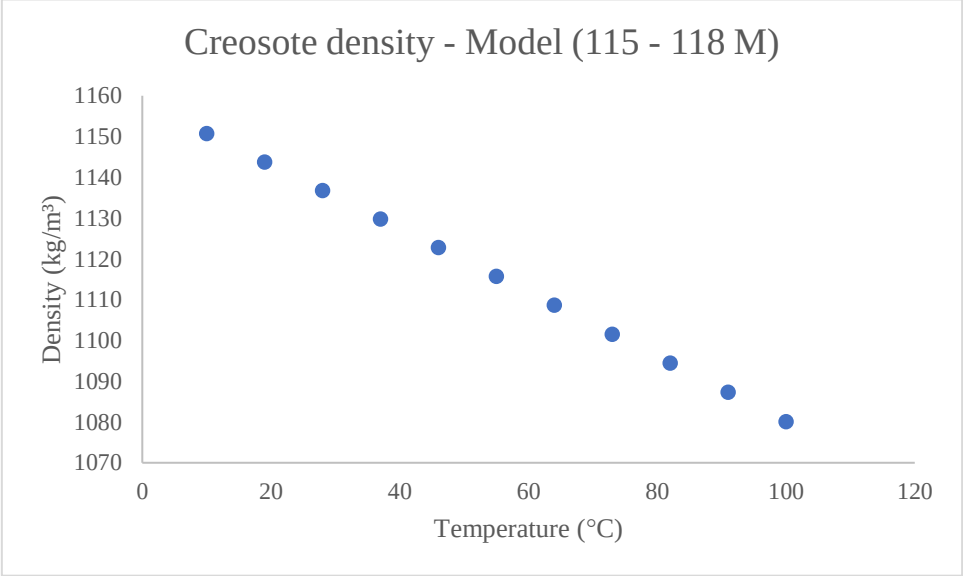

Figure 8-11: Light creosote density distribution for 115 - 118 M Pitch process.

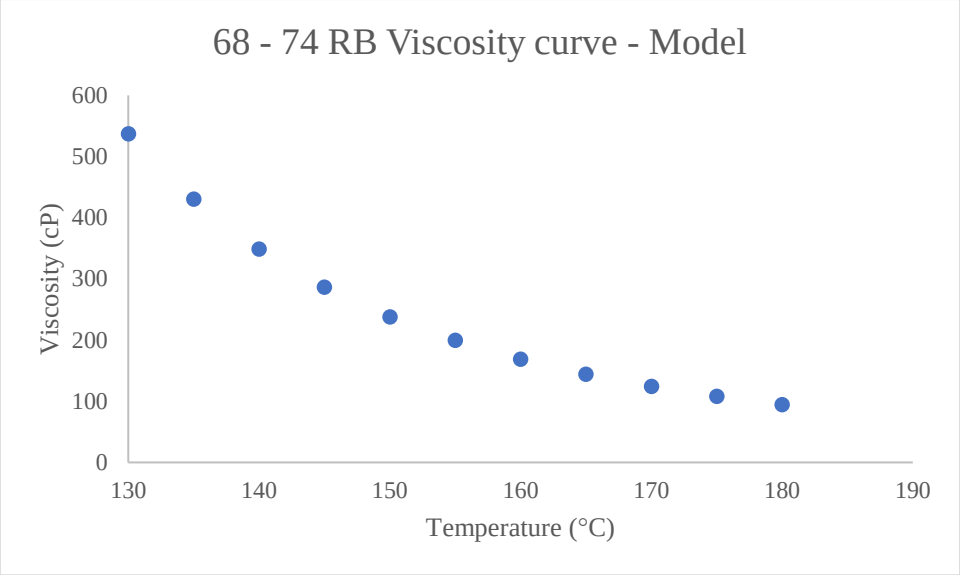

Figure 8-12: 68 - 73 RB Pitch viscosity curve.

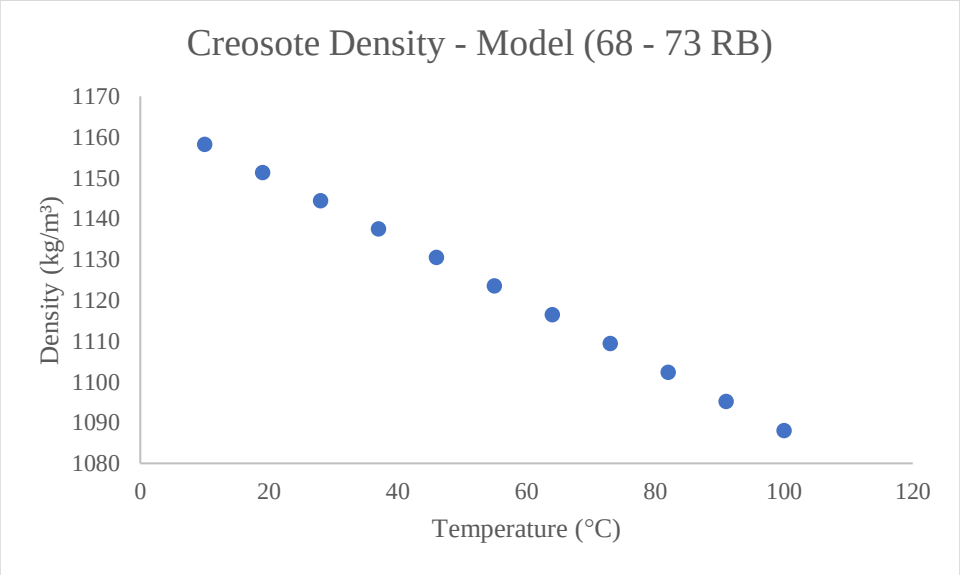

Figure 8-13: Light creosote density distribution for 68 - 73 RB process.

8.10 Appendix J: Process operating conditions.

Table 8-11: Operating conditions specified for the production of 115 - 118 M pitch product.

Column	Top temperature (°C)			Bottom temperature (°C)			Top pressure (kPa)			Bottom pressure (kPa)		
	Range	*Actual*	*Model*	*Range*	*Actual*	*Model*	*Range*	*Actual*	*Model*	*Range*	*Actual*	*Model*
Dehydrator	95 - 110	137,98 ± 18,79	159,4	200 - 220	-	245,5	95	95,32 ± 4,69	95	100	100	100
Fractionator	200 - 215	253,92 ± 29,62	266,9	-	288,49 ± 36,39	330	50 - 70	62,35 ± 7,76	60	-	102,71 ± 3,73	105
Creosote	310	308,85 ± 30,14	313,7	-	-	385,6	45 - 60	55,12 ± 7,26	55	-	55,15 ± 7,70	55
Flash	-	356,37	366,6	-	-	367,1	-	-	18,35	-	-	-

Table 8-12: Operating conditions specified for the production of 68 - 73 RB pitch product

Column	Top temperature (°C)		Bottom temperature (°C)		Top pressure (kPa)		Bottom pressure (kPa)	
	Range	*Model*	*Range*	*Model*	*Range*	*Model*	*Range*	*Model*
Dehydrator	96	151,4	200 - 220	246,8	95	95	100	100
Fractionator	200 - 210	220,1	-	339,2	50 - 70	65	-	105
Creosote	285 - 305	283,3	-	326,6	35	35	-	35
Flash	-	326,9	-	327,1	-	25	-	-

8.11 Appendix K: Column temperature profiles and flash column conditions.

Table 8-13: Dehydrator column temperature profile.

Tray position	Temperature (°C)
Condenser	101,1668908
1__Main Tower	151,3910791
2__Main Tower	192,7241932
3__Main Tower	205,5662557
4__Main Tower	170,8560563
5__Main Tower	177,0382875
6__Main Tower	191,6742625
7__Main Tower	246,7641271
Reboiler	289,8338969

Table 8-14: Fractionator column temperature profile.

Tray position	Temperature (°C)
Condenser	212,8981066
1__Main Tower	220,1214593
2__Main Tower	225,7164072
3__Main Tower	230,6583683
4__Main Tower	235,3474959
5__Main Tower	239,988349
6__Main Tower	244,7189929
7__Main Tower	249,7766042
8__Main Tower	255,5476696
9__Main Tower	264,8445939
10__Main Tower	285,7604685
11__Main Tower	290,8655787
12__Main Tower	297,0643066
13__Main Tower	298,8768545
14__Main Tower	302,3536647
15__Main Tower	307,1477861
16__Main Tower	311,0620306
17__Main Tower	314,6178795
18__Main Tower	320,573632
19__Main Tower	328,5182196
20__Main Tower	339,1588829
Reboiler	365,6431292

Table 8-15: Creosote column temperature profile.

Tray position	Temperature (°C)
Condenser	256,907361
1__Main Tower	283,3125916
2__Main Tower	301,2193555
3__Main Tower	310,7831022
4__Main Tower	316,4824926
5__Main Tower	320,2589562
6__Main Tower	322,8331229
7__Main Tower	324,5575057
8__Main Tower	325,6838829
9__Main Tower	327,2879999
10__Main Tower	327,2804512
11__Main Tower	327,266307
12__Main Tower	326,7367352
13__Main Tower	326,6126949
14__Main Tower	326,575873
15__Main Tower	326,5642604
16__Main Tower	326,5611861
17__Main Tower	326,5634706
18__Main Tower	326,5799063
Reboiler	327,5291934

Table 8-16: Flash column process conditions.

Name	Soft Pitch	Residue Pitch	Heavy oil
Vapour	0	0	1
Temperature [C]	327,529193	327,0854078	326,9301635
Pressure [kPa]	35	34,5	26,5
Molar Flow [kgmole/h]	70,8178554	70,59515184	0,222703588
Mass Flow [kg/h]	16216,6905	16172,22689	44,46359912
Std Ideal Liq Vol Flow [m3/h]	12,8404909	12,803747	3,67E-02
Molar Enthalpy [kJ/kgmole]	-244752,368	-245663,7916	44161,10115
Molar Entropy [kJ/kgmole-C]	-674,466835	-676,1204435	-147,9912572
Heat Flow [kJ/h]	-17332837,8	-17342672,67	9834,835697

8.12 Appendix L: Analysis of the naphthalene distribution in the dehydrator and fractionator columns.

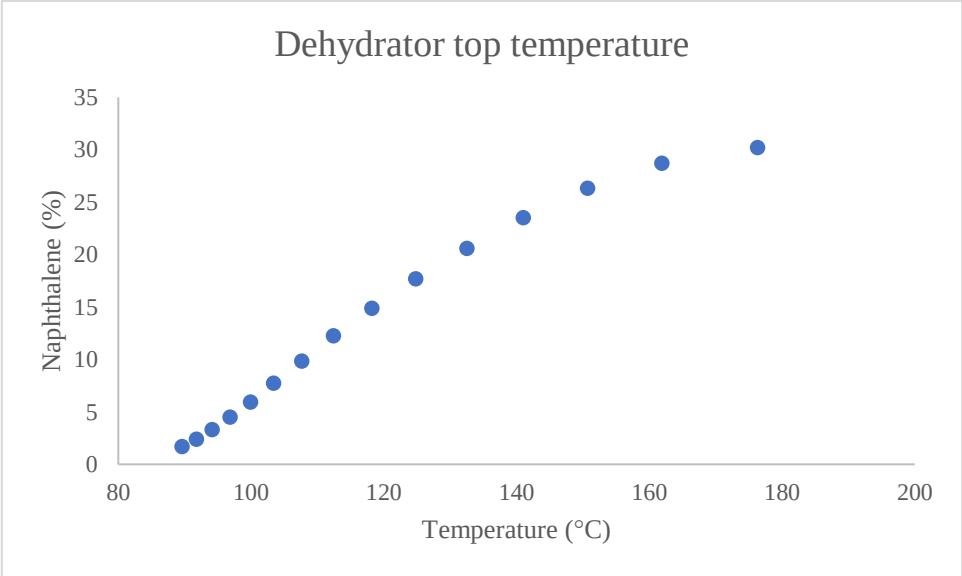

Figure 8-14: Naphthalene distribution in light oil fraction with changes in dehydrator top temperatures.

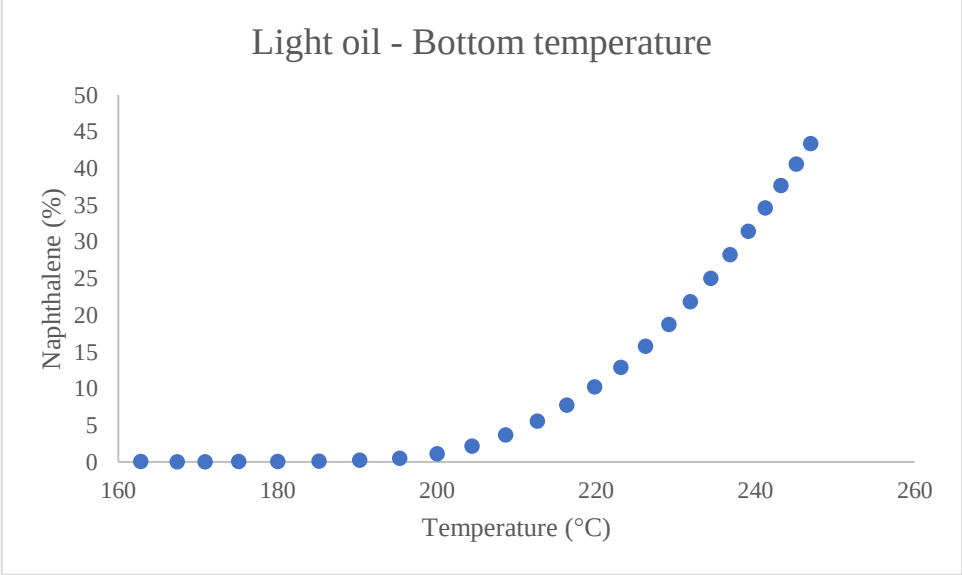

Figure 8-15: Naphthalene distribution in light oil fraction with changes in dehydrator bottom temperatures.

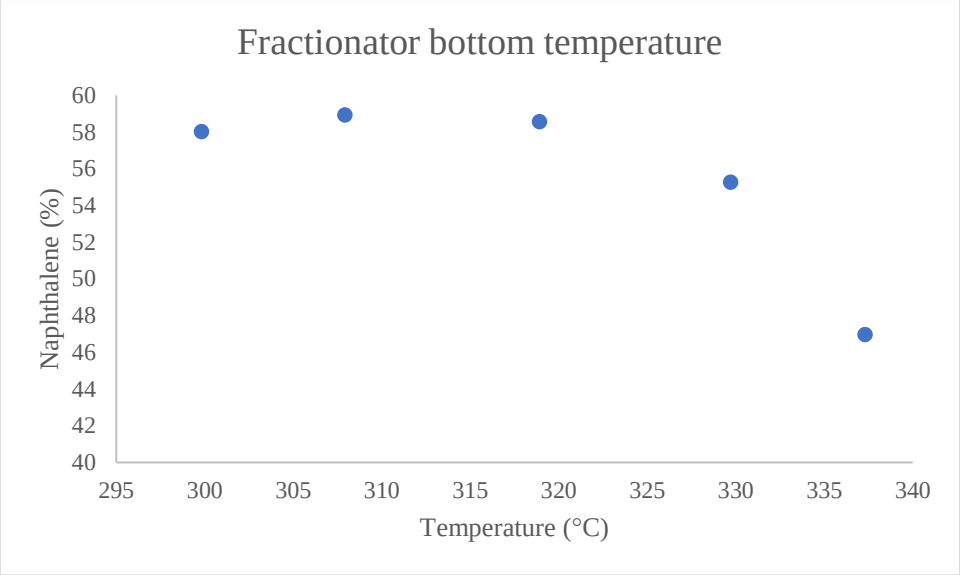

Figure 8-16: Bottom temperature effect on RCO naphthalene distribution.

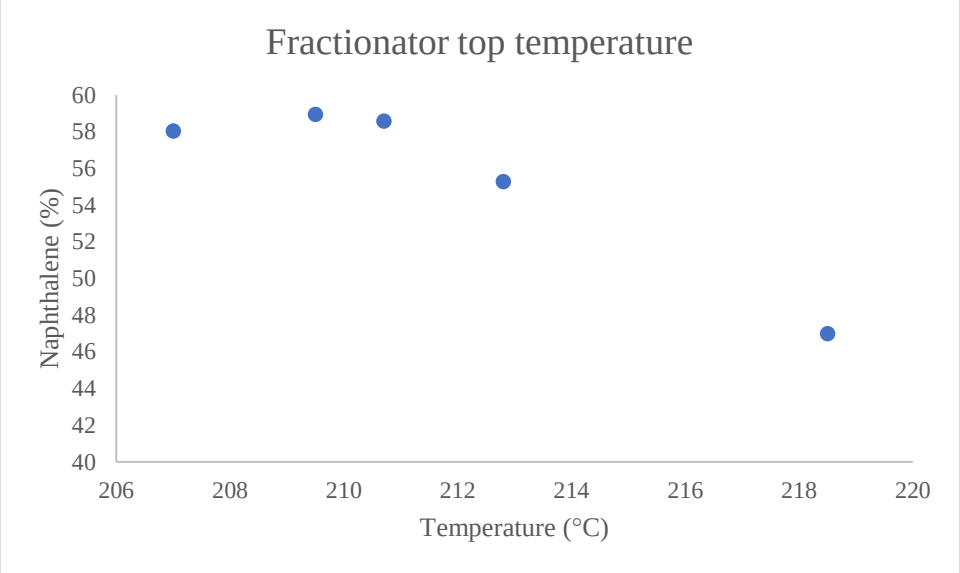

Figure 8-17: Top temperature effect on RCO naphthalene distribution.

8.13 Appendix M: Product revenue calculations.

Table 8-17: Product pricing for the year 2022.

Product	Cost (Rands/t)
Light oil	3100
RCO	4400
Light creosote	4200
Heavy oil	3800
115 - 118 M Pitch	4500
68 - 73 RB Pitch	11700

Table 8-18: 115 - 118 M pitch process base product revenue.

115 - 118 M Base revenue				
Product	**Simulation (t/h)**	**tons/t of tar**	**Cost (R/t)**	**R/t of tar**
Light oil	2,32	0,0928	3100	287,68
RCO	3,92	0,1568	4400	689,92
Light creosote	6,7	0,268	4200	1125,6
Heavy oil	1,56	0,0624	3800	237,12
115 - 118 M	10,5	0,42	4500	1890
				4230,32
			Revenue p/a	**501667303,3**

Table 8-19: 115 - 118 M pitch process product revenue after optimisation.

115 - 118 M maximum revenue				
Product	**Simulation (t/h)**	**tons/t of tar**	**Cost (R/t)**	**R/t of tar**
Light oil	0,08475	0,00339	3100	10,509
RCO	2,1975	0,0879	4400	386,76
Light creosote	10,08	0,4032	4200	1693,44
Heavy oil	0,205	0,0082	3800	31,16
115 - 118 M	12,43	0,4972	4500	2237,4
				4359,269
			Revenue p/a	**516959171,8**

Table 8-20: 68 - 73 RB pitch process base product revenue.

68 - 73 RB Base revenue				
Product	**Simulation (t/h)**	**tons/t of tar**	**Cost (R/t)**	**R/t of tar**
Light oil	1,62	0,0648	3100	200,88
RCO	4,76	0,1904	4400	837,76
Light creosote	2,4	0,096	4200	403,2
Heavy oil	0,044	0,00176	3800	6,688
68 - 73 RB	16,17	0,6468	11700	7567,56
				9016,088
			Revenue p/a	**806592756,6**

Table 8-21: 68 - 73 RB pitch process product revenue after optimisation.

68 - 73 RB Maximum revenue				
Product	**Simulation (t/h)**	**tons/t of tar**	**Cost (R/t)**	**R/t of tar**
Light oil	0,006	0,00024	3100	0,744
RCO	3,54	0,1416	4400	623,04
Light creosote	4,37	0,1748	4200	734,16
Heavy oil	0,1475	0,0059	3800	22,42
68 - 73 RB	16,935	0,6774	11700	7925,58
				9305,944
			Revenue p/a	**832523709,2**